CHEMICAL REVIEWS

Review

pubs.acs.org/CR

# Upconversion Nanoparticles: Design, Nanochemistry, and Applications in Theranostics

Guanying Chen,*[,†,‡] Hailong Qiu,[†,‡] Paras N. Prasad,*[,‡,§] and Xiaoyuan Chen*[,∥]

[†]School of Chemical Engineering and Technology, Harbin Institute of Technology, Harbin, Heilongjiang 150001, China

[‡]Department of Chemistry and the Institute for Lasers, Photonics, and Biophotonics, University at Buffalo, State University of New York, Buffalo, New York 14260, United States

[§]Department of Chemistry, Korea University, Seoul 136-701, Korea

[∥]Laboratory of Molecular Imaging and Nanomedicine, National Institute of Biomedical Imaging and Bioengineering, National Institutes of Health, Bethesda, Maryland 20892-2281, United States


## CONTENTS



**Received:** August 5, 2013
**Published:** March 10, 2014

   dx.doi.org/10.1021/cr400425h | *Chem. Rev.* 2014, 114, 5161−5214

## 1. INTRODUCTION

Theranostics is a concept of integrating imaging and therapy into a single platform for use in the next generation of personalized medicine to meet the challenges in modern health care.[1] The diagnostic role of theranostic agents reports the presence of a disease, its status, and its response to a specific treatment, while the therapeutic role of the agent can be implemented in several forms:[2] (i) The first is imaging-guided surgery for tumor resection and postsurgery evaluation. Intraoperative visualization of diseased areas is important for precision surgery, as the location of the tumor may change after presurgical imaging and during resection.[3−6] Furthermore, postsurgical assessment is valuable in ensuring complete removal of the diseased sections. (ii) The second is delivery or release of therapeutic entities to the intended site. The delivered entities can be small molecule chemotherapeutics (such as cisplatin, doxorubicin, and paclitaxel), biologics (such as protein drugs and antibodies), gene products (DNA, siRNA, and miRNA), nanotherapeutic agents, and even cells.[7−9] The release/therapy can be light-activated such as in photodynamic therapy (PDT) for destruction of the tumor or heat activated by nonradiative conversion of absorbed photon energy into heat such as in photothermal therapy (PTT),[10] which disrupts the structure of the cells and shrinks the tumor volume.[11] (iii) The third is disruption of a cellular or metabolic pathway.[2] An occupation of specific cell surface receptors by introduced theranostic agents with appropriate chemistry can disrupt cell regulation, producing a therapeutic effect.[12] Theranostics offers an opportunity to embrace multiple techniques to arrive at a comprehensive imaging/therapy regimen. Incorporation of therapeutic functions into molecular imaging contrasts plays a pivotal role in developing theranostic agents.[13] Molecular imaging using photoluminescence (PL) spectroscopy is an important technique in biochemistry and molecular biology. It has become the dominant method revolutionizing medical diagnostics, bioassays, DNA sequencing, and genomics.[14−17] It can be used to study a wide range of biological specimens, from cells to ex vivo tissue samples, and to in vivo imaging of live objects; it can also cover a broad range of length scale, from submicrometer-sized viruses and bacteria, to macroscopic-sized live biological species.[17−19] Thus, PL imaging provides a powerful noninvasive tool to visualize morphological details in tissue with subcellular resolution. However, the imperfect optical properties of conventional PL imaging agents and the challenge in incorporation of therapeutic functions onto them have severely limited their abilities for use in theranostics.

PL imaging generally employs exogenous contrast agents, which encompass organic dyes,[20,21] organically modified silica,[22−24] fluorescent proteins,[25−28] metal complexes,[11,29−31] and semiconductor quantum dots (QDs).[32−35] Most of these conventional contrast agents utilize Stokes-shifted emission using excitation in the ultraviolet (UV) or blue-green visible spectral ranges. These conventional PL imaging agents when excited in such spectral range have a number of limitations: (i) low signal-to-background ratio (SBR) caused by unwanted autofluorescence as well as by strong light scattering from the biological tissues (such as fur, skin, and tissues) when excited at short wavelengths; (ii) low penetration depth of UV and visible excitation and/or emission light in biological tissues; and (iii) potential DNA damage and cell death due to long-term exposure to short wavelength, particularly UV excitation. In addition, there is also a serious concern about the toxicity of heavy metal-based QDs for bioimaging, as they contain toxic elements (e.g., cadmium, mercury, and lead). It is well-known that biological tissues have an "optical transparency window" in the near-infrared (NIR) range of 700−1100 nm.[17−19] Utilization of NIR excitation light not only allows for deeper light penetration and reduced photodamage effects, but also offers lower autofluorescence, reduced light scattering, and phototoxicity.[36−38] Two-photon-excitation or second harmonic generation contrast agents, which utilize longer wavelength light, have been recently developed to overcome these limitations for imaging of cells and small animals.[39−43] However, they require expensive ultrashort pulsed lasers (e.g.,


dx.doi.org/10.1021/cr400425h | Chem. Rev. 2014, 114, 5161−5214

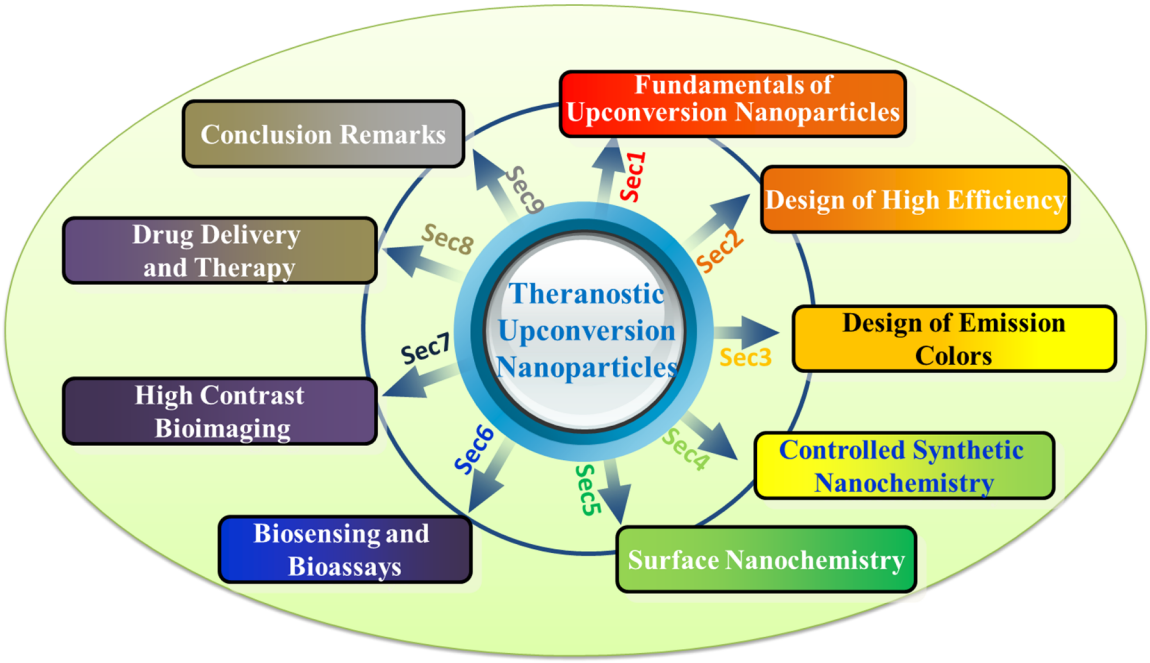


**Figure 1.** Schematic illustration of the structure of this Review.

a femtosecond laser) to perform the excitation as they involve inefficient nonlinear optical processes.

Lanthanide-doped upconversion nanoparticles (UCNPs) are a promising new generation of imaging agents for bioimaging.[44−57] Upconversion (UC) utilizes sequential absorption of multiple photons through the use of long lifetime and real ladder-like energy levels of trivalent lanthanide ions embedded in an appropriate inorganic host lattice to produce higher energy anti-Stokes luminescence.[51,58] It thereby converts two or more low-energy excitation photons, which are generally NIR light, into shorter wavelength emissions (e.g., NIR, visible, and UV). This process is different from nonlinear multiphoton absorption in organic dyes and QDs, which involves simultaneous absorption of two or more photons through virtual states.[59] The efficiency of a UC process is generally several orders of magnitude higher than that of nonlinear multiphoton absorption, thus enabling UC to be produced by a low-cost continuous-wave (cw) diode laser instead of the need of ultrashort pulsed lasers for nonlinear multiphoton excitation. UCNPs have multiple attributes that make them well-suited for use in theranostics comprised of imaging, drug delivery, and therapy. Their unique frequency conversion capability is usually unavailable for existing endogenous and exogenous fluorophores, thus providing UCNPs numerous distinctive characteristics for medical diagnostics and therapy. For bioimaging, some of the advantages are virtually zero autofluorescence background to improve signal-to-noise ratio, large anti-Stokes shifts allowing us to easily separate the PL from the excitation wavelength, narrow emission bandwidths allowing ease of multiplexed imaging, and high resistance to photobleaching making it suitable for long-term repetitive imaging. In addition, UCNPs are nonblinking, less light scattering, and allow for deep tissue penetration because of excitation being in the NIR region that is within the optical transparency window. Moreover, a new direction for theranostic UCNPs utilizes hierarchically built nanostructures to combine UC PL imaging with other imaging modalities such as magnetic resonance imaging (MRI),[55] computed tomography (CT),[60] single-photon emission tomography (SPECT),[61] positron emission tomography (PET),[62] as well as with therapeutics of PTT,[63] PDT,[64] gene and drug delivery,[53] for in vitro and in vivo theranostics. Indeed, significant advances in theranostic UCNPs have recently been made by the use of nanochemistry that allows for nanocontrol of their optical properties to enhance upconversion at a selected wavelength,[36] surface modification for phase transfer,[65] and surface coupling chemistry for ligands that target biomarkers.[66]

This Review aims to summarize recent progress in design and applications of UCNPs with an emphasis on the role of nanochemistry in the advancement of this field. The organization and the scope of this Review are represented in Figure 1. In section 1, we introduce the basic concepts of UC that are utilized in sections 2 and 3. Sections 2 and 3 describe recent advances in controlling optical properties needed to achieve high UC efficiency and tunabilty of output colors, respectively. Sections 4 and 5 are dedicated to nanochemistry for controlled synthesis and surface engineering of UCNPs. Sections 6−8 summarize recent advances in theranostic applications of UCNPs in biosensing and bioassays, high contrast bioimaging, and drug delivery and therapy, respectively. Finally, section 9 concludes the overall current status, challenges, and future perspectives.

### 1.1. Upconversion Nanoparticles (UCNPs)

Lanthanide-doped UCNPs are dilute guest−host systems where trivalent lanthanide ions are dispersed as a guest in an appropriate dielectric host lattice with a dimension of less than 100 nm. The dopants of lanthanide are optically active centers, which produce emission when excited. Through judicious selection of lanthanide dopants, UCNPs can display wavelength (color) selective upconversion, such as NIR to shorter NIR, visible (blue, green, red), or UV. Generally, the UC PL arises from the 4f−4f orbital electronic transitions with concomitant wave functions localized within a single lanthanide ion. The shielding of 4f electrons by the outer complete 5s and 5p shells results in line-like sharp emissions, which exhibit high resistance


dx.doi.org/10.1021/cr400425h | Chem. Rev. 2014, 114, 5161−5214

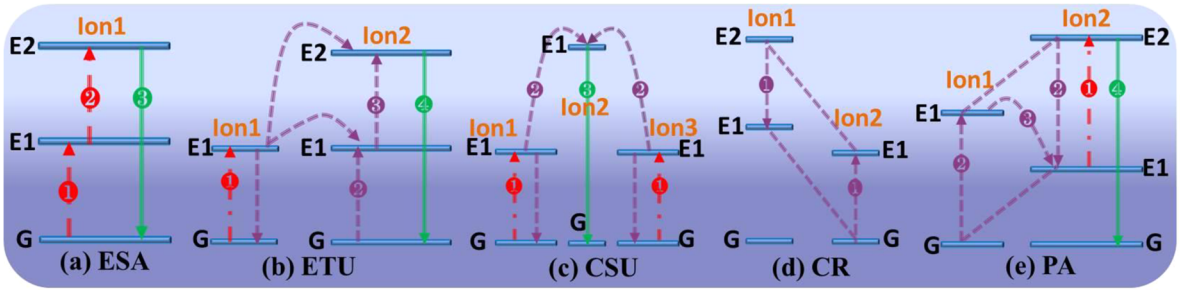


**Figure 2.** Principal UC processes for lanthanide-doped UCNPs: (a) excited-state absorption (ESA), (b) energy transfer upconversion (ETU), (c) cooperative sensitization upconversion (CSU), (d) cross relaxation (CR), and (e) photon avalanche (PA). The red, violet, and green lines represent photon excitation, energy transfer, and emission processes, respectively.

to photobleaching, and photochemical degradation. These intra-4f electronic transitions of lanthanide ions are electric dipoles forbidden by quantum mechanical selection rules, which, however, are relaxed due to local crystal field-induced intermixing of the f states with higher electronic configurations.[67,68] The primary forbidden nature of the 4f−4f transition yields very long lifetimes (up to tens of millisecond) for energy levels of lanthanide ions, thus favoring the occurrence of sequential excitations in the excited states of a single lanthanide ion as well as permitting favorable ion−ion interactions in the excited states to allow energy transfers between two or more lanthanide ions. These resulting features of lanthanide dopants determine the basic UC mechanisms (see section 1.2). The UC PL intensity generally has a nonlinear dependence on the excitation light density:[69−71]

$$I_{\mathrm{UCPL}} = KP^{n} \tag{1}$$

where $I_{\mathrm{UCPL}}$ is the photoluminescence intensity, $P$ is the power of pump laser, $K$ is material-related coefficient, and $n$ is the number of the excitation photons required to produce the UC PL. The log−log relation of eq 1 is very useful to determine the "$n$" values for the UC PL peaks at very low excitation density. However, it should be noted that "$n$" values can be affected by the competition process between "the decay rate" and "the upconverted rate" at the intermediate states, leading to smaller "$n$" values (not integral numbers) at high excitation density.[69−71] This phenomenon is termed the "saturation effect", which needs to be carefully avoided when determining the photon processes of UC PL peaks. Because of the nonlinear nature of UC PL, the upconversion quantum yield (UCQY) or the efficiency of a UCPL peak is strongly dependent on the excitation density. UCQY is defined as the ratio of the number of the emitted upconverted photons to the number of the absorbed NIR photons, according to the following formula:

$$\begin{aligned}\mathrm{UCQY} &= \frac{\text{photons emitted}}{\text{photons absorbed}} \\ &\propto \frac{\text{emitted UC PL intensity}}{\text{absorbed exciation light}} \\ &= \frac{I_{\mathrm{UCPL}}}{\alpha P}\end{aligned} \tag{2}$$

where $\alpha$ is the absorption coefficient of the host material at the excitation wavelength. By inserting eq 1 into eq 2, it can be easily obtained that:

$$\mathrm{UCQY} \propto P^{n-1} \tag{3}$$

According to this equation, it is clear that UC PL involving different photon processes will have distinct dependence on the excitation power density. Because the dependence of the PL intensity on the excitation density can be easily measured for a given UC PL peak, the UC QY for a given peak at any excitation density can be determined by referencing to a quantified UCQY at one particular excitation density.

UCNPs have optical properties similar to those of the corresponding bulk forms. They both generally produce the same UC PL peaks due to the well-shielded 4f−4f orbital electronic transitions by the outer complete 5s and 5p shells. However, the efficiency and the relative intensity between different UC PL peaks of UCNPs are quite different from their bulk counterpart due to nanosize-induced surface effects. Because of the high surface-to-volume ratio of UCNPs, most of the lanthanide dopants are exposed to surface deactivations (due to surface defects, as well as to ligands and solvents that possess high phonon energy). Surface-related deactivations encompass two ways: (i) dopants located on or around the nanoparticle surface can be deactivated directly by neighboring surface quenching centers; and (ii) the energy contained in dopants located in the center of UCNPs can randomly migrate and travel a long distance to the dopant on/around surface or directly to the surface quenching sites. In addition to the influence of phonons from the host lattice, the optical properties of UCNPs are significantly affected by the surface properties, which are not so pronounced in bulk crystals. Indeed, UCNPs are found to exhibit much lower efficiency than their bulk form due to surface-induced deactivations. To produce high efficiency UCNPs, appropriate nanochemistry for engineering the surface of these nanoparticles plays a pivotal role (see sections 2.5−2.6). UCNPs have intrinsic attributes such as nonblinking, nonphotobleaching, high chemical stability, sharp emission bands, NIR light excitation, and large anti-Stokes emissions, making them promising for theranostic applications.

The UCNPs have to meet many key technical requirements for bioapplications: (i) The first is high efficiency and multicolor emissions. High efficiency is required for all UCNPs to accomplish improved limit of detection (LOD) in sensing (see section 6), high SBR bioimaging (see section 7), and increased therapy effect (see section 8). Single-wavelength excited multicolor emissions are of critical importance for multiplexing (simultaneously detecting multiple analytes/targets in a sample) capabilities in imaging or the throughput increase of bioassays. (ii) Next is monodispersed small size, uniform shape, and stoichiometric composition (see section 4). The monodispersed small size and uniform shape are required


dx.doi.org/10.1021/cr400425h | Chem. Rev. 2014, 114, 5161−5214

to have identical optical properties as well as cellular uptake and biological effects for intracellular theranostics, while a precise stoichiometric composition is necessary to allow control over the concentration of lanthanide dopants to manipulate the optical attributes. (iii) The third is a nanochemically engineered surface for phase transfer and for coupling to targeting ligands. The as-synthesized UCNPs are generally hydrophobic due to their capping by long-chain hydrophobic ligands. Engineering the surface of UCNPs to allow their dispersion in aqueous phase for biological applications is required. In addition, UCNPs lack the targeting moieties to identify regions of interest in the body such as angiogenic tumor area. Appropriate coupling chemistry is required to incorporate a range of antibodies, peptides, biotin, avidin, and proteins onto the nanoparticle surface. (iv) The final requirement is biocompatibility. UCNPs should be nontoxic and biocompatible to cells and to the body.

### 1.2. Upconversion Mechanisms

As depicted in Figure 2a−e, there are five basic UC mechanisms encompassing (a) excited-state absorption (ESA), (b) energy transfer upconversion (ETU), (c) cooperative sensitization upconversion (CSU), (d) cross relaxation (CR), and (e) photon avalanche (PA).[69,72−74] The mechanism of cooperative upconversion luminescence is not included in this review, as it is an inefficient process that is not explored in UCNPs up to now. These five basic mechanisms are discussed below.

**1.2.1. Excited-State Absorption.** Excited-state absorption (ESA) takes the form of successive absorption of pump photons by a single ion due to the ladder-like structure of a simple multilevel system as illustrated in Figure 2a by a three-level system for two sequential photon absorption. The occurrence of this mechanism is due to the equal separation from G to E1 and from E1 to E2 as well as the reservoir capability of the intermediate level E1. When an ion is excited from the ground state to the E1 level, another pump photon has a high possibility of promoting the ion from E1 to the higher-lying state E2 due to the long lifetime of E1 state, before its decay to the ground state. Consequently, upconverted emission will occur from the E2 level. To achieve highly efficient ESA, a ladder-like arrangement of the energy states of lanthanide is required. Only a few lanthanide ions such as $Er^{3+}$, $Ho^{3+}$, $Tm^{3+}$, and $Nd^{3+}$ have such energy level structures,[58] which also find a good excitation wavelength match with the output of commercially available diode lasers (at ∼975 and/or 808 nm).

**1.2.2. Energy Transfer Upconversion.** Energy transfer upconversion (ETU) in Figure 2b is quite different from ESA in Figure 2a, as ESA is operated within a single lanthanide ion, while ETU involves two neighboring ions. In an ETU process, an ion 1 known as the sensitizer is first excited from the ground state to its metastable level E1 by absorbing a pump photon; it then successively transfers its harvested energy to the ground-state G and the excited-state E1 of ion 2, known as the activator, exciting ion 2 to its upper emitting state E2, while sensitizer ion 1 relaxes back to ground-state G twice. The upconversion efficiency of an ETU process is sensitive to the average distance between the neighboring sensitizer-activator, which is determined by the concentrations of dopants. In contrast to ETU, the efficiency in an ESA process is independent of the dopant concentration due to its single ion characteristic.

The ETU process is of crucial importance for UCNPs, as the most efficient theranostic UCNPs to date utilize ion pairs (sensitizer/activator) of $Yb^{3+}/Tm^{3+}$, $Yb^{3+}/Er^{3+}$, and $Yb^{3+}/Ho^{3+}$ for enhanced excitation at ∼975 nm.[36,75−82] It is worth noting that biological tissues have relatively small scattering and absorption at 975 nm, which is within the "optical transparency window" of tissue. Here, $Yb^{3+}$ works perfectly as a sensitizer, as it has a sufficiently large absorption cross-section in the NIR region at ∼975 nm. Moreover, its optimized concentration can be kept high (20−100% for fluoride nanoparticles) without evoking deleterious cross-relaxations (see section 1.2.4) because of the fact that $Yb^{3+}$ has an only two energy level structure. To date, most efforts have been devoted to develop $Yb^{3+}$-sensitized UCNPs pumped at around 975 nm.

Efficient ETU can also be observed in single lanthanide doped systems utilizing lanthanide ion itself as the sensitizer, for example, in $Er^{3+}$-doped $LiYF_4$ when excited at telecom wavelength of 1490 nm,[83] or in $Ho^{3+}$-doped $NaGdF_4$ nanoparticles when excited at 1200 nm.[84] The utilization of other sensitizers can be used to quench and enhance certain emission bands. For instance, $Nd^{3+}$, $Ce^{3+}$, and $Ho^{3+}$ have been used as sensitizers to enhance the blue emission band of $Tm^{3+}$, red emission band of $Ho^{3+}$, and NIR emission band of $Tm^{3+}$, respectively.[85−88]

**1.2.3. Cooperative Sensitization Upconversion.** Cooperative sensitization upconversion (CSU) in Figure 2c is a process involving the interaction of three ion centers, with ion 1 and ion 3 generally being of the same type. After absorbing excitation photons, both ion 1 and ion 3 can be excited to the excited state, respectively. Both ion 1 and ion 3 then can interact with ion 2 simultaneously, cooperatively transfer the contained energy, and excite ion 2 to a higher state. The excited ion 2 can relax back to its ground state by emitting an upconveted photon. The efficiency of CSU is generally orders of magnitude lower than the ESA or ETU process, as it involves quasi-virtual pair levels during transitions, which have to be described quantum mechanically in a higher order of perturbation. Despite this, the need for confined excitation to compensate the low efficiency may provide a possibility to achieve high-resolution imaging that is unavailable from the other UC mechanisms. The CSU mechanism has been reported for $Yb^{3+}/Tb^{3+}$,[89] $Yb^{3+}/Eu^{3+}$,[90] and $Yb^{3+}/Pr^{3+}$ ion pairs.[91]

**1.2.4. Cross Relaxation.** Cross relaxation (CR) in Figure 2d is an energy transfer process, resulting from ion−ion interaction in which ion 1 transfers part of its excited energy to ion 2 through a process of E2 (ion 1) + G (ion 2) → E1 (ion 1) + E1 (ion 2). Ion 1 and ion 2 can be either the same or different, and ion 2 can also be in its excited state in some cases. The CR process is a fundamental result of ion−ion interaction; its efficiency is in close relation with the dopant concentration. CR is the main reason for the well-known "concentration quenching mechanism" of emission, but it can be intentionally used to tune the color output in UCNPs or construct efficient photon avalanche mechanism (see section 1.2.5).

**1.2.5. Photon Avalanche.** Photon avalanche (PA) in Figure 2e is a process that produces UC above a certain threshold of excitation power. Below the threshold, very little up-converted fluorescence is produced, while the PL intensity increases by orders of magnitude above the pump threshold. Actually, the PA is a looping process that involves processes of ESA for excitation light and an efficient CR that produces feedback. The level E1 of ion 2 is initially populated by nonresonant weak ground-state absorption. The looping


dx.doi.org/10.1021/cr400425h | Chem. Rev. 2014, 114, 5161−5214

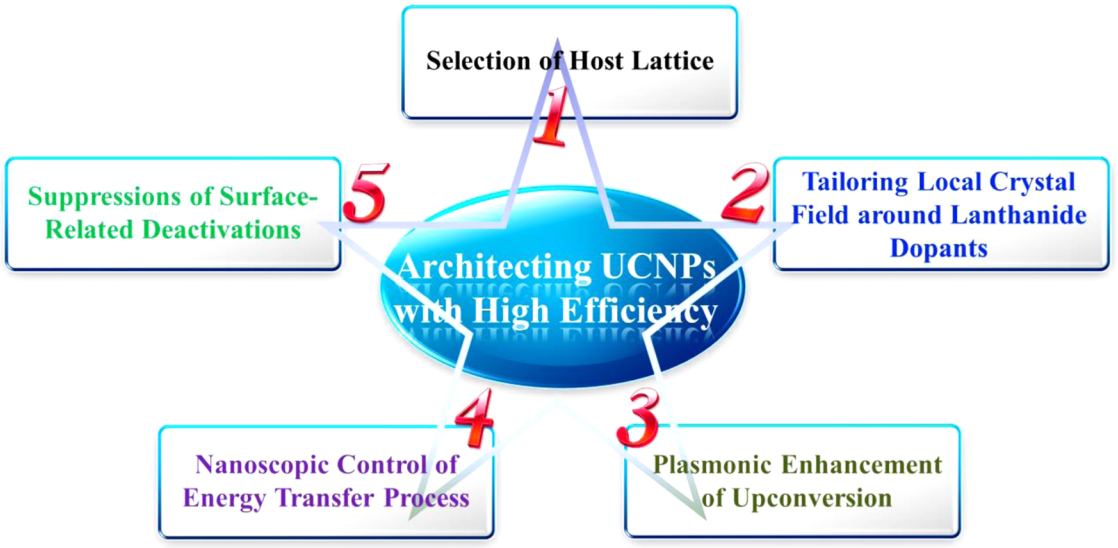


**Figure 3.** General strategies to achieve the high efficiency of UCNPs.

process starts with the ESA process to elevate ion 2 at the level E1 to the emitting level E2. An efficient CR process of E2 (ion 2) + G (ion 1) → E1 (ion 2) + E1 (ion 1) between ion 1 and ion 2 then occurs. Last, ion 1 transfers its energy to ion 2 to populate its level E1, forming a complete loop. The net effect of the looping process is that one ion 2 at metastable E1 state produces two ion 2's at this state. When the looping process ensues, two ion 2's at the E1 state will produce four; four will produce eight, evoking an avalanche effect for populating ion 2 in its E1 state, and thus the PA UC from the emitting level of E2. It is easy to identify PA, as it generally requires a pump threshold and a long time (seconds) to build up. Moreover, the dependence of UC PL on the pump power becomes extremely strong around the threshold pumping power.

## 2. ARCHITECTING UPCONVERSION NANOPARTICLES WITH HIGH EFFICIENCY

Photon upconversion has been known and studied over a long period of time, which was generally based on bulk materials. An extensive review of the early work on bulk materials was given by Auzel in 2004 as well as recently by other reviews on specific topics of UCNPs.[46,51,52,57,58,92−107] However, none of the previous reviews provide a comprehensive review on the design, nanochemistry, and theranostic applications of UCNPs. It is not until recently that UCNPs became available for biomedical applications due to the success achieved in producing highly efficient UCNPs. The accomplishment of high efficiency is of particular importance, as it is the basic optical function of UCNPs to perform high performance theranostic application. For this reason, we first highlight in this section recent progress made on this aspect. Figure 3 displays five general strategies that have been employed to achieve high efficiency in UCNPs: (i) selection of novel host materials; (ii) tailoring local crystal field; (iii) plasmonic enhancement; (iv) engineering energy transfers; and (v) suppression of surface-related deactivations.

### 2.1. Selection of Novel Host Materials

Selection of appropriate host materials is essential for high efficiency UC emissions. Basically, an ideal host material should be transparent in the spectral range of interest, have high optical damage threshold, and be chemically stable. Moreover, the host lattice can affect the UC efficiency in two ways: (i) by the phonon dynamics, and (ii) by the local crystal field.

The phonon-induced nonradiative process is the main loss mechanism for UC emissions; the luminescence efficiency is quite sensitive to the distribution of phonon density of states in UCNPs. A nonradiative process involves multiphonon-assisted relaxations whereby the energy difference between the higher and the lower energy level is converted into many lattice phonons.[92] A good indicator of how many phonons may be needed is the cutoff phonon energy of the host lattice. The host materials investigated in nanophosphors encompass oxides (e.g., $Y_2O_3$, cutoff phonon energy ~550 $cm^{-1}$; $ZrO_2$, cutoff phonon energy ~500 $cm^{-1}$),[108,109] fluorides (e.g., $NaYF_4$, cutoff phonon energy ~350 $cm^{-1}$),[110] vanadates (e.g., $YVO_4$, cutoff phonon energy ~890 $cm^{-1}$),[111] oxysulfide (e.g., $Y_2O_2S$, cutoff phonon energy ~520 $cm^{-1}$),[112] and oxy-fluorides or -chlorides (e.g., GdOCl, cutoff photon energy ~500 $cm^{-1}$).[113] Generally, the larger is the number of phonons needed to convert the excitation energy into phonon energy, the lower is the efficiency of the nonradiative process. Hence, to enhance the emission efficiency by reducing nonradiative rate, it is desirable to have the lanthanide ions incorporated into a dielectric host of very low frequency phonons. Among investigated hosts, fluoride materials have the lowest phonon cutoff energy and generally exhibit the highest UC efficiency due to the minimization of nonradiative losses in the intermediate states or the emitting states.

The crystal field of a host material has a profound effect on the UC efficiency of lanthanide emitters, as the local crystal symmetry surrounding a lanthanide ion strongly influences its optical properties. A less symmetric crystal phase is generally favorable for the UC efficiency, as the intermixing of the lanthanide ion's f states with higher electronic configurations can be more manifested. For example, hexagonal $NaYF_4$:$Yb^{3+}$/$Er^{3+}$ microcrystals exhibit visible upconversion PL, which is 4.4 times higher than its cubic counterparts,[77] and monoclinic $ZrO_2$ nanoparticles emit higher UC PL than the tetragonal phase nanoparticles.[109] Selection of an appropriate host lattice with a low phonon cutoff energy and low crystal field symmetry is therefore important to realize an efficient UC process.


dx.doi.org/10.1021/cr400425h | *Chem. Rev.* 2014, 114, 5161−5214

### 2.2. Tailoring Local Crystal Field

It is well-known that the local environment around the lanthanide determines its optical parameters, as it enables the parity-forbidden intra-4f electronic transitions of the lanthanide ion to become partially allowed by intermixing the f states with higher electronic configurations. As discussed in section 2.1, selection of certain host lattice of low crystal field is a promising way to enhance the UC PL of UCNPs. However, the drawback of this strategy is that once the host lattice is fixed, it is unable to further modify the local environment around the lanthanide ion. When the crystal phase of the selected host lattice is fixed, another promising route to enhance the UC PL is to tailor the local environment around the lanthanide ion through an intentional doping of nonluminescent cationic ions. The nonluminescent ions can replace the cationic ions in the lattice points or occupy the interstitial sites around the lanthanide ions, thus lowering the local symmetry around the lanthanide dopants and favoring the UC efficiency. In separate works of Chen et al. and Bai et al., $Li^+$-doping was a found to be able to enhance the UC emission in oxide UCNPs of varying host lattice and lanthanide dopants by 2 orders of magnitude.[114−118] In some recent reports, it was shown that $Li^+$ can produce similar results in fluoride UCNPs.[119−121] Dou et al. investigated the impact of the alkali ions on lanthanide-doped fluoride nanoparticles, and found a significant UC PL enhancement.[122] Li et al. demonstrated that up to 10-fold enhancement of UP PL in singly $Er^{3+}$-doped $YAlO_3$ phosphor by exchanging about 40% of $Y^{3+}$ to larger $Gd^{3+}$ (1.159 vs 1.193 Å) due to the expansion of the host lattice and the distortion of the local symmetry.[123] The blue, green, red, and UV UC PL of hexagonal $NaYF_4$:$Yb^{3+}$/$Er^{3+}$ nanoparticles were shown to be obviously enhanced by tridoping with nonluminescent cationic ions of $Sc^{3+}$.[124] Although significant progress has been made by utilizing nonluminescent ion doping to enhance the PL of UCNPs, the direct evidence of tailoring the local crystal field remains lacking. Investigations on the local structure of lanthanide ions, for example, by using extended X-ray absorption fine structure (EXAFS) spectroscopy, are needed to provide such proof.

### 2.3. Plasmonic Enhancement

Localized surface plasmon resonance (LSPR) is the collective oscillation of electrons at the interface of metallic structures, and is produced by the electromagnetic interaction of the metal with incident light of a specific wavelength.[11,125−129] It is well-known that LSPR of metallic structures can enhance the fluorescence from adjacent fluorophores (dyes or QDs),[130−138] when the distance between the metallic structure and the fluorophore is appropriate. Similarly, LSPR can also be used to enhance the efficiency of UC PL of UCNPs. The interaction of UCNPs with the metallic structures has been investigated in three ways: (i) UCNPs of $NaYF_4$ doped with lanthanide ion pairs of $Yb^{3+}$/$Er^{3+}$ or $Yb^{3+}$/$Tm^{3+}$ were deposited on a metallic film of gold islands,[139] dense metal nanoparticles (Au or Ag),[140,141] or 3D plasmonic antenna.[142,143] It was found that the PL of UCNPs can be enhanced by ∼5−310-fold due to the plasmonic-induced coupling effect by optimizing pertinent experimental parameters. However, the challenge in this approach is to tune the distance between the nanoparticles and the metallic structure, which the plasmonic-enhanced UC PL is highly dependent upon. These investigations have produced efficient thin-film UC materials, which have not been explored for biophotonic applications up to now, but are expected to provide a platform for highly sensitive biosensing applications. (ii) Metallic nanoparticles are attached or self-assembled onto the surface of lanthanide-doped fluoride, oxide, or vanadate UCNPs.[144−151] The surface modification of the as-synthesized UCNPs with new ligands is implemented to make them dispersible in aqueous phase and carry positive charges,[144−149] which is important to attract the negatively charged metallic nanoparticles to the surface of UCNPs in water or for in situ growth of gold nanorods.[150] The UCNPs dispersed in organic phase can also be directly assembled with silver nanowires or gold nanoparticles synthesized in organic phase to investigate the plasmonic effect.[151] When irradiated with 980 nm laser, the specifically designed plasmonic metallic nanoparticles were shown to clearly enhance NIR-to-visible UC luminescence from the UCNPs. It is very important to study the surface plasmon enhancement mechanism at single nanoparticle level to provide an optimal design of hybrid UCNPs and metallic nanoparticles. Schietinger et al. coupled single $NaYF_4$:$Yb^{3+}$/$Er^{3+}$ nanoparticles with a gold nanosphere (30 and 60 nm in diameter) to enhance UC emission and observed an overall enhancement factor of 3.8.[147] This work provides direct evidence of plasmonic-enhanced UC PL at the single particle level. (iii) The third is by core/shell structures of metallic/silica/UCNPs or UCNPs/silica/metallic.[47,152−156] The UC PL has been demonstrated to be enhanced by 4−10-fold with the assistance of metallic nanostructure. The core/shell design is of particular importance for theranostic applications, as it provides a novel platform to integrate plasmonics and UC PL at nanoscale. Moreover, the distance between the metallic nanoparticles and the UCNPs can be precisely controlled by the thickness of the spacer silica shell.

Most previous works have clearly shown plasmonic-enhanced UC PL, but some works also reported on plasmonic-induced quenching of UC PL.[157−159] Time-resolved measurements did reveal that both the excitation and the emission processes are influenced by the coupling to plasmon resonance in the metallic nanospheres. However, these results cannot determine which enhancement and/or quenching mechanism is undertaking. The plamonic-induced PL enhancement is known to result from the increase of the radiative rate and/or the excitation intensity by the LSPR of metallic nanostructures, while the quenching of the PL stems from resonance energy transfer from the fluorophore to the metallic structure or the absorption of the emitted light by the metallic nanoparticle.[160,161] For the Stokes-shifted PL of a fluorophore, the measurement of intrinsic quantum yield (QY) of the fluorophore can determine which mechanism takes places and how much it contributes, as the increased radiative rate can increase the intrinsic QY, while the increased excitation field is independent of the intrinsic QY of the fluorophore. However, for the UC PL, the measurement of UC PL QY becomes ineffective for such purpose, as the QY of UC PL is overall a nonlinear process and is strongly dependent on the excitation density. To unravel the complex mechanisms of plasmonic-induced UC PL, a direct measurement of the QY of the Stokes-shifted PL (where the UC PL shares the same peak position) of the lanthanide activator is helpful. Such a measurement can quantify the amount of gain that is due to the increased radiative rate produced by the plasmonic coupling. In addition, a measurement of the enhancement factors of different UC PL bands is constructive to understand the enhancement mechanism, as the plasmonic-increased local excitation field generally results in more pronounced effects on a multiphoton-involved UC PL band,


dx.doi.org/10.1021/cr400425h | Chem. Rev. 2014, 114, 5161−5214

when utilizing a low excitation power density that cannot produce a saturation effect. It is known that the plasmonic-induced quenching effect only occurs efficiently when the UCNPs and metallic structures are placed in direct contact or at a quite close distance. Thus, it is imperative to introduce a spacer layer between the UCNPs and the metallic structure to avoid the quenching effect. Moreover, the ability to precisely control the thickness of the spacer provides an opportunity to maximize the UC PL under NIR light excitation. Theoretical investigations on the interaction of plasmonic metallic structures of varying shapes and sizes with UCNPs are needed in the future to provide the guidance on chemical preparations of an optimized plasmonic-enhanced UCNPs system for theranostic applications.

### 2.4. Engineering Energy Transfers within Lanthanide Dopants

The energy transfer is an important process in UC mechanisms (consult Figure 2); in particular, it plays a major role in the ETU mechanisms for the $Yb^{3+}/Tm^{3+}$, $Yb^{3+}/Er^{3+}$, and $Yb^{3+}/Ho^{3+}$ combinations, which are identified to be the most efficient ion pairs up to date, when excited at ~980 nm.[92] The main mechanism for nonradiative energy transfer involves fundamental multipolar and/or exchange interactions between two lanthanide ions that are strongly dependent on their distance.[58] Because the lanthanide dopant concentration within one single UCNP determines the average ion−ion distance, the control of dopant concentration becomes a useful tool to manipulate energy transfer processes. One has to be aware that a higher concentration of lanthanide ions can introduce CR process, which is usually detrimental to the luminescence efficiency. This sets a hurdle on increasing the lanthanide concentration to shorten the ion−ion distance to enhance the energy transfer process for the increased UC PL efficiency. However, it is important to note that, unlike the activator ions of $Tm^{3+}$, $Er^{3+}$, and $Ho^{3+}$, the sensitizer $Yb^{3+}$ ion has one exclusive excited energy level, the $^2F_{5/2}$ state, produced by absorptions at ~980 nm. The variation of its concentration generally is unable to induce a CR process, thus excluding any general "concentration quenching effect". Interestingly, a recent investigation revealed that the "concentration quenching effect" from a high concentration of activators can be circumvented by utilization of a high laser irradiance density (~$10^6$ W/cm$^2$), producing a higher brightness of UCNPs due to a higher concentration of activator as luminescent centers.[162] However, this uncovered UC PL enhancement strategy is limited to applications that permit a high irradiance density.

It has recently been established that the NIR-to-NIR (consult Figure 4),[36] NIR-to-blue,[163] as well as the NIR-to-UVUC PL in $NaYF_4$:$Yb^{3+}/Tm^{3+}$ nanoparticles or in ($NaYF_4$:$Yb^{3+}/Tm^{3+}$)/$CaF_2$ nanoparticles can be enhanced by orders of magnitude through increasing the $Yb^{3+}$ ion concentration up to 100%.[164] Despite previous reports on $Yb^{3+}/Tm^{3+}$-doped UC materials utilizing the $Yb^{3+}$ concentration of around 20−40%,[77,165−168] these recent results have clear implications that energy transfers between $Yb^{3+}$ and $Tm^{3+}$ can be manipulated to produce tunable UC PL enhancement through monotonous increase of the concentration of $Yb^{3+}$ ions. It is noted that the UC PL in $Yb^{3+}/Er^{3+}$ (or $Ho^{3+}$) doped fluoride UCNPs can be gradually increased for $Yb^{3+}$ ions below 20% (10% for oxide nanoparticles), but produce quenching effect above this concentration.[77] These quenching effects were previously interpreted by back energy transfer processes from $Er^{3+}$ to $Yb^{3+}$ ions, that

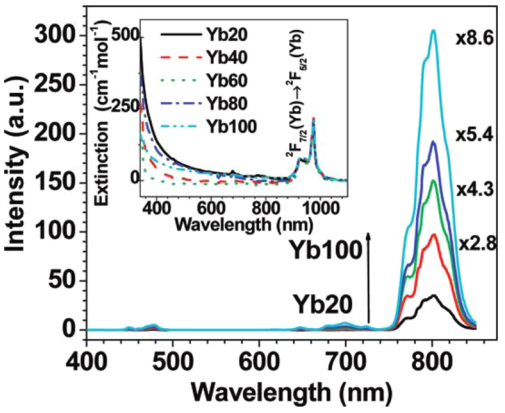


**Figure 4.** UC PL spectra of colloidal $NaYF_4$ nanoparticles codoped with 2% $Tm^{3+}$ and with various concentrations of $Yb^{3+}$ ions (20−100%), under diode laser excitation at 975 nm. Their absorption spectra have been normalized at 975 nm for the $^2F_{7/2} \rightarrow {}^2F_{5/2}$ transition of $Yb^{3+}$ ions, as displayed in the inset. Reprinted with permission from ref 36. Copyright 2010 American Chemical Society.

is, $^4S_{3/2}(Er) + {}^2F_{7/2}(Yb) \rightarrow {}^4I_{13/2}(Er) + {}^2F_{5/2}(Yb)$ or $^2H_{11/2}(Er) + {}^2F_{7/2}(Yb) \rightarrow {}^4I_{11/2}(Er) + {}^2F_{5/2}(Yb)$. However, these back energy transfer processes in combination with energy transfers from $Yb^{3+}$ to $Er^{3+}$ form a closed positive looping (similar to the PA), which can enhance the UC PL. The observed quenching effect for higher $Yb^{3+}$ ion concentrations in $Yb^{3+}/Er^{3+}$ (or $Ho^{3+}$) doped fluoride UCNPs (or other UC materials) might arise from $Yb^{3+}$-induced energy migrations from the lattice points inside the particle to the surface quenching sites around the particle (refer to section 2.5 for details on the quenching mechanism). Suppressions of surface quenching sites can display a real benefit of engineering the energy transfers to enhance the UC PL of $Er^{3+}$ (or $Ho^{3+}$) via increasing $Yb^{3+}$ ion concentration up to 100%. In analogy, a recent investigation found that minimizing the migration of excitation energy to defects in $KYb_2F_7$:$Er^{3+}$ 2% UCNPs can yield 8 times more efficient violet UC PL from $Er^{3+}$ ions than the previously reported value of $NaYF_4$:$Yb^{3+}$ 20%, $Er^{3+}$ 2% UCNPs.[169]

### 2.5. Suppression of Surface-Related Deactivations

The surface characteristics of UCNPs are important for the efficiency of UC PL, as they expose numerous lanthanide dopants to surface deactivations (caused by surface defects, lattice strains, as well as ligands and solvents that possess high phonon energy, Figure 5). These processes are strongly manifested in nanoparticles because of the high surface-to-volume ratio at nanometer dimensions. Surface-related deactivations may occur in two ways: (i) Photoexcited dopants located on or around the surface can be deactivated directly by neighboring quenching centers; and (ii) the energy contained in the photoexcited dopants located in the center of nanophosphors can randomly migrate and travel a long distance to the dopant on/around surface or directly to the surface quenching sites (Figure 5). This second way is more prominent for UCNPs, as a high sensitizer concentration of $Yb^{3+}$ (more than 18%) is often introduced into nanophosphors, doped with $Yb^{3+}/Tm^{3+}$, $Yb^{3+}/Er^{3+}$, $Yb^{3+}/Ho^{3+}$, to achieve high UC PL.[58] The long distance transportation of energy in a $Yb^{3+}$ sublattice is due to the unique two-energy-level structure of $Yb^{3+}$ in association with its long-lived excited state. It is of note that the harvested UV energy can travel 5 nm with no losses through a $Gd^{3+}$ sublattice in the $NaGdF_4$ host lattice.[170] In


dx.doi.org/10.1021/cr400425h | Chem. Rev. 2014, 114, 5161−5214

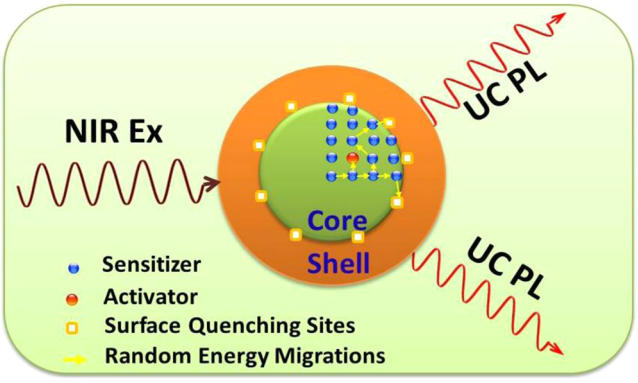


**Figure 5.** Schematic illustration of a cross section of core/shell structure and random energy migration among lanthanide ions in the core nanoparticles.

analogy, the absorbed NIR energy in a $Yb^{3+}$ sublattice might be able to travel several or even 10 nm in nanophosphors with a high $Yb^{3+}$ concentration. Hence, suppressions of surface-related quenching mechanisms in these UCNPs are of particular significance to accomplish a high efficiency of UC PL. The most effective way toward this is the utilization of a core/shell structure, in which the host material of the shell should exhibit a low lattice mismatch with the core materials. There are three types of core/shell structures that have been utilized to enhance the UC PL. The classification is based on the host matrix composition of the core and the shell, or the distribution of dopant ions within the core and the shell.

**2.5.1. Enhancing Upconversion Photoluminescence with a Homogeneous Core/Shell Structure.** An important classification of core/shell structure is that the shell and the core have the identical host material.[171] This kind of core/shell structure is simple but very effective, as it guarantees the epitaxial growth and creates a homogeneous interface between the core and the outer shell. Yi et al. reported that the visible UC emissions in hexagonal phase $NaYF_4$:$Yb^{3+}$/$Er^{3+}$ and $NaYF_4$:$Yb^{3+}$/$Tm^{3+}$ were enhanced by 7.4 times and 29.6 times, respectively, by growth of a thin layer of $NaYF_4$ (~2 nm).[172] Later, the same conclusion has independently been verified in ($NaYF_4$:$Yb^{3+}$/$Er^{3+}$)@$NaYF_4$ core/shell UCNPs.[173−177] The absolute quantum yield of the 30 nm ($NaYF_4$:$Yb^{3+}$/$Er^{3+}$)@$NaYF_4$ core/shell UCNPs is 3 times higher than that of $NaYF_4$:$Yb^{3+}$/$Er^{3+}$ core nanoparticles of the same size, reaching as high as 0.3% under excitation of 150 W/$cm^2$ at ~980 nm.[177] Significant enhancement of luminescence efficiency has also been observed in core/shell nanoparticles of ($KYF_4$:$Yb^{3+}$/$Er^{3+}$)@$KYF_4$,[178] ($SrF_2$:$Yb^{3+}$/$Er^{3+}$)@$SrF_2$,[179] ($NaGdF_4$:$Yb^{3+}$/$Tm^{3+}$)@$NaGdF_4$,[180,181] ($KGdF_4$:$Yb^{3+}$/$Tm^{3+}$)@$KGdF_4$,[182] (YOF:$Yb^{3+}$/$Er^{3+}$)@YOF,[183] and ($YF_3$:$Ln^{3+}$)@$YF_3$ ($Ln^{3+}$ = $Yb^{3+}$/$Er^{3+}$, $Yb^{3+}$/$Tm^{3+}$, or $Yb^{3+}$/$Er^{3+}$/$Tm^{3+}$) when compared to the core counterpart under NIR excitation at ~980 nm.[184] The core/shell/shell design ($NaGdF_4$:$Er^{3+}$)@($NaGdF_4$:$Ho^{3+}$)@$NaGdF_4$ nanoparticles showed a broad excitation in the NIR range. More importantly, a clear enhancement is observed when the third inert $NaGdF_4$ shell was incorporated onto the core/shell ($NaGdF_4$:$Er^{3+}$)@($NaGdF_4$:$Ho^{3+}$) nanoparticle.[84] Indeed, the core/shell structure with the shell being an identical host lattice to the host material of the core has been extensively investigated. It is clear that this structure allows an effective suppression of surface-related deactivations by elimination of the quenching sites on the surface of the core nanoparticle as well as spatial isolation of the core from surrounding deactivators (ligands, solvents, etc.). However, it is challenging to show direct evidence of formation of this kind of core/shell structure, as the core and the shell generally have identical contrast in the transmission electron microscope. The formation of the core/shell structure often can be suggested by the increase in the size distribution, the elevated luminescence efficiency, as well as the prolonged decay of the UC PL.

**2.5.2. Enhancing Upconversion Photoluminescence with a Heterogeneous Core/Shell Structure.** The core/shell nanoparticle with the core and the shell host matrix of different composition has also been investigated for the enhancement of the UC efficiency of the core nanoparticles. The requirement for the shell host matrix is to have a low lattice mismatch with that of the core nanoparticle. One advantage of this type of core/shell nanoparticle is that it entails the incorporation of two or more imaging modalities into a single conduct. For example, core/shell ($NaYF_4$:$Yb^{3+}$/$Er^{3+}$)@$NaGdF_4$ or ($NaYF_4$:$Yb^{3+}$/$Tm^{3+}$)@$NaGdF_4$[37,185] structures have a luminescent upconverting core protected by a $NaGdF_4$ shell,[37,179,186] whereas the paramagnetic $Gd^{3+}$ in the shell allows for integrating magnetic resonance imaging (MRI) properties. Recently, Wang et al. reported ~300-fold enhancement of UC emission yield in the 10−13 nm $NaYF_4$:$Ln^{3+}$@$CaF_2$ heterogeneous core/shell nanoparticles in comparison to the parent $NaYF_4$:$Ln^{3+}$ nanoparticles (Figure 6c and d).[187] The heteroshell of $CaF_2$ was chosen as well by us to coat $NaYbF_4$:$Tm^{3+}$, leading to a 35-fold enhancement of NIR-to-NIR upconversion intensity (Figure 6a and b) and reaching a quantum yield as high as 0.6% under an excitation power density of 0.3 W/$cm^2$.[38] Han et al. reported on 2 orders of magnitude enhancement of NIR-to-UV UC emission in a series of $NaYF_4$:(20−100%)$Yb^{3+}$/$Tm^{3+}$@$CaF_2$ core/shell nanoparticles when compared to the core nanoparticles.[164] As compared to the typically used $NaYF_4$ shell, the $CaF_2$ coating is found to be more effective in resisting quenching in aqueous medium to preserve the upconverting emissions, and more efficient in suppression of lanthanide leakage. It is interesting to note that the silica coating has slightly increased the UC emission of the $Y_2O_3$:$Yb^{3+}$/$Tm^{3+}$,[188] and $NaYF_4$:$Yb^{3+}$/$Tm^{3+}$ or $Yb^{3+}$/$Er^{3+}$.[189] The core/shell $NaYF_4$:$Ln^{3+}$@$NaGdF_4$ nanoparticles with fixed or tunable shell thickness have been successfully prepared to provide a hard proof of the epitaxial growth of the core/shell structure, and to provide a paradigm for the investigation of the shell thickness on the enhancement of UC emissions.[190−194] From a chemical point of view, in addition to the merits of enhancement of UC PL and the integration of multimodalities, another unique advantage of the heterogeneous core/shell structure is that it allows for in-depth characterization of the core−shell morphology, while it remains a challenge for the homogeneous core/shell structure (discussed in section 2.5.1).

**2.5.3. Enhancing Upconversion Photoluminescence with an Active Core/Active Shell Structure.** The active core/active shell strategy is similar to the homogeneous and heterogeneous core/shell method to enhance the upconverting efficiency. The difference is that instead of using an inert homogeneous or heterogeneous shell material, a reasonable concentration of lanthanide dopants (generally the sensitizer) is introduced to the shell layer. The shell layer now takes two roles: (i) Suppression of surface-related deactivations, which is the same as the homogeneous and heterogeneous core/shell structure. (ii) The lanthanide dopants in the shell further


dx.doi.org/10.1021/cr400425h | Chem. Rev. 2014, 114, 5161−5214

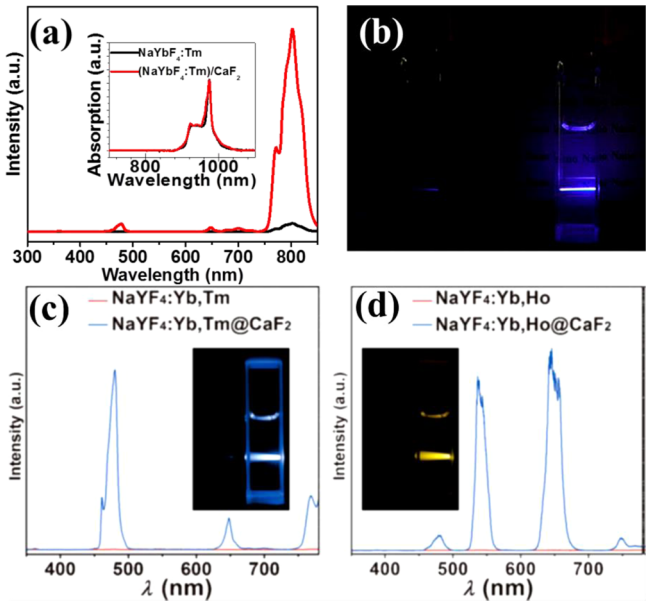


**Figure 6.** (a) The UC PL spectra of the ~20 nm $NaYbF_4$:0.5%$Tm^{3+}$ core, and the ~27 nm ($NaYbF_4$:0.5%$Tm^{3+}$)@$CaF_2$ core/shell nanoparticles; the inset shows the corresponding absorption spectra of the core and the core/shell nanoparticles; (b) photographic images of cuvettes with suspensions of the $NaYbF_4$:0.5%$Tm^{3+}$ core and the ($NaYbF_4$:0.5%$Tm^{3+}$)@$CaF_2$ core/shell nanoparticles (ref 38); (c) UC emission spectra and digital photographs (inset) of ~7 nm $NaYF_4$:$Yb^{3+}$/$Tm^{3+}$ core and the $NaYF_4$:$Yb^{3+}$/$Tm^{3+}$@$CaF_2$ core/shell nanoparticles; and (d) UC emission spectra and digital photographs (inset) of the $NaYF_4$:$Yb^{3+}$/$Ho^{3+}$ core and the $NaYF_4$:$Yb^{3+}$/$Ho^{3+}$@$CaF_2$ nanoparticles (ref 187). The excitation wavelength is ~980 nm. The excitation power density for (a) and (b) is around 0.3 W/$cm^2$, while it is about 8 W/$cm^2$ for (c) and (d). Reprinted with permission from refs 38 and 187. Copyright 2012 American Chemical Society and 2012 John Wiley and Sons.

enhance the UC PL by interacting with lanthanide dopants located in the core nanoparticles. Capobianco et al. reported on $NaGdF_4$:$Yb^{3+}$/$Er^{3+}$ active-core@$NaGdF_4$:$Yb^{3+}$ active shell nanoparticles, displaying a significant increase in the intensity of NIR-to-visible upconversion when compared to either the $NaGdF_4$:$Yb^{3+}$/$Er^{3+}$ active-core@$NaGdF_4$ inert shell or the $NaGdF_4$:$Yb^{3+}$/$Er^{3+}$ core-only nanoparticles.[195] In addition to the suppression of surface-related deactivations, the enhancement of upconversion was also believed to be caused by energy transfer of excited $Yb^{3+}$ ions in the active shell to the dopant ions in the active core. The active core/active shell strategy has also been investigated in the $LaPO_4$:$Er^{3+}$@$LaPO_4$:$Yb^{3+}$ nanorods,[196] the $BaGdF_5$:$Yb^{3+}$/$Er^{3+}$@$BaGdF_5$:$Yb^{3+}$ nanoparticles,[120] as well as $BaF_2$:$Ln^{3+}$@$SrF_2$:$Ln^{3+}$ nanoparticles.[120] The concept of incorporating lanthanide dopants into different layers in the active core/active shell structure has important implications for the design of UCNPs. The detrimental effects of cross-relaxation process between different lanthanide dopants can be eliminated now by the spatial confinement of the lanthanide ions into different layers, providing numerous opportunities for the design of UCNPs while maintaining high luminescence efficiency.

### 2.6. Future Directions of Improving Upconversion Efficiency

Despite recent advances in improving the efficiency of UCNPs, the insufficient brightness of UCNPs is still the major reason that limits their popularity in biology. The insufficient brightness is aroused from two parts: (i) The first is the low extinction coefficient of UCNPs, which is an intrinsic feature of 4f–4f optical transitions in lanthanide ions. To alleviate the extinction limit of trivalent lanthanide ions, one important way is to utilize an antenna effect from dyes, plasmons, quantum dots, or other doping elements with a strong absorption to sensitize the UCNPs. Recently, the work on dye-sensitized upconversion is a good example toward this direction, which increases the UC PL by 3000 times due to the orders of magnitude higher extinction coefficient of the dye than that of the lanthanide ion.[197] Moreover, the antenna effect provides opportunities to engineer the excitation wavelength for a given UCNP, eliminating the required matching of the excitation

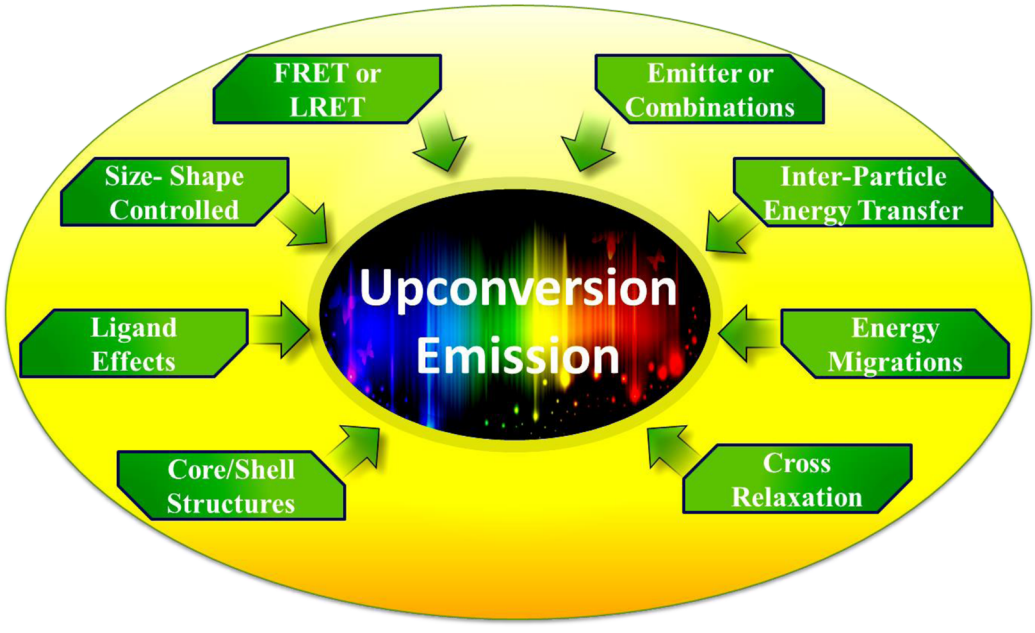


**Figure 7.** Schematic illustration of the various strategies to manipulate the wavelength of emission in lanthanide-doped UCNPs.


dx.doi.org/10.1021/cr400425h | *Chem. Rev.* 2014, 114, 5161–5214

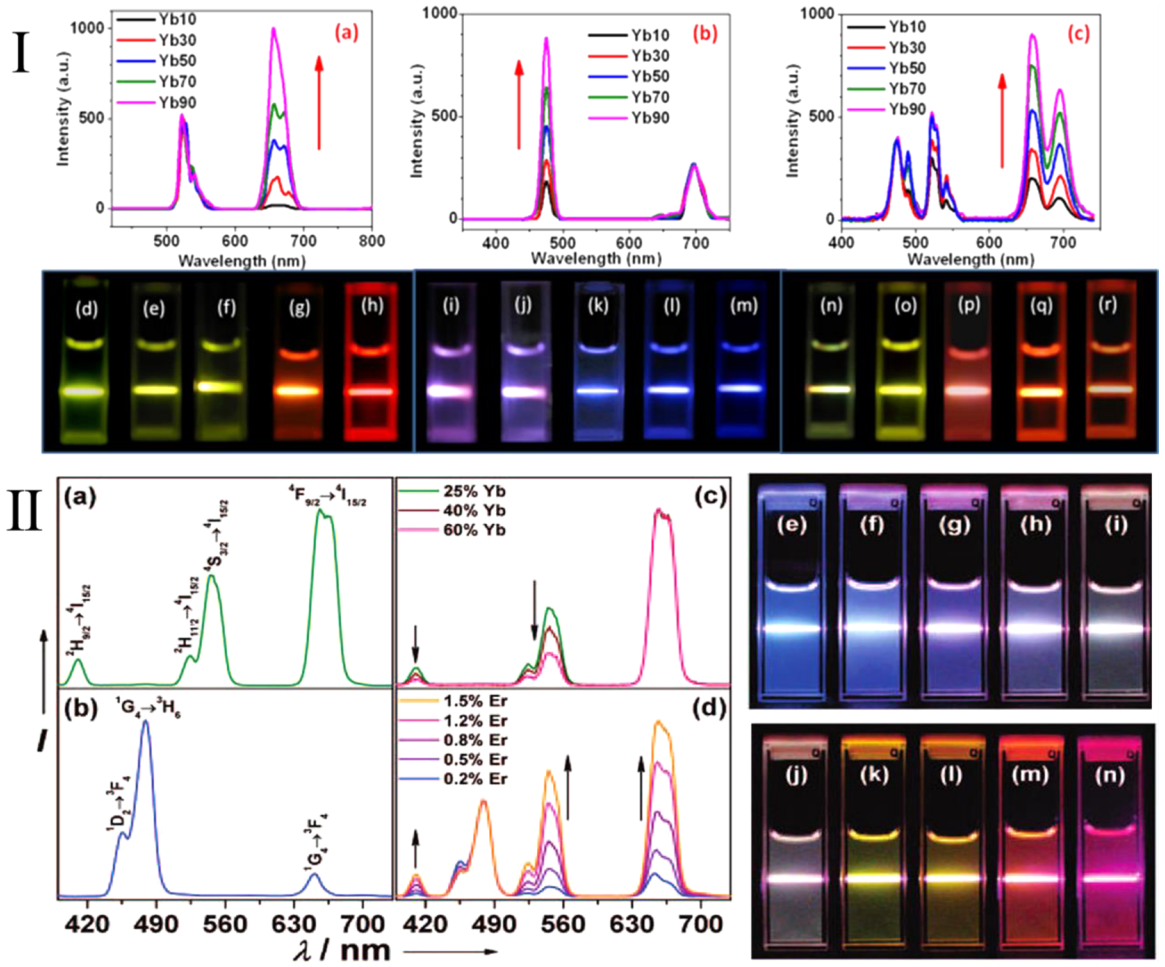


**Figure 8.** Panel (I): UCPL of colloidal $YF_3$ nanoparticles doped with (Ia) $Er^{3+}$ ions of 0.5% and $Yb^{3+}$ ions of 10- 90%; (Ib) $Tm^{3+}$ ions of 2% and $Yb^{3+}$ ions of 10−90%; (Ic) $Er^{3+}$ ions of 0.5%, $Tm^{3+}$ ions of 2%, and $Yb^{3+}$ ions of 10−90%. The spectra in (Ia), (Ib), and (Ic) in order were normalized to the emissions of $Er^{3+}$ ions at 520 nm, $Tm^{3+}$ ions at 475 nm, and $Tm^{3+}$ ions at 475 nm, respectively. Compiled UCPL images of colloidal nanoparticles of $YF_3$ doped with (Id-h) $Er^{3+}$ ions of 0.5% and $Yb^{3+}$ ions of 10- 90%; (Ii-m) $Tm^{3+}$ ions of 2% and $Yb^{3+}$ ions of 10−90%; (In-r) $Er^{3+}$ ions of 0.5%, $Tm^{3+}$ ions of 2%, and $Yb^{3+}$ ions of 10−90% (ref 184). Panel (II): UC PL spectra of (IIa) $NaYF_4$:$Yb^{3+}$/$Er^{3+}$ (18% and 2%), (IIb) $NaYF_4$:$Yb^{3+}$/$Tm^{3+}$ (20% and 0.2%), (IIc) $NaYF_4$:$Yb^{3+}$/$Er^{3+}$ (25−60% and 2%), and (IId) $NaYF_4$: $Yb^{3+}$/$Tm^{3+}$/$Er^{3+}$ (20%, 0.2%, and 0.2−1.5%) particles in ethanol. Compiled luminescent photos showing corresponding colloidal solutions of (IIe) $NaYF_4$:$Yb^{3+}$/$Tm^{3+}$ (20% and 0.2%), (IIf-j) $NaYF_4$: $Yb^{3+}$/$Tm^{3+}$/$Er^{3+}$ (20%, 0.2%, and 0.2−1.5%), and (IIk-n) $NaYF_4$: $Yb^{3+}$/$Er^{3+}$ (18−60% and 2%) (ref 82). Reprinted with permission from refs 82 and 184. Copyright 2008 American Chemical Society and 2012 Royal Society of Chemistry Publishing.

wavelength with the absorption of the lanthanide ion. (ii) The second is the inadequate quantum yield of UCNPs at an excitation density that is safe to human skin. According to *American National Standard Z136.1−2007* (American National Standard for Safe Use of Lasers), the maximum permissible skin exposure for the commonly utilized 980 nm cw laser irradiation is 0.73 W/cm$^2$. Until now, the highest upconversion quantum yield, at cw 980 nm laser irradiation of 0.3 W/cm$^2$, is reported to be 0.6% for ($NaYbF_4$:$Tm^{3+}$ 0.5%)@$CaF_2$ core/shell UCNPs.[38] We found that the enhancement strategies described in sections 2.1−2.5 are compatible with each other but generally are implemented independently. Hence, to accomplish high quantum yield UCNPs, one obvious but promising way is to combine two or more of these strategies together in the design of lanthanide-doped nanoparticles. Moreover, designing UCNPs with saturated PL intensity at low excitation density is also favorable to reach a high quantum yield, as this enables a much higher upconverting rate than the decay rate at the intermediate states of the lanthanide dopants.

## 3. UPCONVERSION EMISSION COLOR TUNABILITY

Manipulation of UC emission color is of particular importance for multiplexed bioimaging and multiplexed assays. Multiplexed imaging enables real-time tracking of multiple targets such as proteins and genes, which are important for bioanalysis, clinical diagnosis, as well as for the therapeutic treatments.[198−200] Multiplexed assays entail parallel detection of multiple analytes, which enables genotyping, DNA sequencing, and high-throughput screening of combinatorial libraries.[201−204] As shown in Figure 7, tuning of the color output of UCNPs has been implemented by using a number of strategies: (i) control of compositions (a combination of different host/activator or controlling dopant concentrations), (ii) utilization of appropriate energy transfer or migration pathways, (iii) manipulation of nanosize- and shape-induced surface effects, (iv) control of relaxation processes induced by phonons of the surrounding ligands, (v) utilization of an appropriate core/shell design, and (vi) the use of Förster resonance energy transfer (FRET) or luminescence resonance energy transfer (LRET) between the UCNPs and the coupled dyes or QDs. Although great efforts


dx.doi.org/10.1021/cr400425h | *Chem. Rev.* 2014, 114, 5161−5214

have been dedicated to achieve tunable color output, it is still a challenge to develop a general protocol to precisely tune the color output of UCNPs over a broad spectral range, while still maintaining high efficiency. Described in the following subsections are these various strategies presented in Figure 7.

### 3.1. Multicolor Emission Using Different Activators or Combinations

Because each lanthanide ion has its own set of energy level structures, different lanthanide ions can produce distinct sharp emission peaks, thus covering collectively a broad spectrum, from NIR to the UV range. In addition, the luminescence from a given lanthanide ion is almost independent of different host materials due to the weak coupling of the f−f transition with the local crystal field provided by the host lattice. Thus, these features enable production of a range of selective color output by selecting different lanthanide dopants or using their combinations. It is worth pointing out that the phonon distribution from the host lattice and the surface ligands can produce a pronounced effect on the color output on the UCNPs, because it can adjust the population between two close energy levels of a given lanthanide ion through multiphonon-assisted nonradiative processes (see sections 3.7 and 3.8). Generally, a fixed lanthanide ion or its combination with others can produce a similar set of emission peaks in a given type of host material, for example, the fluoride host lattice.

The most common activators in UCNPs are generally restricted to $Er^{3+}$, $Tm^{3+}$, and $Ho^{3+}$ ions, characterized by their ladder-like energy levels. Interestingly, all of these lanthanide ions can be efficiently sensitized by the $Yb^{3+}$ ion whose absorption is much stronger and located around 975 nm for the $^2F_{7/2} \rightarrow {}^2F_{5/2}$ transition. The ability of the sensitizer $Yb^{3+}$ ion to efficiently transfer its absorption energy to $Er^{3+}$, $Tm^{3+}$, and $Ho^{3+}$ ions enables a single wavelength excitation (975 nm) of UCNPs doped with these lanthanide ions or their various combinations for multicolor emissions. The $Er^{3+}$ ions have mainly three UC emissions bands, including two green emission bands at around 525/545 nm originated from the transitions $^2H_{11/2}/{}^4S_{3/2} \rightarrow {}^4I_{15/2}$, and a red emission band at around 660 nm originated from the transition $^4F_{9/2} \rightarrow {}^4I_{15/2}$.[79,205] The $Ho^{3+}$ ions have two main UC bands of green and red emission at 541 and 647 nm, corresponding to the transitions $^5S_2/{}^5F_4 \rightarrow {}^5I_8$ and $^5F_5 \rightarrow {}^5I_8$, respectively.[206] The main UC band of the $Tm^{3+}$ ions is in the NIR range at 800 nm originated from the $^3H_4 \rightarrow {}^3H_6$ transition. This NIR UC band is located within the "optical transparency window" for biological tissues, in which both light absorption and scattering are significantly reduced.[17] This feature makes $Tm^{3+}$-doped UCNPs particularly interesting for imaging deep-lying tissue in rodents. The $Tm^{3+}$ ions have another three UC emission bands at around 479, 450, and 350 nm, generated by the transitions of $^1G_4 \rightarrow {}^3H_6$, $^1D_2 \rightarrow {}^3F_4$, and $^1D_2 \rightarrow {}^3H_6$, respectively.[207] The selection of different emitters or combinations of lanthanide dopants is a straightforward approach to tune the upconversion multicolor emission. The first demonstration of efficient multicolor UC emission in colloidal lanthanide-doped nanoparticles was reported by Haase and co-workers. They utilized $Yb^{3+}/Er^{3+}$ and $Yb^{3+}/Tm^{3+}$ codoped $NaYF_4$ nanoparticles to yield strong yellow and blue emissions, respectively.[165] Similar observations have also been reported by Capobianco et al. in $NaYF_4$ nanoparticles.[208] Later, Nann et al. demonstrated four-color emissions from $NaYbF_4$:$Tm^{3+}$ (blue), $NaYbF_4$:$Ho^{3+}$ (green), $NaYbF_4$:$Er^{3+}$ (red), and $NaYF_4$:$Yb^{3+}$ (magenta) nanoparticles, respectively.[209] Liu et al. reported on a general and versatile approach to fine-tune the UC emission in a broad range of color output by a single wavelength excitation at 980 nm.[82] By selecting the $Er^{3+}$ and/or $Tm^{3+}$ as an activator and the $Yb^{3+}$ as the sensitizer, the color output in lanthanide-doped cubic $NaYF_4$ can be finely tuned by variation of the concentration of lanthanide dopants (Figure 8, panel II). Recently, it has been established by Chen et al. that the color output in $YF_3$ nanoparticles doped with different lanthanide dopants and combinations can be manipulated by adjusting the concentration of $Yb^{3+}$.[184] Chan et al. used combinatorial screening of multiply doped $NaYF_4$ nanoparticles to identify a series of doubly and triply doped upconverting nanoparticles that exhibit narrow and spectrally pure emission spectra at various visible wavelengths.[210] It is known that blue, green, and red are three primary colors that can be combined to produce a palette of colors. The simultaneous use of green and red color through $Er^{3+}$ or $Ho^{3+}$ and the blue emission through $Tm^{3+}$ can yield white UC emission in UCNPs.[72] Given the broad range of emission wavelengths from lanthanide dopants, an appropriate selection of different lanthanide dopants or their combinations can generate a large library of emission spectra in the NIR−UV spectral region that are particularly useful for multiplexed labeling and encoding.

### 3.2. Tuning Upconversion Emission by Interparticle Energy Transfer or Antenna Effect

Mahalingam and co-workers have reported the first observation of upconversion via interparticle energy transfer (IPET).[211] A colloidal mixture containing ∼5 nm $BaLuF_5$:$Tm^{3+}$ and $BaLuF_5$:$Yb^{3+}$ nanoparticles showed intense blue UC emission upon excitation at 980 nm. In contrast, a solution containing only $BaLuF_5$:$Tm^{3+}$ or $BaLuF_5$:$Yb^{3+}$ nanoparticles did not emit, clearly displaying the energy transfer from the $Yb^{3+}$-doped nanoparticles to the $Tm^{3+}$-doped nanoparticles. This result has important applications, as a range of color output can be produced using similar mechanisms. Moreover, energy transfer between two nanoparticles is strongly dependent on the distance between them. This feature is quite similar to the FRET process, which can measure distance and detect molecular interactions in an excitation donor/acceptor pair that has found wide applications in biology and chemistry. However, further work in characterizing and understanding the basic energy transfer mechanism is required, particularly on the interactions between two single nanoparticles.

Recently, energy transfers from dye molecules to $NaYF_4$:$Yb^{3+}/Er^{3+}$ UCNPs have been established to significantly improve the intensity of UC green emission.[197] This process utilizes an organic dye as an antenna to sensitize small sized UCNPs due to the fact that the absorption of the dye is orders of magnitude stronger than the absorption by the lanthanide ion, and a large amount of lanthanide ions are located at or around the nanoparticle surface due to its unique high "surface-to-volume" ratio produced by the nanoscale dimension. Despite the achieved high UC PL intensity from dye-sensitized UCNPs, the net UCQYs in this system remained relatively low (∼0.1%). Further work on increasing the UCQYs in dye-sensitized UCNPs will be of value. In addition, although no multicolor UC emissions are reported in this work,[197] the antenna mechanism can be easily extended to other lanthanide ions or combinations to produce efficient multicolor emissions.


dx.doi.org/10.1021/cr400425h | Chem. Rev. 2014, 114, 5161−5214

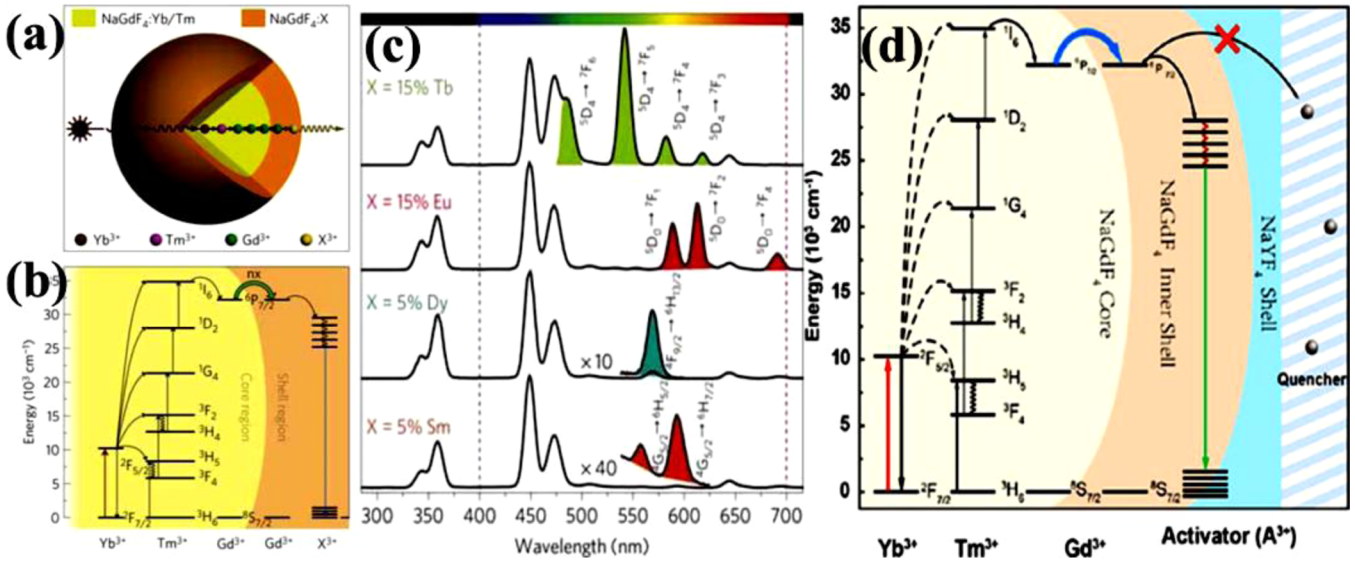


**Figure 9.** Tuning upconversion through energy migration in UCNPs. (a) Schematic illustration of a lanthanide-doped NaGdF4@$NaGdF_4$ core–shell nanoparticle for energy migration-mediated upconversion (X: activator ion); (b) proposed energy transfer mechanisms in the system; (c) upconversion fluorescence spectra of the as-prepared $NaGdF_4$@$NaGdF_4$ core–shell nanoparticles doped with different activators (activator emissions are highlighted with color) (ref 170); and (d) the effective suppression of surface-related quenching mechanism in the $NaGdF_4$@$NaGdF_4$@$NaYF_4$ UCNPs (ref 193). Reproduced with permission from refs 170 and 193. Copyright 2011 Nature Publishing Group and 2012 American Chemical Society.

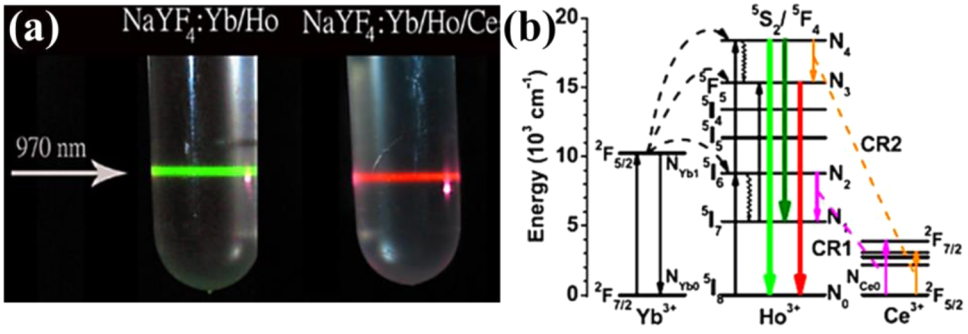


**Figure 10.** (a) Digital images of colloidal $NaYF_4$:20%$Yb^{3+}$,2%$Ho^{3+}$ (green, left) nanoparticles and $NaYF_4$:20%$Yb^{3+}$,2%$Ho^{3+}$,10%$Ce^{3+}$ (red, right) under 970 nm diode laser excitation; and (b) cross-relaxation (CR) energy transfer diagrams of $Ho^{3+}$, $Yb^{3+}$, and $Ce^{3+}$ ions as well as proposed UC mechanisms. Reproduced with permission from ref 86. Copyright 2009 IOP Publishing.

### 3.3. Tuning Upconversion Emission through Energy Migration

As discussed in section 3.1, efficient upconversion emission is generally limited to lanthanide activators of $Er^{3+}$, $Tm^{3+}$, and $Ho^{3+}$ ions when excited at ~980 nm. However, Liu et al. reported that efficient upconversion emission is also possible for lanthanide activators ($Eu^{3+}$, $Tb^{3+}$, $Dy^{3+}$, and $Sm^{3+}$) without long-lived intermediate energy states via energy migration-mediated upconversion processes.[170] The $NaGdF_4$:$Yb^{3+}$,$Tm^{3+}$@$NaGdF_4$: $X^{3+}$ (X = Eu, Tb, Dy, or Sm) core–shell nanoparticle is prepared with lanthanide ions separately incorporated into the core and the shell layer of the nanoparticle, respectively (Figure 9a). In this system, the sensitizer ion ($Yb^{3+}$) first transfers its excitation energy to the accumulator ion ($Tm^{3+}$) and excites it to the high-lying excited state. The energy is then transferred from the high-lying excited state of $Tm^{3+}$ to the migrator ion ($Gd^{3+}$), followed by the migration of excitation energy via $Gd^{3+}$-sub lattice through the core–shell interface. Last, the migrating energy in $Gd^{3+}$-sub lattice is trapped by the activator ion ($X^{3+}$), resulting in upconverting emission (Figure 9b,c). The ability to accomplish UC PL for a rather wide range of activators would expand the applications for lanthanide-doped nanoparticles. Unfortunately, the reported core/shell design suffers from limited conversion of the migrating energy stored in the migrator to activator emission due to surface-related quenching mechanisms (refer to section 2.5). The problem has been addressed by growing an inert shell $NaYF_4$ on the $NaGdF_4$:$Yb^{3+}$, $Tm^{3+}$@$NaGdF_4$:$X^{3+}$ (X = Eu, Tb, Dy, or Sm) core–shell nanoparticle (Figure 9d).[193] However, the drawback of this migration strategy to tune upconversion is that it is strongly dependent on the efficiency of the population of $^1I_6$ state of $Tm^{3+}$ ions, which generally is low due to the involvement of five-photon process. Development of high upconverting efficiency in $Gd^{3+}$-based UCNPs doped with $Yb^{3+}$/$Tm^{3+}$ will be advantageous for this approach.

### 3.4. Tuning Upconversion Emission Using Cross-Relaxation Processes

As described in section 1, the cross-relaxation (CR) process is a typical energy transfer process in which one ion will transfer part of its excited energy to the other ion. The CR process is a fundamental consequence of ion–ion interaction; its efficiency


dx.doi.org/10.1021/cr400425h | Chem. Rev. 2014, 114, 5161–5214

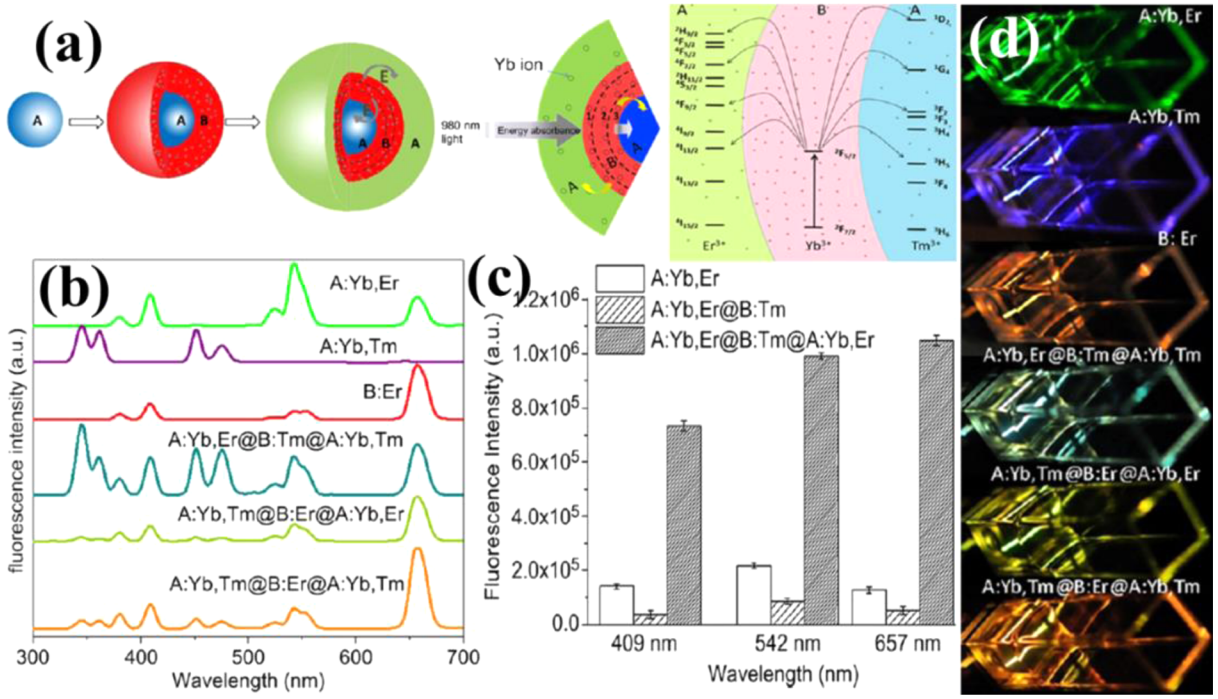


**Figure 11.** (a) Schematic illustration of a sandwich construct to tune the UCNPs' emission color; (b) UC PL spectra of the sandwich-structured nanoparticles; (c) fluorescence intensity comparison of core, core−shell, and sandwich structured UCNPs; and (d) photographic images of multicolor UCNPs. Reproduced with permission from ref 216. Copyright 2013 Elsevier B.V.

is strongly dependent on the dopant concentration. The CR process can be judiciously used to tune the color output in a UCNP by enhancing emission from one excited level, while quenching it from another. Chen et al. demonstrated for the first time that tuning UC PL from green to red (Figure 10a) can be realized in monodispersed cubic $NaYF_4$:$Yb^{3+}$/$Ho^{3+}$ nanoparticles via tridoping with $Ce^{3+}$ ions under 970 nm diode laser excitation.[86] Two CR processes of $^5S_2/^5F_4(Ho) + {}^2F_{5/2}(Ce) \rightarrow {}^5F_5(Ho) + {}^2F_{7/2}(Ce)$ and $^5I_6(Ho) + {}^2F_{5/2}(Ce) \rightarrow {}^5I_7(Ho) + {}^2F_{7/2}(Ce)$ between the $Ho^{3+}$ and $Ce^{3+}$ ions (Figure 10b) were employed to select the dominant UC pathways to tune the radiation from green to red. Capobianco et al. utilized the CR between the two $Er^{3+}$ ions to reduce the green UC emission ($^2H_{11/2}/^4S_{3/2} \rightarrow {}^4I_{15/2}$) while increasing the red UC emission ($^4F_{9/2} \rightarrow {}^4I_{15/2}$).[212] Moreover, they utilized the cross relaxations between $Tm^{3+}$ and $Dy^{3+}$ to preferentially suppress high-energy upconverted emissions of $Tm^{3+}$ in $Yb^{3+}$/$Tm^{3+}$/$Dy^{3+}$ codoped $LiYF_4$ colloidal nanoparticles.[213] As pointed out in section 1, the CR process generally is the main reason for the well-known "concentration quenching mechanism". Caution should be exercised to avoid any decrease of the PL intensity while tuning the color output.

### 3.5. Tuning Upconversion Emission Using Core/Shell Structures

The use of core/shell architecture with two or more lanthanide activators incorporated into the core and different shells is a typical strategy to tune the luminescence of UCNPs, while maintaining high luminescence efficiency.[214] This strategy also explores different combinations of lanthanide activators to produce multicolor emissions, but exercises a spatial isolation of these lanthanide activators using an appropriate core/shell structure. It eliminates deleterious cross relaxations between the lanthanide activators and suppresses surface-related quenching mechanism in the core nanoparticles, thus yielding a range of tunable emission with high efficiency. Zhang et al. reported on hexagonal-phase core-shell-structured $NaYF_4$:$Yb^{3+}$/$Tm^{3+}$@$NaYF_4$:$Yb^{3+}$/$Er^{3+}$ and $NaYF_4$:$Yb^{3+}$/$Tm^{3+}$@$NaYF_4$:$Yb^{3+}$/$Er^{3+}$@$NaYF_4$:$Yb^{3+}$/$Tm^{3+}$ nanoparticles to produce multiple emission peaks.[215] Different from the $Tm^{3+}$/$Er^{3+}$-codoped $NaYF_4$ nanoparticles in which $Tm^{3+}$ emission was quenched, both $Tm^{3+}$ and $Er^{3+}$ emissions were observed from the sandwich-structured nanoparticles. They also reported on sandwich-structured multicolored core/shell/shell nanoparticles of $NaYF_4$:$Yb^{3+}$/$Er^{3+}$@$NaYbF_4$:$Tm^{3+}$@$NaYF_4$:$Yb^{3+}$/$Tm^{3+}$, $NaYF_4$:$Yb^{3+}$/$Tm^{3+}$@$NaYbF_4$:$Er^{3+}$@$NaYF_4$:$Yb^{3+}$/$Er^{3+}$, and $NaYF_4$:$Yb^{3+}$/$Tm^{3+}$@$NaYbF_4$:$Er^{3+}$@$NaYF_4$:$Yb^{3+}$/$Tm^{3+}$, for multicolor cellular imaging (Figure 11).[216] It is intriguing to further explore the possibility of tuning upconversion through the core/shell structure combined with the use of energy migration described in section 3.3.

### 3.6. Tuning Upconversion Emission Using Ligand Effects

The use of the ligand is essential for controlling the size and the shape of resulting UCNPs using chemical reaction in a solution phase. However, it is found by Wu et al. that multicolor emissions from $NaYF_4$:$Yb^{3+}$/$Er^{3+}$ or $NaYF_4$:$Yb^{3+}$/$Tm^{3+}$ nanoparticles could be obtained by changing the ratio of two ligands, octadecylamine and the oleamide, coordinated to the nanoparticle surface.[217] They also found that the multicolor output of *N*-octadecyloleamide coated $NaYF_4$:$Yb^{3+}$/$Er^{3+}$ nanoparticles can be subtly tuned by a "cooperative effect" resulting from the amidation reaction of the carboxylic acid group of oleic acid and the amine group of oleylamine.[218] Tuning the emission color by a "cooperative effect" might arise from two effects: (i) the change of the size and shape of resulting nanoparticles; and (ii) the change of vibrational modes at the interface between the nanoparticle surface and the ligands. A direct measurement of the change of the phonon density distribution of UCNPs can


dx.doi.org/10.1021/cr400425h | *Chem. Rev.* 2014, 114, 5161−5214

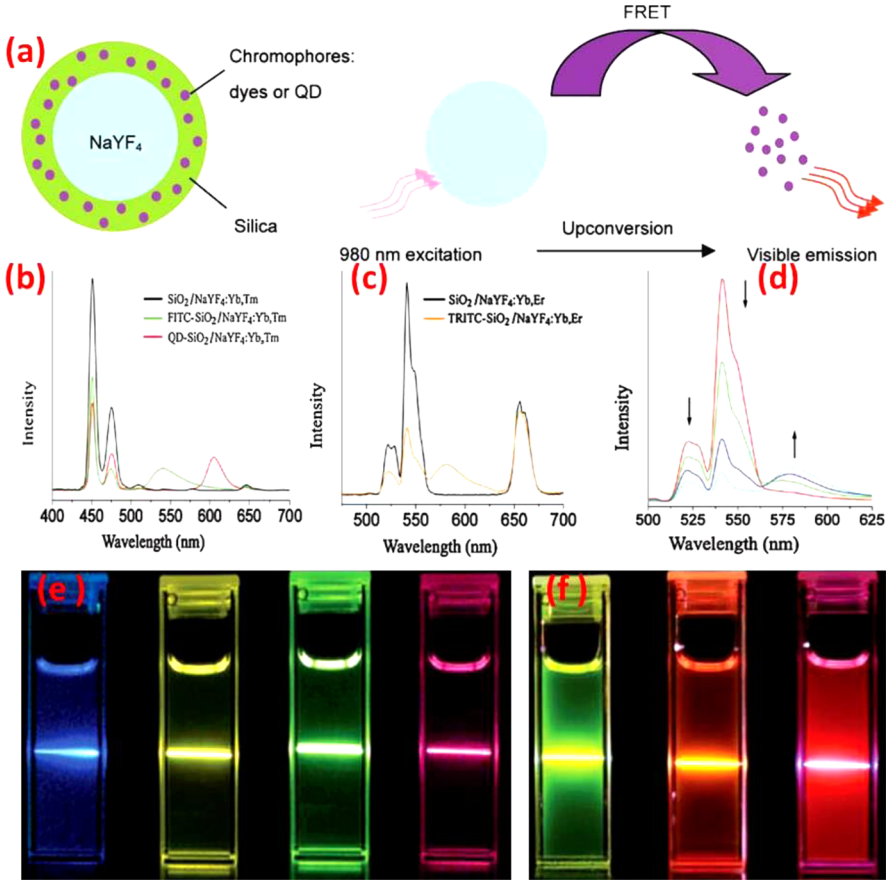


**Figure 12.** (a) Schematic illustration of FRET-based lanthanide-doped core/shell $NaYF_4$@silica UCNPs; (b) PL spectra of pure $NaYF_4$:$Yb^{3+}$/$Tm^{3+}$@silica nanospheres (black line), and of $NaYF_4$:Yb,Tm@silica nanospheres doped with FITC (green line) and QD605 (red line); (c) fluorescence spectra of pure $NaYF_4$:$Yb^{3+}$/$Er^{3+}$@silica nanospheres (black line) and $NaYF_4$:$Yb^{3+}$/$Er^{3+}$@silica nanospheres doped with TRITC (red line); (d) PL spectra of $NaYF_4$:$Yb^{3+}$, $Er^{3+}$@silica nanospheres doped with different amounts of TRITC; (e) photographic images of UCPL of $NaYF_4$:$Yb^{3+}$/$Tm^{3+}$ nanospheres (blue), UCPL of $NaYF_4$:$Yb^{3+}$/$Er^{3+}$ nanospheres (yellow green), UCPL of $NaYF_4$:$Yb^{3+}$/$Er^{3+}$ nanospheres through green and red filters; and (f) photographic images of UC PL of $NaYF_4$:$Yb^{3+}$/$Tm^{3+}$@FITC-doped silica nanospheres (left), $NaYF_4$:$Yb^{3+}$/$Er^{3+}$@TRITC-doped silica nanospheres (middle), and $NaYF_4$:$Yb^{3+}$/$Tm^{3+}$@QD605-doped silica nanospheres (right). Reproduced with permission from ref 224. Copyright 2008 John Wiley and Sons.

be utilized to illustrate the details of the mechanism for the variation of color output.

### 3.7. Tuning Upconversion Emission Using Size- and Shape-Induced Surface Effects

Several groups have examined the size- and shape-dependent optical properties of the $Ln^{3+}$-doped UCNPs. Song and co-workers observed that the relative UC intensity of the red to the green increased gradually with decreasing particle size in the $Y_2O_3$:1%$Er^{3+}$,4%$Yb^{3+}$ nanoparticles.[219] Yan et al. reported the size-dependent UC emission of $NaYF_4$:$Yb^{3+}$/$Er^{3+}$ nanoparticles dispersed in solutions.[173] Multicolor UC emissions (green, yellow, and red) can be observed when decreasing the UCNPs size under excitation with a 980 nm laser. A gradual decrease in the blue PL efficiency in $NaYF_4$:$Yb^{3+}$/$Tm^{3+}$ nanoparticles has been observed by decreasing the nanoparticle size.[168] It is known that the quantum-confinement effect is not available for lanthanide ions that are doped into UCNPs.[92] Thus, unlike QDs, the size-dependent emission cannot be interpreted by quantum mechanics. Alternatively, as the size of the UCNPs decreases, the surface-induced (defects, ligands, solvents) effect becomes more prominent, which can produce more efficient multiphonon-assisted nonradiative relaxations to modify the relative population among close-lying excited states or to deactivate UC PL. Liu et al. have investigated UC PL of $NaGdF_4$:$Yb^{3+}$/$Tm^{3+}$ nanoparticle of varying size (15, 20, and 30 nm). Despite a large disparity in the particle size, the emission spectra are essentially identical when coated with an inert shell of $NaGdF_4$.[181] This result provided for the first time direct evidence to support surface-related effects accounting for the size-dependent behavior of UC PL. In addition, Zhang et al. and Murray et al. reported that $NaYF_4$:$Yb^{3+}$/$Er^{3+}$/$Tm^{3+}$ nanoplates, nanospheres, and nanoellipses or $NaYF_4$:$Yb^{3+}$,$Er^{3+}$/$Ho^{3+}$ nanorods, nanoplates, and nanoprisms emitted varied UC PL fluorescence.[220,221] Although detailed explanations are not provided in both works, we believe that the varied color might arise from shape-related surface mechanisms that produce varied phonon influence on the lanthanide ions in UCNPs.

### 3.8. Tuning Upconversion Emission Using FRET or LRET

Fluorescence resonance energy transfer (FRET) is a mechanism describing energy transfer from a donor fluorophore to an acceptor fluorophore through nonradiative dipole−dipole coupling.[15,26,27,129,222,223] When utilizing the UCNP as an energy donor and the dye or QDs as an energy acceptor, it offers a larger freedom for upconverted emission wavelengths than the one produced merely by the lanthanide ions. Indeed,


dx.doi.org/10.1021/cr400425h | Chem. Rev. 2014, 114, 5161−5214

**Table 1. Typical UC Host Materials and Their Synthetic Strategies**

| synthetic method | solvent | hosts | shape control | size distribution (nm) | ref |
|---|---|---|---|---|---|
| thermolysis | OA, ODE | $NaYbF_4$ | sphere, polyhedron, sphere, polyhedron | 15−30 very narrow | 38,237,238 |
| | | $NaGdF_4$ | | 6−15 very narrow | 85,195,237,239 |
| | | $NaYF_4$ | hexahedron, sphere, nanorod, nanocubic, nanoplate, nanoprism | 10−100 very narrow | 192,221,237,240,241 |
| | | $LiYF_4$ | nanospindle, hexahedron, sphere, nanorod, nanocubic, sphere, nanocubic | 20−100 very narrow | 83,166,242 |
| | | $NaLnF_4$ (Ln = Nd, Sm, Eu, Tb, Dy, Ho, Er, Tm, Lu) | | 10−150 very narrow | 237 |
| | | $CeO_2$ | | 5−80 very narrow | 243,244 |
| | | $LaF_3$ | nanozigzag, nanoplate | 10−50 very narrow | 245,246 |
| | | $YF_3$ | sphere, parallelogram | 3−10 very narrow | 184,246 |
| | | $MF_2$ (M = Mg, Ca, Sr) | nanoneedle, nanocubic | 30−100 narrow | 179 |
| | | $LnF_3$ (Ln = Ce, Pr, Nd, Sm, Eu, Gd, Tb, Dy, Ho, Tm, Yb, Lu) | nanoplate, sphere, nanozigzag, truncated-octahedron, nanorods, nanopolyhedra | 5−20 nm very narrow | 246 |
| | | LnOF (Ln = Er, Tm, Yb, Lu, Tb, Dy, Ho, Y) | | | |
| | | $NaScF_4$ | nanocubic, nanohexahedron | 20−30 narrow | 247 |
| | OM | $NaYF_4$ | sphere | 10−50 narrow | 248 |
| | | LaOF | sphere | 3−10 very narrow | 246,249 |
| | | GdOF | sphere, nanorods | 2−10 very narrow | 249 |
| | OM, ODE | LnOCl | nanorod, nanoplate | 3−200 very narrow | 250 |
| | OA, OM | $NaYF_4$ | sphere | 5−20 narrow | 36,218 |
| | | EuOF | nanowire, polyhedron | 3−5 very narrow | 246 |
| | | GdOF | nanorod, polyhedron | 3−5 very narrow | 246,249 |
| | | $LnF_3$ (Ln = Dy, Ho, Er) | triangular, nanoplate, nanozigzag, nanoquadrilateral, nanopolygonal, nanorod | 2−20 very narrow | 246 |
| | | LnOF (Ln = Ce, Pr, Nd, Sm, Tb, Dy, Ho, Y) | | | |
| | | $Ln_2O_3$ (Ln = La, Pr, Nd, Sm, Eu, Y) | nanodisk, nanoplate, nanocubic | 5−20 very narrow | 251 |
| | | $LnPO_4$ (Ln = Ln, Eu, Tb, Y, Ho) | nanopolyhedron, nanowire, nanoplate, nanorod, nanowormlike wire, nanoquasirod | 3−200 very narrow | 252 |
| | OA, OM, ODE | $Eu_2O_2S$ | nanoplate, nanorod | 10−15 very narrow | 253 |
| | | $La_2O_2S$ | nanoplate | 25−30 very narrow | 254 |
| | | $Gd_2O_3$ | nanoplate, nanodisk | 8−10 very narrow | 251,252 |
| | | $Ln_2O_3$ (Ln = Tb, Dy, Ho, Er, Tm, Yb, Lu, Y) | nanoplate, nanodisk | 5−20 very narrow | 251 |
| | | $NaLnS_2$ (Ln = La, Sm, Tb, Ce) | nanoplate, nanocubic | 10−200 very narrow | 255 |
| | | $NaLnF_4$ (Ln = Pr, Nd, Sm, Eu, Tb, Dy, Ho, Er, Tm, Yb, Lu, Gd) | nanopolyhedron, nanorod, hexahedron | 5−500 very narrow | 237 |
| | | $NaYF_4$ | nanopolyhedron, nanorod, hexahedron, nanocage | 10−200 very narrow | 237,256 |
| | | $LiYF_4$ | sphere | 10−12 very narrow | 257 |
| | OA, TOPO | $Y_2O_3$ | nanodisk | 4−6 very narrow | 258 |
| | | $NaYF_4$ | nanorod, sphere, nanoplate, nanocubic | 9−150 narrow | 259−261 |
| Ostwald-ripening | | $NaYF_4$ | nanoplate, sphere, nanorod | 10−300 very narrow | 82,176,224,262,263 |
| | | $NaGdF_4$ | sphere, nanoplate | 10−20 very narrow | 180,181 |


dx.doi.org/10.1021/cr400425h | Chem. Rev. 2014, 114, 5161−5214

Table 1. continued

| synthetic method | solvent | hosts | shape control | size distribution (nm) | ref |
|---|---|---|---|---|---|
| | | $KMnF_3$ | nanocubic | 10−40 narrow | 264 |
| | | $NaMnF_3$ | sphere | 8−10 very narrow | 265 |
| | | YOF | sphere | 15−18 very narrow | 183 |
| hydrothermal | | $NaYF_4$ | sphere, nanoplate nanocubic | 5−500 narrow | 66,78,215,266−270 |
| | | $Er_2O_3$ | sphere, nanorod | 3−3000 narrow | 271 |
| | | $BaYF_5$ | sphere, microcubic | 10−1000 narrow | 272 |
| | | $CeO_2$ | sphere, microcubic | 5−15 narrow | 273 |
| | | $SrF_2$ | sphere | 5−6 very narrow | 274 |
| | | $CaF_2$ | nanocubic | 5−8 very narrow | 81 |
| | | $LaF_3$ | sphere, nanoplate | 5−65 narrow | 267,268,275 |
| | | $GdF_3$ | sphere | 10−20 narrow | 267 |
| | | $NaYbF_4$ | sphere, polyhedron | 5−25 narrow | 267,269 |
| | | $CeF_3$ | sphere, nanocubic | 5−8 very narrow | 276,277 |
| | | $NaCeF_4$ | nanowire, nanorod | 100−1000 narrow | 276 |
| | | $Na_3MF_7$ (M = Zr, Hf) | nanocubic | 6−8 very narrow | 278 |
| | | $BaY_2F_8$ | nanobelt | 75 × 1000 narrow | 279 |
| | | $YbPO_4$, $LuPO_4$ | sphere | 5−10 narrow | 280 |
| | | $NaLnF_4$ (Ln = Pr, Nd, Sm, Eu, Gd, Dy, Ho, Er, Tm, Tb) | polyhedron, nanotube, nanodisk, nanorod | 3−800 narrow | 269 |
| | | $KYF_4$ | sphere | 20−50 not narrow | 178 |
| | | $NaLuF_4$ | nanoplate | 15−150 very narrow | 269,281 |

Zhang et al. reported that an expanded range of multicolor emission can be obtained from the core/shell $NaYF_4$:$Yb^{3+}$/$Er^{3+}$($Tm^{3+}$)@silica nanostructures whereby organic dyes or QDs are encapsulated into the silica shell (Figure 12).[224] For each type of lanthanide-doped UCNPs, a wide range of multiple colors can be produced through the FRET from the UCNPs to the organic dyes or QDs that produce new emission colors (Figure 12). A new multiplexed NIR in vivo imaging has also recently been shown by using NIR QDs and $NaYF_4$:$Yb^{3+}$/$Tm^{3+}$ nanoparticles.[225] Instead of utilizing the emitting dye to produce additional UC color, the emission bands of UC can also be selectively quenched to produce varied color outputs via utilizing the strong absorption of unremitting dye or nanoparticles. For example, Wolfbeis et al. reported tuning of dual UC emission from either the $NaYF_4$:$Yb^{3+}$/$Er^{3+}$ or the $NaYF_4$:$Yb^{3+}$/$Tm^{3+}$ nanoparticles for ratiometric optical encoding by introducing various amounts of amino-reactive organic dye on the UCNP surface to selectively quench an intended UC band.[226] Alternatively, gold nanoparticles can also be utilized as a FRET quencher to quench the green UC peak in $NaYF_4$:$Yb^{3+}$/$Er^{3+}$.[76,227] It is worth noting that the time-resolved downconversion FRET process has been established to detect trace amounts of interested analytes using lanthanide-doped nanoparticle that exhibit long-time PL as an energy donor.[228−231] This suggests that the FRET upconversion mechanism can have important implications for sensing applications.

Luminescence resonance energy transfer (LRET) is a radiative process where light emitted by the donor is absorbed by acceptor molecules. The difference between LRET and FRET resides in that the energy transfer process in LRET is radiative, whereas it is nonradiative for FRET. Liu et al. reported on multicolor in vivo imaging of UCNPs with their emission tuned by LRET to dyes, indicating the effectiveness of LRET for expanding UC PL emissions.[232] In addition, UC LRET has been used for sensitive detection of $CN^-$ in water and for lection recognition.[233,234] However, until now, both FRET and LRET mechanisms are utilized without clarification. Discerning these two mechanisms is essential for selecting the type of energy acceptor molecules, which can be accomplished by measuring the time-resolved spectroscopy of the donor emission.

### 3.9. Future Opportunities for Tuning Upconversion Emission

The reported strategies to tune upconversion often result in reduction of the luminescence efficiency, as they cannot avoid the deleterious cross relaxations between different lanthanide ions. Also, unwanted increased nonradiative relaxations induced by the size, shape, and ligand effects, and coupling losses between the UCNPs and the energy receptors of dyes or QDs


dx.doi.org/10.1021/cr400425h | Chem. Rev. 2014, 114, 5161−5214

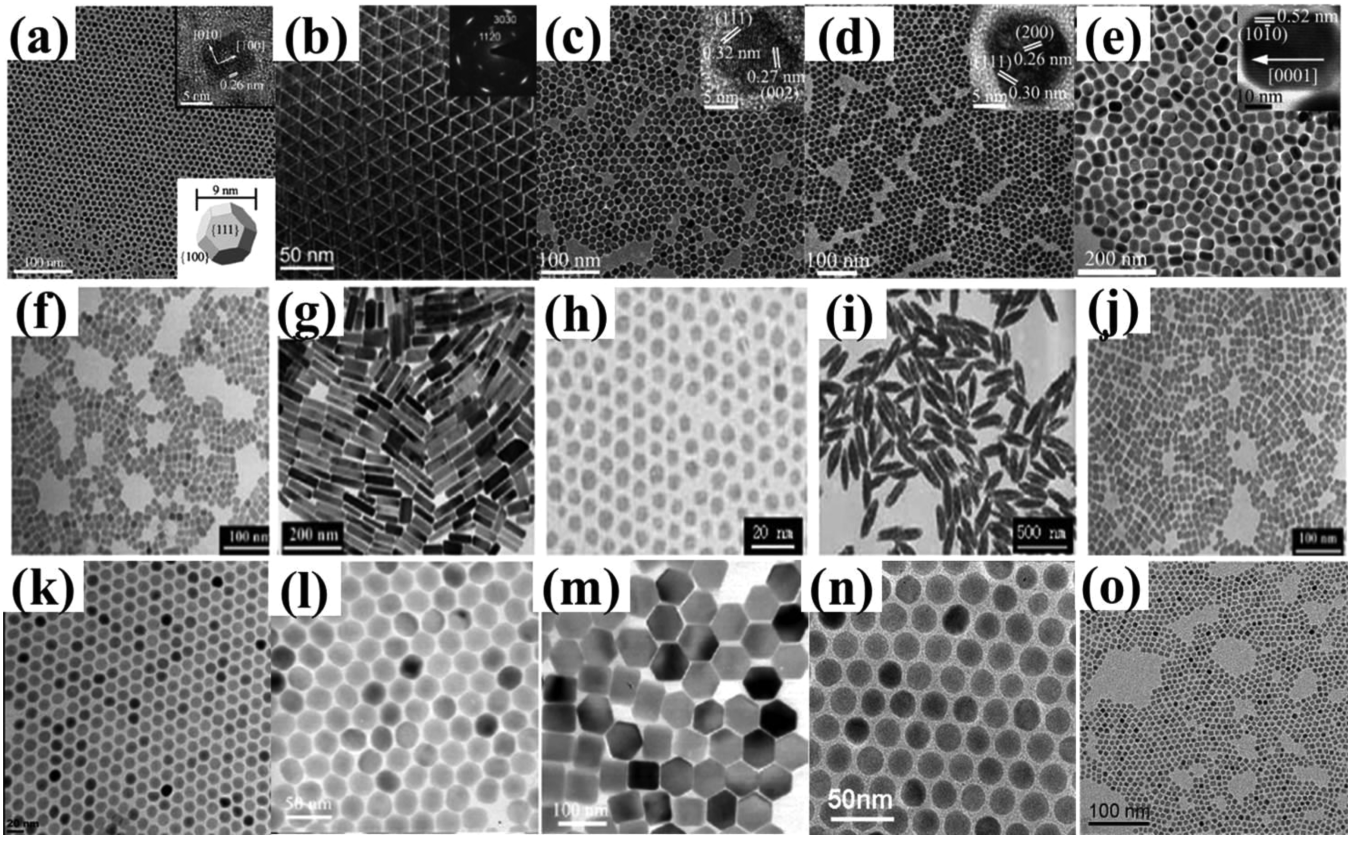


**Figure 13.** Typical TEM images of lanthanide-doped (a) LuOF, (b) $LaF_3$, (c) $\alpha$-$NaYF_4$, (d) $NaYbF_4$, (e) $\beta$-$NaEuF_4$ (refs 237, 245, and 246) synthesized by the thermolysis method; (f) $\alpha$-$NaYF_4$:$Yb^{3+}$, $Er^{3+}$, (g) $\beta$-$NaYF_4$:$Yb^{3+}$, $Er^{3+}$, (h) $LaF_3$, (i) $YF_3$, (j) $\alpha$-$NaYF_4$, synthesized by the hydro(solvo)-thermal method (refs 100 and 266); (k–o) $\beta$-$NaYF_4$ or $CaF_2$ nanoparticles synthesized by the Ostwald-ripening method (refs 175, 224, 220, 215, and 231). Reprinted with permission from refs 237, 245, 246, 100, 266, 175, 224, 220, 215, and 231. Copyright 2006 American Chemical Society, 2005 American Chemical Society, 2007 John Wiley and Sons, 2011 American Chemical Society, 2005 Nature Publishing Group, 2012 American Chemical Society, 2008 John Wiley and Sons, 2008 IOP Publishing, 2008 American Chemical Society, and 2013 John Wiley and Sons.

can lead to energy loss. The core/shell structure to tune upconversion seems promising, but surface-related deactivations have to be addressed. In addition, the range of upconverted emission is still limited, unable to cover all of the panchromatic range. In our opinion, there exist a great deal of future opportunities for tuning upconversion emission in two directions: (i) Tuning upconversion using core/shell structures with minimized surface-related deactivations. Spatial isolation of lanthanide emitters is necessary to avoid cross relaxations to maintain high dopant concentration and high luminescence efficiency. Meanwhile, the shell is able to effectively suppress surface-related deactivations. Variation of different shell host lattice to tune upconversion emission in the core nanparticle can also be promising. (ii) Finally, combining two or more existing color-tuning approaches (for example, the energy migration in section 3.3 and the color/shell structure in section 3.5), as well as coupling upconversion mechanisms to other types of emitters through FRET or LRET, may open totally new design criteria for achieving wide tunability at higher efficiency. Last, a new dimension to tune upconversion for multiplexing is to produce a tunable lifetime for a specific UC color, which can then be exploited to encode biochemical process in the time domain, extending the freedom of existing wavelength-encoded upconversion multiplexing.[235] Tunable lifetime for UCNPs can be produced by size-induced surface effect as well as dopant-concentration-induced cross-relaxation effect.[235,236] However, the caveat here is that the produced tunable lifetime is generally accompanied by a decrease of the upconversion efficiency.

## 4. NANOCHEMISTRY FOR CONTROLLED SYNTHESIS

Development of facile synthesis strategies for high-quality lanthanide-doped luminescent nanoparticles with controlled composition, crystalline phase, shape, and size is crucial to tune their chemical and optical properties and explore their potential applications in diverse fields. This section describes the various nanochemistry approaches utilized to produce upconversion nanoparticles in a highly controlled manner. A range of synthetic approaches such as thermal decomposition, hydro-(solvo)thermal synthesis, Ostwald-ripening method, sol–gel processing, coprecipitation method, as well as ionic liquid-based synthesis have been investigated to synthesize high-quality lanthanide-doped UCNPs. This Review mainly focuses on thermolysis, hydro(solvo)thermal, and Ostwald-ripening, which are the most widely used methods, as they can offer precise control over the phase, shape, size, and stoichiometric composition of the core only and/or the core/shell UCNPs. Table 1 is a summary of UCNPs of varied host materials prepared by these three methods, while Figure 13 illustrates some examples of TEM images of UCNPs prepared by these methods.


dx.doi.org/10.1021/cr400425h | *Chem. Rev.* 2014, 114, 5161–5214

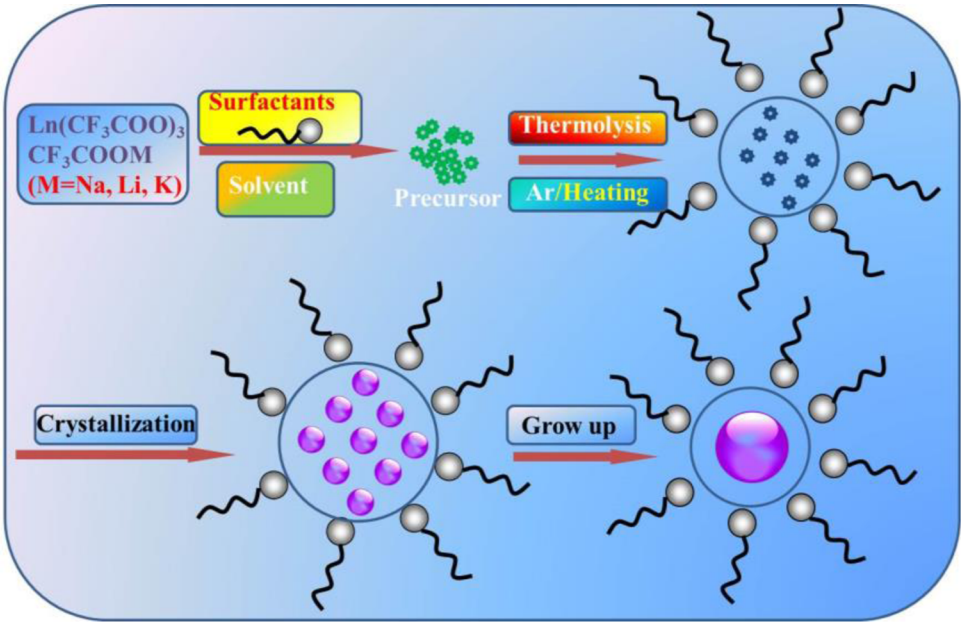


**Figure 14.** Schematic illustration of the growth of UCNPs using the thermolysis strategy. The metallic precursors decompose at high temperature to yield monomers, which are then crystallized and grow into monodispersed UCNPs.

### 4.1. Thermolysis Strategy

The thermolysis strategy generally employs organometallic compounds as precursors, which decompose in a high boiling point organic solvent with the assistance of surfactants at an elevated temperature. The various steps of the involved nanochemistry are represented in Figure 14. The commonly used precursors are metallic trifluoacetate salts; the solvent can be 1-octadecene (ODE); the surfactants can be oleic acid (OA), oleylamine (OM) or trioctylphosphine oxide (TOPO), which typically contain a functional capping group to coordinate the metallic elements and the long hydrocarbon chain to prevent nanoparticle aggregation. It is important to note that the rapid decomposition of metallic trifluoroacetate creates a burst of nucleation, which is essential for producing monodispersed nanophosphors. By carefully tailoring the experimental variables, such as the nature of the solvents, concentration of metal precursors, reaction temperature, and time, high-quality UCNPs with a narrow size distribution, good crystallinity, and exceptional optical properties can be readily obtained from the thermolysis process. The drawback of the thermolysis strategy is that it involves a fast nucleation or growth process, which naturally can have a higher possibility to produce more defects in the synthesized UCNPs, thus leading to a relatively lower upconversion quantum yield. In addition, the toxic byproducts of fluorinated and oxyfluorinated carbon species mandate a carefully exercised synthetic procedure.

**4.1.1. Thermolysis in Oleic Acid and Octadecene.** The thermolysis method was first developed by the Yan group to synthesize highly monodispersed $LaF_3$ nanoparticles.[245] The approach was later extended as a common route to synthesize high-quality cubic lanthanide-doped $NaYF_4$ UC nanoparticles.[208,237,240] For example, Capobianco and co-workers have reported the synthesis of cubic $NaYF_4$ nanoparticles codoped with $Yb^{3+}/Er^{3+}$ or $Yb^{3+}/Tm^{3+}$ via thermal decomposition of metal trifluoroacetate precursors in the presence of OA and ODE.[208] In their studies, the noncoordinating ODE was used as the primary solvent due to its high boiling point. OA was chosen not only as a solvent but also as a passivating ligand that prevents the nanoparticles from agglomeration. The same approach was further refined by Capobianco et al. to synthesize cubic UC $NaYF_4$ nanoparticles with a remarkably narrow size distribution without the need for size-selective fractionation.[240] The approach was based on temporal separation of nucleation and crystal growth by slow addition of the precursors to the solution and subsequent manipulation of the temperature. Another outstanding demonstration was reported by Murray and co-workers who prepared highly uniform hexagonal $NaYF_4:Yb^{3+}/Er^{3+}$ nanoparticles with controlled sizes and morphologies (spheres, nanorods, and hexagonal prisms) by using the same synthetic strategy.[221] These as-prepared nanoparticles can be easily assembled into large-area superlattices under appropriate conditions. The decomposition method has also been extended to synthesize other RE fluorides, oxides, and oxyfluorides such as $LiREF_4$,[83,166,242] $KRE_3F_{10}$,[282] $NaScF_4$,[247] $YF_3$,[184,246] $MF_2$ (M = Mg, Ca, and Sr),[179] $BaREF_5$,[283] $CeO_2$,[243,244] and LnOF (Ln = Er, Tm, Yb, Lu, Tb, Dy, Ho, Y).[246]

**4.1.2. Thermolysis in Oleic Acid/Oleylamine, Oleic Acid/Oleylamine/Octadecene, and Oleylamine Solvents.** Yan and co-worker also presented systematic and general synthesis of high-quality $Ln_2O_3$ (Ln = Tb, Dy, Ho, Er, Tm, Yb, Lu, Y)[251] and LnOF (Ln = Ce, Pr, Nd, Sm, Tb, Dy, Ho, Y) nanoparticles with diverse shapes in OA/OM, as well as $NaYF_4$ and $NaLnF_4$ (Ln = Pr, Nd, Sm, Eu, Tb, Dy, Ho, Er, Tm, Yb, Lu, Gd) nanoparticles in OA/OM/ODE solvents.[173,179,187,237,246,249,251] They refined this technique to the general synthesis of a whole range of rare earth fluorides, rare earth oxide, and rare earth oxyfluoride nanoparticles with multiform crystal phases and morphologies by manipulating the ratio of precursors, solvent composition, reaction temperature, and time. For the synthesis of fluoride nanoparticles, it is found that the combined use of coordinating ligands of the OA and the OM can produce sub-10 nm cubic lanthanide-doped $NaYF_4$ nanoparticles, which is generally much smaller than the ones produced using OA as the ligand and the ODE as a high-boiling solvent.[36] It is interesting to note that ~10 nm monodisperse


dx.doi.org/10.1021/cr400425h | Chem. Rev. 2014, 114, 5161−5214

hexagonal phase $NaYF_4$:$Yb^{3+}$/$Er^{3+}$ (or $Tm^{3+}$) nanoparticles can be synthesized through thermal decomposition of sodium and lanthanide trifluoroacetates by using the single solvent of OM, which served both as a reaction medium and as a capping ligand.[248] However, the resulting hexagonal-phase $NaYF_4$:$Yb^{3+}$/$Er^{3+}$ (or $Tm^{3+}$) UCNPs have relatively poor shape. Subsequently, there has been a series of excellent reports on the thermolysis approach in using OA/OM, OA/OM/ODE, or OM solvents to prepare monodispersed lanthanide-doped $Eu_2O_2S$,[253] $La_2O_2S$,[254] $Gd_2O_3$,[251,252] LnOCl,[250] $LiYF_4$,[257] and $NaLnS_2$ (Ln = La, Sm, Tb, Ce) nanoparticles.[255] The advantage of utilizing OM for the preparation of UCNPs lies in its ability to produce ultrasmall UCNPs that are attractive for bioimaging due to their more efficient clearance from the body. In addition, the weak coordination bond between the amine group and the lanthanide ions on the surface of UCNPs facilitates the utilization of a popular ligand exchange procedure for phase transfer (consult section 5.1).

**4.1.3. Thermolysis in Oleic Acid/Trioctylphosphine Oxide/Octadecene.** Besides the most frequently used organic capping agents OA, OM, and ODE, Shan et al. first reported the use of TOPO as a coordinating ligand for the synthesis of ultrasmall, monodispersed, and pure hexagonal phase $NaYF_4$ UCNPs.[259−261] As compared to other available coordination solvents such as OA and OM, the free-energy barrier for the cubic → hexagonal phase transition was significantly reduced in TOPO. Unfortunately, the solubility of the as-obtained TOPO-capped nanoparticles was low in common organic solvents like cyclohexane or chloroform. This problem was solved by combined use of trioctylphosphine (TOP)/OA to replace TOPO to synthesize $NaYF_4$ nanoparticles. It was found that the cooperative actions of OA and TOP also can decrease the energy barrier of $\alpha/\beta$ phase transition, allowing the preparation of hexagonal $NaYF_4$ at lowered temperatures.[259−261]

### 4.2. Ostwald-Ripening Strategy

Ostwald ripening refers to the process that larger particles with smaller surface-to-volume ratios are favored over energetically less stable smaller particles, resulting in the growth of larger particles at the expense of smaller ones.[284] In one pioneering work, Zhang and co-workers synthesized highly uniform hexagonal phase $NaYF_4$:$Yb^{3+}$/$Er^{3+}$ (or $Tm^{3+}$) UCNPs with controllable shapes and sizes by using OA as the capping ligand and ODE as the high-boiling solvent.[215,220,224] This synthetic strategy was based on the formation of small amorphous sacrificial $NaYF_4$ coprecipitates at room temperature (RT) followed by the growth of nanoparticles using the Ostwald-ripening process at elevated temperatures (300 °C). As compared to the thermal decomposition method, this approach offers relatively mild reaction conditions, nontoxic byproducts, simple protocols, and short reaction time. A control of the ripening process through control of temperature and reaction time allows one to produce monodispersed nanoparticles, often hexagonal phase, with narrow size distribution. This method has been extensively adapted to prepare monodispersed $Ln^{3+}$-doped $LiYF_4$,[242] $NaYF_4$,[82,176,224] $NaGdF_4$,[180,181] $NaTbF_4$, $NaLuF_4$,[285] $NaScF_4$,[247] and $CaF_2$ UCNPs.[231] Ostwald-ripening strategy has also been used to produce hierarchical core/shell nanoparticles due to the ability to precisely control the shell thickness by stoichiometric regulation of the number of sacrificial nanoparticles or monomers involved in the Ostwald-ripening process. As the Ostwald-ripening approach involves a relatively long time to nucleate and grow, it generally can produce well-crystallized hexagonal UCNPs with decreased defects, and thus might have a relatively higher UC efficiency. Comparison of the absolute quantum yields of the same type of UCNPs that are produced with thermolysis, Ostwald-ripening, or hydrothermal strategy will be a straightforward method to evaluate the production embodiment of these synthetic approaches.

### 4.3. Hydro(solvo)thermal Strategy

The hydro(solvo)thermal method is a typical solution-based chemical synthesis approach in which reactions occur in a sealed environment under high pressure and temperature, usually above the critical point of the solvent to increase the solubility and reactivity of the inorganic substances. Possible advantages of this method over other types of synthetic methods include the ability to create highly crystalline phases at much lower temperatures and to implement a set of reactions at the same time. Disadvantages of the method include the need for specialized reaction vessels known as autoclaves and the inability to observe nanoparticles as they grow. In a typical procedure of hydro(solvo)thermal synthesis, appropriate reaction precursors, solvents, and surfactants with functional groups are mixed and then heated in a specialized reaction vessel. Surfactants like polyethylenimine (PEI),[82] ethylenediaminetetraacetic acid (EDTA),[272] cetyltrimethylammonium bromide (CTAB),[286] and OA provide chelating ability with cationic ions to regulate their reacting concentration,[287] which are essential for the control of the crystalline phase, size, and morphology as well as the surface functional groups of resulting UCNPs. The most representative example of hydro(solvo)-thermal synthesis is provided by the work of Li and co-workers who reported on a general "liquid−solid−solution (LSS)" strategy for the synthesis of monodisperse (semiconductor, metallic, and dielectric) nanoparticles,[266] whereby the reaction, phase transfer, and separation take place at the interfaces. Adapted from the LSS method, a variety of lanthanide-doped UCNPs with well-controlled crystal phase, size, and shape have been synthesized, such as $NaYF_4$,[28,31,88,126] $NaLaF_4$,[287] $NaLuF_4$,[269,281] $BaGdF_5$,[288] $KMnF_4$,[289] $YF_3$,[290−292] $LaF_3$,[267,268,287] LaOF,[293] $GdF_3$,[267] $CaF_2$,[81] and $SrF_2$.[274] Another interesting development was reported by Zhao and co-workers, who utilized an oleic acid-mediated hydrothermal method for the synthesis of uniform UC $NaYF_4$ nanorods, nanotubes, and flower-patterned nanodisks.[294] Very recently, Liu et al. developed a novel $Gd^{3+}$-doping approach to give simultaneous control over the crystal phase, size, and optical properties of the resulting $NaYF_4$ UCNPs during the hydro(solvo)thermal synthesis.[262] It was discovered that $Gd^{3+}$ doping not only can result in a rapid cubic-to-hexagonal phase transformation within 2 h, but also lead to the reduction of size, producing ultrasmall hexagonal $NaYF_4$ UCNPs at a substantially decreased reaction temperature. The phase transformation and size and morphology optimization induced by impurity doping were further verified by some other groups. Li and co-workers reported the synthesis of $NaLuF_4$:$Gd^{3+}$/$Yb^{3+}$/$Tm^{3+}$ nanoparticles with controllable size and phase by doping different amounts of $Gd^{3+}$ ions.[295] The addition of $Gd^{3+}$ ions promoted the phase transformation from cubic to hexagonal and reduced the particle size from large microtubes to small cubes. Wang and co-workers extended this impurity doping strategy for the controlled synthesis of $MF_2$ (M = Ca, Sr, and Ba) and $LnF_3$ (Ln = La, Ce, and Pr) nanoparticles.[274] In addition to the aforementioned fluoride nanoparticles, monodispersed $Ln^{3+}$-


dx.doi.org/10.1021/cr400425h | Chem. Rev. 2014, 114, 5161−5214

doped inorganic oxide nanoparticles can also be readily obtained by using the hydro(solvo)thermal synthesis, as exemplified by the synthesis of $Er_2O_3$,[271] $BaYF_5$,[272] $CeO_2$,[273] $NaYbF_4$,[267,269,296] $NaCeF_4$,[276] $Na_3MF_7$ (M = Zr or Hf),[278] $YbPO_4$,[280] $LuPO_4$,[280] $KYF_4$,[178] and $NaLnF_4$ (Ln = Pr, Nd, Sm, Eu, Gd, Dy, Ho, Er, Tm, Tb).[269]

### 4.4. Hierarchical Core/Shell Upconversion Nanoparticles

As described in sections 2.5, 3.3, and 3.5, core/shell UCNPs play important roles there. Moreover, core/shell structures provide opportunities to incorporate a functional shell at nanoscale for bioimaging applications (e.g., combined UC PL and MRI). Two techniques have been generally used to grow a shell layer on the core nanoparticle surface, as illustrated in Figure 15. Both approaches take two steps. The first step is to synthesize the core nanophosphors utilizing the nanochemistry described in sections 4.1−4.3, which are then used as seeds in the second step to induce further epitaxial growth. To ensure an epitaxial growth and to create a homogeneous interface between the core and the outer shell, the host material of the shell should exhibit a low lattice mismatch with the core material. The epitaxial growth can be implemented using two strategies: (i) The first is the use of precursors of the shell material in the second growth solution. The monomer of shell material, produced by either mixing or thermal decomposition of corresponding chemical precursors in the solvents of OA and ODE, is able to gradually and stably deposit on the seeding core nanoparticles and finally form the shell layer. (ii) The second is the use of small sacrificial nanoparticles of shell composition. The Ostwald ripening process is able to dissolve energetically less stable small sacrificial nanoparticles into shell monomers, which can then deposit on the larger stable core nanoparticles. Utilizing these two strategies, a large variety of homogeneous or heterogenerous core/shell nanoparticles have been prepared such as $NaYF_4$@$NaYF_4$,[172] $NaYF_4$@$NaGdF_4$,[192] $NaYF_4$@$CaF_2$,[187] $\alpha$-($NaYbF_4$:$Tm^{3+}$)@$CaF_2$,[38] $NaGdF_4$:$Yb^{3+}$/$Er^{3+}$@$NaGdF_4$:$Yb^{3+}$,[195] $KGdF_4$:$Yb^{3+}$/$Tm^{3+}$@$KGdF_4$,[182] ($NaYbF_4$:$Tm^{3+}$)@$NaGdF_4$,[37] ($NaGdF_4$:$Nd^{3+}$)@$NaGdF_4$,[85] and ($YF_3$:$Yb^{3+}$/$Er^{3+}$/$Tm^{3+}$)@$YF_3$.[184] Moreover, high-angle annular dark-field scanning (HAADF) transmission electron microscopy (STEM) coupled with element mapping of a core/shell nanoparticle using electron energy-loss spectroscopy (EELS) and energy dispersive X-ray spectroscopy (EDS) become powerful characterization tools to provide direct evidence of the formation of heterogeneous core/shell UCNP.[38,192] It is worth mentioning that it is also possible to precisely control the shell thickness in the second step utilizing a precisely defined concentration of precursors or sacrificial nanoparticles. The ability to produce core/shell nanoparticle with precisely defined shell thickness provides a versatile platform to investigate the fundamental interaction between lanthanide pairs as well as to manipulate the interested optical attributes.

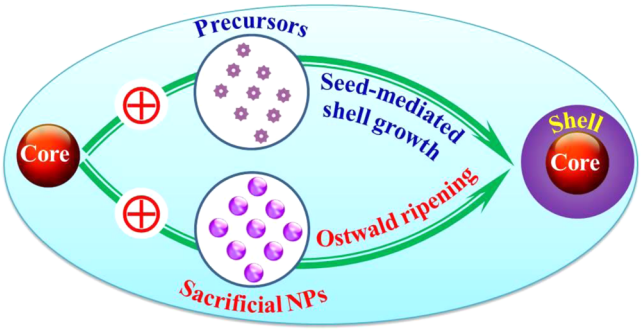


**Figure 15.** Two strategies to produce hierarchical core/shell UCNPs.

### 4.5. Future Opportunities for Synthetic Chemistry

For a specific synthetic approach, the efficiency of resulting UCNPs might vary from bath to batch. However, the evaluation of such efficiency variance has lacked up to now, thus deserving further investigations to provide guidance for experiments that involve UCNPs of different batches. As aforementioned, the thermolysis, Ostwald-ripening, and hydrothermal strategies are three general approaches to produce lanthanide-doped UCNPs. However, the quality of the same resulting UCNPs (the same size, same shape, and same composition ratios) produced by these approaches lacks comparison. Determination of the absolute quantum yields of the same UCNPs produced with these three approaches will be appealing to evaluate the production embodiment of these synthetic approaches. Although synthetic nanochemistries described in sections 4.1−4.4 are able to produce monodisperse UCNPs with a diameter of 20−100 nm, it remains a challenge to produce smaller but efficient UCNPs. The clinical translation requires that imaging agents injected into the human body be completely cleared in a reasonable amount of time.[297,298] Renal clearance is the main clearance route for imaging agents without biodegradation into biologically benign components,[298] which require the hydrodynamic size of nanomaterials be smaller than 10 nm with optimized surface. Hence, developing new or modified synthetic strategies to prepare sub-10 nm UCNPs is of crucial importance in the future. Furthermore, such an ultrasmall size of UCNPs is always associated with a significant decrease of the luminescent efficiency due to the extremely high "surface-to-volume" ratio. Thus, nanochemistry dealing with ultrasmall-size-related quenching mechanisms also needs our attention. Additionally, hierarchical core/shell UCNPs are emerging as new platforms for optical and/or multimodal imaging and as new building blocks to tune upconversion. Nanochemical approaches to produce various shells with precisely controlled thickness will be of interest to investigate the shell thickness-related fundamental UC effect as well as to create an optimal nanostructure for multimodal imaging.

## 5. NANOCHEMISTRY FOR SURFACE ENGINEERING

UCNPs produced by the various methods described in section 4 are generally hydrophobic, as they are capped by OA, OM, TOP, or TOPO, which are hydrophobic. They are dispersible only in nonpolar organic solvents and not in an aqueous solution or biological buffer, which limits their applications for theranostic where hydrophilicity is a prerequisite. Moreover, surface properties dictate the biocompatibility of nanomaterials in vitro and in vivo. As a consequence, a crucial step in the use of these hydrophobic UCNPs for bioapplications is modification and functionalization of their surface, in an effort to render them water-soluble, make them biocompatible, and provide reactive groups for subsequent bioconjugation to various biomolecules for enhanced circulation and targeting. To this end, a variety of surface modification strategies like ligand exchange, ligand oxidation, ligand removal, silanization, layer-by-layer assembly, and amphiphilic polymer coating have been utilized to transfer nanoparticles with hydrophobic surfaces into


dx.doi.org/10.1021/cr400425h | Chem. Rev. 2014, 114, 5161−5214

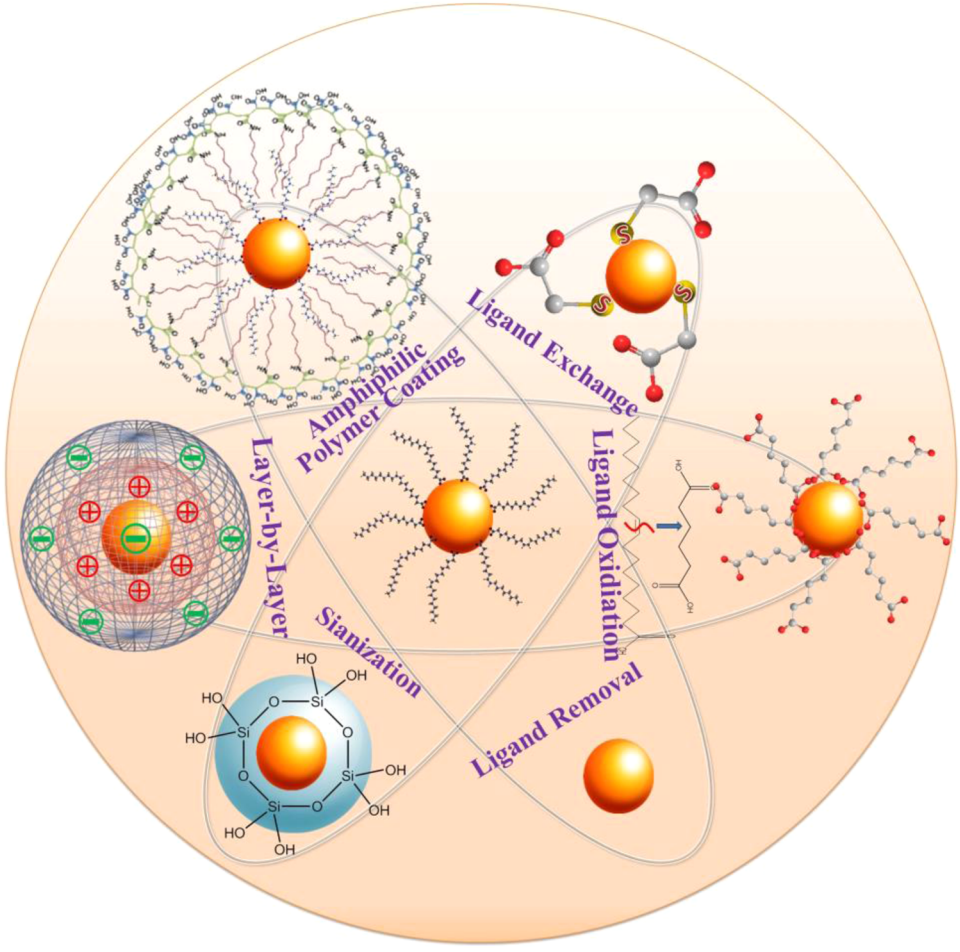


**Figure 16.** Schematic illustration of general strategies used for surface engineering of UCNPs, which include ligand exchange, ligand oxidation, ligand removal, silanization, layer-by-layer assembly, and amphiphilic polymer coating.

water over the past decade (Figure 16), which will be briefly surveyed in the sections 5.1−5.6. The bioconjuation chemistry will be discussed in section 5.7, which enables them to conjugate with a large variety of biological molecules such as peptides, proteins, and antibodies, allowing specific targeting of region of interest. Recent progress in surface modification of UCNPs has also been summarized in some recent reviews.[46,51,96,97,299] In all, surface functionalization of UCNPs also provides an effective way to control the interface between them and the biological systems they are designed to interact with.

### 5.1. Ligand Exchange

Ligand exchange is the most popular method to modify the surface of UCNPs by replacing the original hydrophobic ligands with some hydrophilic ligands without obvious influence on the chemical and optical properties of UCNPs (see Figure 16). Most of as-synthesized UCNPs in section 4 are originally capped by the hydrophobic OA ligand with a long-chain hydrocarbon and a carboxyl group (−COOH), which coordinates with the lanthanide ions on the nanoparticle surface. To allow an efficient exchange with the OA ligand, a multichelating hydrophilic ligand or an excess of single-chelating hydrophilic ligand that has stronger coordinating ability with the lanthanide ions is utilized. To this end, a large variety of ligands have been reported, including poly(acrylic acid) (PAA),[37] poly(ethyleneglycol) (PEG)-phosphate,[176] mercaptopropionic acid (MPA),[300] hexanedioic acid (HDA),[301] 3-dimercaptosuccinic acid (DMSA),[302] mercaptosuccinic acid (MSA),[238] citrate,[303] 1,10-decanedicarboxylic (DDA),[304] mercaptonudecanoic acid (MUA),[304] and poly(amidoamine) (PAMAM).[234] It is noted that after the ligand exchange, most of these commonly used ligand molecules on the UCNP surface carry additional functional groups to facilitate further biofunctionalization and bioconjugation. For example, the thiol group from the MPA ligand coordinates with the lanthanide ions on the surface of UCNP, while the carboxylic group is pointing out to provide an opportunity to covalently link an antibody (e.g., Anti-Claudin 4).[55]

Another common type of UCNPs in section 4 is capped by the hydrophobic OM ligand, which utilizes an amino (−$NH_2$) group to coordinate with the lanthanide ions on the nanoparticle surface. The interaction of OM and the surface lanthanide ions is generally weak, which facilitates ligand exchange with other hydrophilic ligands carrying functional groups. It has been reported that PEG-diacid,[248] PEI,[183] and thioglycolic acid (TGA)[305] can exchange successfully with the original OM anchored on the UCNP surface. In analogy, the coordinating ligand of *N*-(2-hydroxyethyl) ethylenediamine (HEEDA) on the surface of the $NaYF_4$:$Yb^{3+}$/$Er^{3+}$ nanoparticles can be easily replaced by the ligand of ethane-1,1-diphosphonic acid (HEDP).[305] Very recently, Murray and co-workers reported on a general and versatile ligand exchange strategy that enables sequential surface functionalization of nano-


dx.doi.org/10.1021/cr400425h | *Chem. Rev.* 2014, 114, 5161−5214

particles. Nitrosonium tetrafluoroborate ($NOBF_4$) was used to replace the original organic ligands such as OA and OM attached to the nanoparticle surface at room temperature, thereby stabilizing the nanoparticles in various polar media, without aggregation or sedimentation for years.[306] More importantly, the hydrophilic nanoparticles obtained above can be further functionalized by employing functional ligands to create desired surface functionalization of the nanoparticles.

### 5.2. Ligand Removal

Removal of the ligands coordinating the nanoparticle surface is a unique but simple way to disperse the UCNPs into aqueous phase (see Figure 16). This approach has been applied to the UCNPs capped by the ligand of OA. Removal of OA on the lanthanide-doped nanoparticle surface can be achieved through either a direct acid treatment and/or excess ethanol treatment with the assistance of sonication. Xu et al. reported that the OA ligand from the surface of the $NaYF_4$:$Yb^{3+}$/$Er^{3+}$ nanoparticles can be eliminated by thoroughly washing using excess ethanol under ultrasonic treatment.[55] Recently, Capobianco and co-workers reported ligand removal of OA capped on $NaGdF_4$:$Yb^{3+}$/$Er^{3+}$ nanoparticles with acid treatment;[65] this method was later applied by Prasad et al. to lanthanide-doped downconversion nanoparticles.[85] When dispersing lanthanide-doped nanoparticles in an acid environment (pH ≈ 2−4) with the assistance of sonication, the carboxylate groups of the oleate ligand were gradually protonated to yield oleic acid. The small amount of liberated oleic acid in water can be removed by extraction utilizing diethyl ether. The purified nanoparticles can form a stable and transparent solution for a long time. Because abundant naked metallic ions on the particle surface have strong coordination capability, the obtained ligand-free UCNPs are capable of direct conjugation to biocompatible molecules with functional groups such as −COOH, $-NH_2$, −OH in water solution for further bioapplications. Indeed, biomolecules like heparin have been coordinated to the surface of ligand-free $NaGdF_4$:$Yb^{3+}$/$Er^{3+}$ to allow them for use in targeting and delivery of heparin-binding growth factors and imaging of cancer cells.[307]

### 5.3. Ligand Oxidation

The ligand oxidation process is another effective approach to obtain water-soluble UCNPs, based on selectively oxidization of surface carbon−carbon double bonds (R−CH═CH−R′) (see Figure 16). This method is limited to original ligands, which contain at least one unsaturated bond, such as the OA ligand. The OA ligand on the UCNPs surface can be oxidized into hydrophilic azelaic acids ($HOOC(CH_2)_7COOH$), which makes UCNPs water-dispersible. Li et al. were the first to report the ligand oxidation method to oxidize selectively an OA molecule to give two carboxylic acids using the Lemieux−von Rudloff reagent. Alternatively,[66,308] Yan et al. used an ozone, a clean and readily available strong oxidant, to oxidize the OA on the UCNPs surface into azelaic aldehyde or azelaic acid through ozonolysis under specific conditions.[309] The ligand oxidation approach has disadvantages of long reaction time and low yield. However, the method is very simple and straightforward. Moreover, the resulting azelaic acid on the UCNP surface has one free carboxylic acid group, allowing further conjugation with various biomolecules. Indeed, this was validated by a recent work reported by Lin and co-workers, in which water-soluble $NaYF_4$:$Yb^{3+}$/$Tm^{3+}$ UCNPs were initially accomplished by the ligand oxidation method, and then conjugated with hydrazine and doxorubicin (DOX) to fabricate an anticancer drug delivery system.[310]

### 5.4. Layer-by-Layer Assembly

Layer-by-layer assembly involves sequential adsorption of oppositely charged ions on the surface of UCNPs.[311] Electrostatic attraction of oppositely charged species is one of the strongest and most stable interactions known in nature. A specific layer-by-layer modification is often helpful for a particular bioapplication of UCNPs. Li et al. have deposited the oppositely charged poly(allylamine hydrochloride) (PAH), poly(styrene sulfonate) (PSS), and PAH onto $Na(Y_{1.5}Na_{0.5})F_6$:$Yb^{3+}$/$Er^{3+}$(or $Tm^{3+}$) nnaoparticles in a layer-by-layer manner to generate hydrophilic PAH/PSS/PAH-coated nanoparticles with stable amino-rich shells.[227] The advantage of this method is that it permits the preparation of coated colloids of different shapes and sizes, with uniform layers of diverse composition as well as controllable thickness.[312] Most importantly, this method can manipulate the sign and the magnitude of the surface charge or incorporate ligands of functional groups on the surface of the UCNPs, which are important for their cellular internalization and biotargeting. Interestingly, this method has been extended by Duan et al. to produce gold nanoparticles and gold nanoshells on the UCNPs surface, in which the negatively charged coating layer of PAA was deposited by the amino-functionalized PAH ligand that is able to chelate with metallic gold nanoparticles or gold precursors.[144]

### 5.5. Surface Silanization

Surface silanization (or silica coating) is an inorganic surface treatment strategy to make nanoparticles water-dispersible and biocompatible. Silica is known to be highly stable, biocompatible, and optically transparent. When utilized as a coating material, surface silanization methods can flexibly offer abundant functional groups (e.g., −COOH, $-NH_2$, −SH, etc.) and thus satisfy various needs of conjugation with biological molecules. There are two types of related chemistry to coat silica onto the nanoparticles, depending on the polar nature of the capping ligands on the particle surface. One is the Stöber method, which can be utilized to coat silica on hydrophilic UCNPs. Tetraethyl silicate (TEOS) is added to an excess of water containing a low molar-mass ethanol and ammonia, together with the hydrophilic UCNPs. A precise control of the amounts of involved reagents as well the pH value can lead to a uniform growth of silica onto the UCNPs. Veggel et al. reported silica-coated $LaF_3$:$Yb^{3+}$/$Er^{3+}$ (or $Tm^{3+}$) UCNPs by the Stöber method, with the thickness of the silica shell controlled to be below 15 nm.[313] Zhang et al. demonstrated the coating of a very uniform and thin silica shell (1−3 nm) onto polyvinylpyrrolidone (PVP)-stabilized $NaYF_4$ nanoparticles to form a core−shell structure.[314] The other method is sol−gel nanochemistry in a reverse micelle nanoreactor to produce silica coating onto UCNPs with hydrophobic capping ligands.[158,189,315−319] This method utilizes chemical reactions in nanoconfined hydrophilic cavity (nanoreactor space) generated by a homogeneous mixture of ammonia, cyclohexane, surfactant (Igepal CO-520), and tetraethyl orthosilicate (TEOS).[320] This method can precisely control the silica shell thickness by altering the reagent amount or the reaction time, which is very useful to control the distance between the nanoparticles and plasmonic gold nanoparticles for manipulating plasmonic interaction.[159] For example, Li et al. achieved 5 nm silica shell on the surface of $NaYF_4$:$Yb^{3+}$/$Er^{3+}$ UCNPs with good dispersibility via this method.[317] Shan et al.


dx.doi.org/10.1021/cr400425h | Chem. Rev. 2014, 114, 5161−5214

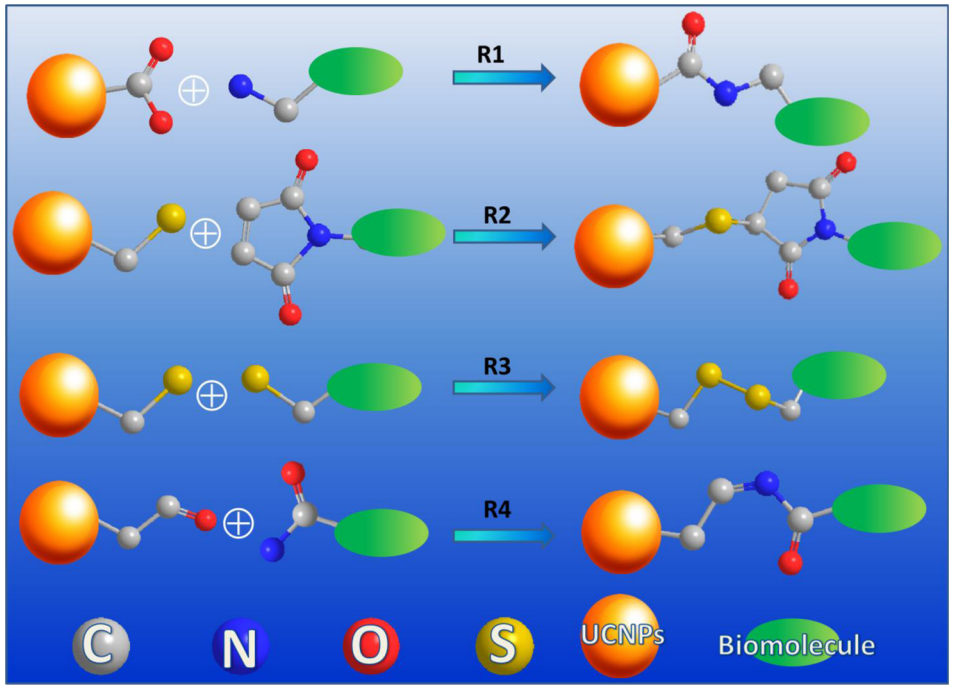


**Figure 17.** Bioconjugation chemistry commonly utilized for UCNPs to couple with selected biomolecules. Reaction 1 describes the chemical reaction of carboxylic acid and primary amine group to produce an amide bond, while reaction 2 presents a covalent bond formation between a thiol group and a maleimide group. Reaction 3 illustrates the coupling reaction between two thiol groups to form a disulfide bond, while reaction 4 displays the reaction of an aldehyde group and an amine group to produce an imine bond.

modified OA-coated UCNPs using $SiO_2$ shell for biofunctionalization in biological applications.[261]

Another advantage of silica coating is that mesoporous organically modified silica shell can be easily obtained by replacing a part of TEOS with (3-aminopropyl)triethoxysilane (APTES)[321] or in combination with the use of TEOS with cetyl trimethylammonium bromide (CTAB).[322] The mesoporous silica, with open mesopores, is immobilized on nanoparticles and offers many sites for the accommodation of functional biomolecules and drugs onto the surface of UCNPs.[322] Zhang et al. prepared the core/shell $NaYF_4$:$Yb^{3+}$/$Er^{3+}$@$SiO_2$@m$SiO_2$ nanoparticles to incorporate a photosensitizer into the mesoporous silica for UC PDT.[323] In addition, this method is also one of the most frequently used one for UC-imaging guided drug delivery.[323−325] Lin's group has reported on the use of $Fe_3O_4$@$SiO_2$@m$SiO_2$@$NaYF_4$:$Yb^{3+}$/$Er^{3+}$,[326] and $Gd_2O_3$:$Er^{3+}$@$SiO_2$@ m$SiO_2$ nanomaterials,[327] core/shell nanoparticles as drug carriers for cellular imaging and drug delivery. It is noted that the flexibility to introduce various functional groups on the silica shell provides another important advantage for mesoporous silica to load and deliver drugs into a selected target area guided by imaging using UC luminescence.

### 5.6. Amphiphilic Polymer Coating

Amphiphilic polymer coating is another strategy to convert the hydrophobic UCNPs to the hydrophilic ones. This approach involves the van der Waals interaction between the hydrophobic part of the amphiphilic polymer and the original hydrophobic ligand capped on the UCNP surface to immobilize the amphiphilic polymer onto the nanoparticle surface. The outer hydrophilic part of the amphiphilic polymer coated on UCNPs leads to aqueous dispersion and further bioapplication.[263] It is noted that the hydrophobic layer of the ampliphilic polymer is effective to isolate the UCNPs from the water molecules that can quench UC PL through the OH group with high frequency vibrations that facilitate multiphonon-induced relaxations. Thus, this method not only can produce exceptionally stable water-soluble UCNPs, but also can preserve the optical properties of UCNPs. The reported amphiphilic polymers up to now encompass poly(maleic anhydride-alt-1-octadecene) (PMAO),[328] octylamine-poly-(acrylic acid)-poly(ethylene glycol) (OA-PAA-PEG),[329] poly-(ethylene glycol)-*block*-poly(carprolactone) (PEG-*b*-PCL),[330] poly((ethylene glycol)-*block*-lactic acid) (PEG-*b*-PLA),[330] 6-aminohexanoic acid (6AA),[331] and poly(L-lysine) (PLL).[332] For example, Liu et al. have employed an amphiphilic polymer OA-PAA-PEG to render OA-coated $NaYF_4$:$Yb^{3+}$/$Er^{3+}$ nanoparticles water-soluble.[329] Veggel et al. reported the use of amphiphilic PMAO to transfer oleate-stabilized $NaYF_4$ core/shell UCNPs from hydrophobic to aqueous phase, with long-term dispersion stability in buffers and biological medium.[328] In addition, by using the octylamine and isoprolylamine-modified PAA as coating polymers, Chow and Yi successfully treated the surface of $NaYF_4$:$Yb^{3+}$/$Tm^{3+}$@$NaYF_4$ core/shell UCNPs with a necessary carboxylic functional group via amphiphilic polymer coating method.[172]

### 5.7. Bioconjugation Chemistry

The surface modifications of UCNPs mentioned so far are limited to the surface nanochemistry that enables nanoparticles to become dispersible and stable in aqueous solutions. However, bioconjugation of UCNPs with various functional biomolecules is generally required for their theranostic applications such as tumor targeted imaging, multimodal imaging, biosensing, photodynamic therapy, etc. The process of coupling biocomelecules to UCNPs can be provided primarily by two methods: (i) First is electrostatic or physisorption; it provides a straightforward noncovalent force to couple with the biomolecules.[238] However, the attached biomolecules might experience detachment when the UCNP−


dx.doi.org/10.1021/cr400425h | *Chem. Rev.* 2014, 114, 5161−5214

biomolecule bioconjugate is circulated inside the body systems that have complicated environments. (ii) Second is a covalent linkage that resulted from a chemical reaction between one reactive group on the particle surface and the other one incorporated in the biomolecules. In this Review, we shall only focus on this covalent type of bioconjugation. Actually, during the phase transfer of UCNPs from an organic solvent to an aqueous solution (see sections 5.1−5.6), a variety of functional groups such as −COOH, $-NH_2$, or maleimide (MA) groups generally have been introduced on the UCNP surface, providing numerous opportunities for them to covalently conjugate to biomolecules such as folic acid (FA), peptides, proteins, and DNAs, etc.

Figure 17 illustrates some of the commonly utilized bioconjugation chemistry. Reaction 1 describes the well-known 1-ethyl-3-(3-dimethylaminopropyl)carbodiimide hydrochloride (EDC) chemistry, which deals with chemical reaction of a carboxylic acid with a primary amine group to produce an amide bond. In a typical procedure, the carboxylic acid (−COOH) group can first be activated by EDC and *N*-hydroxysulfosuccinimide sodium salt (sulfo-NHS) in buffer to produce active *O*-acylisourea intermediate, which can then react with the $-NH_2$ group contained in the biomolecules to yield a stable amide bond. The second one involves reaction between a thiol group and a maleimide group, which can produce a stable thio−ether bond at physiological pH; this is very useful for bioconjugation of proteins with SH groups (containing cysteine moieties) onto the surface of UCNPs. The third reaction utilizes a disulfide linkage for bioconjuation of targeting ligands, which is attractive when a cross-linker with the thiol group at its end is used. However, the instability of disulfide bond in biological fluids might result in nonspecific binding of cysteine-containing proteins. Another approach involves chemical reaction between an aldehyde group and an amine group to give carbinolamines, which then dehydrate to give substituted imines. The aldehyde group can be derived from a cross-linker (e.g., glutaraldehyde) or from the oxidation of the present carbohydrate group. In the following, we summarize recent major investigations in this field based on three general types of functional groups, that is, the carboxylic acid (−COOH), the amino ($-NH_2$), and the maleimide group.

The carboxylic acid group on the UCNPs surface can be provided by the surface treatment with PAA,[37,239] azelaic acid,[49,66] HAD,[301,333] DMSA,[302] MSA,[238] citrate,[44,303] DDA,[304] MUA,[304] and MPA.[55,300] The incorporation of these ligands on the surface is discussed in sections 5.1−5.6. The carboxylic acid (−COOH) group on the particle surface is particularly suitable to establish to a covalent linkage with the biological molecules containing an $-NH_2$ group such as diamino-PEG,[49] antibodies,[55] streptavidin,[334,335] FA-chitosan,[302] Concanavalin A (ConA),[336] and DNA.[337−339] The involved bioconjugation chemistry is described by reaction 1 in Figure 14. One example is the MPA-modified $NaYF_4$:$Gd^{3+}$/$Yb^{3+}$/$Er^{3+}$ UCNPs, which were reported to conjugate with anticlaudin-4 antibody for targeted imaging of cancer cells.[55]

A number of hydrophilic ligands on the surface of UCNPs can provide an $-NH_2$ moiety to react with the carboxylic group contained in the functional biomolecules. These ligands include aminoundecanoic acid (ADA),[340] PEI,[82,341−343] diamino PEG,[53,63] poly(allylamine hydrochloride) (PAH),[76,227] etc. Moreover, the $-NH_2$ group can be easily introduced to silica-coated UCNPs during the coating by replacing TEOS with part of 3-aminopropyltrimethoxysilane (APS) in the last step.[50,158,313,344−347] The moiety of $-NH_2$ on the surface of UCNP can then create a link to different biomolecules containing the carboxylic group, such as FA,[331,348] biotin,[227] antibodies,[238] and DNAs.[76] The amino group on the surface (positively charged under certain pH) can also provide for electrostatic binding with a genetic material for gene therapy and RNA therapy.

The maleimide group can be introduced to the UCNPs surface via maleimide-modified polymers such as maleimide PEG, or by reaction of *N*-hydroxysuccinimide (NHS) ester that contains maleimide group with amine-functionalized UCNPs. The double carbon bond in the maleimide group readily reacts with the thiol group found in proteins like cysteine or thiolated peptide to form a stable carbon−sulfur bond. For example, Zako et al. reported on the coupling of the $Y_2O_3$@$SiO_2$−$NH_2$ UCNPs with the thiolated RGD (arginylglycylaspartic) peptide by use of bifunctional PEG in which the NHS group and the maleimide group are at each end.[349] The NHS group in the PEG provides covalent coupling with the $-NH_2$ group on silica, while the maleimide group in PEG provides covalent binding to the thiol group in the thiolated RGD peptide. Song et al. reported the use of bifunctional linker, sulfo-*N*-succinimidyl 4-(maleimidomethyl) cyclohexane-1-carboxylate (sulfo-SMCC), to link Ni-nitrilotriacetate (NiNTA) to the $NaGdF_4$:$Yb^{3+}$/$Er^{3+}$/$Tm^{3+}$ nanoparticles.[350] Li et al. reported on the maleimide functionalization of the amine-terminated $NaYF_4$:$Yb^{3+}$/$Er^{3+}$(or $Tm^{3+}$) UCNPs via 6-maleimidohexanoic acid *N*-hydroxysuccinimide ester, which reacts with the amino group on the particle surface.[49]

### 5.8. Future Opportunities for Surface Engineering

Most of the surface-modified UCNPs are stable in aqueous dispersion, but they often suffer from a poor colloidal stability under physiological conditions, some of which are only stable for a few hours in physiological buffers (phosphate, tris, and borate buffers). This stems from the presence of salts in buffers, which shows high affinity toward lanthanide ions on the surface of UCNPs, thus detaching the ligand or amphiphilic polymer anchored on the surface of the nanoparticles. The ligand here refers to the one produced from either the ligand oxidation or the ligand exchange procedure. The ligand-stripped UCNPs (removal of ligand) might become aggregated in physiological buffers due to the coordination of salts ions with exposed lanthanide ions on the particle surface. Even though silica coating makes the nanoparticles very stable in physiological buffers, the inability to remove completely the excess surfactants might also result in a low colloidal stability over time. As a consequence, developing modified surface modifications strategies to ensure a long stability of UCNPs in psychological buffers will be the next focus in the future. In addition, PEGylation of the surface of UCNPs to enable long-circulating in blood for passive targeting and/or active targeting delivery will be appealing for in vivo applications in the future.

## 6. BIOSENSING AND BIOASSAYS

Optical sensing and assays play vital roles in theranostics due to the capability to detect hint biochemical entities or molecular targets as well as to precisely monitor specific fundamental physiological processes. UCNPs are promising for these endeavors due to the unique frequency converting capability of biocompatible NIR light that is silent to tissues. They have the potential to reach a high detection sensitivity deeply located in the living body systems. However, the PL of UCNPs is not


dx.doi.org/10.1021/cr400425h | *Chem. Rev.* 2014, 114, 5161−5214

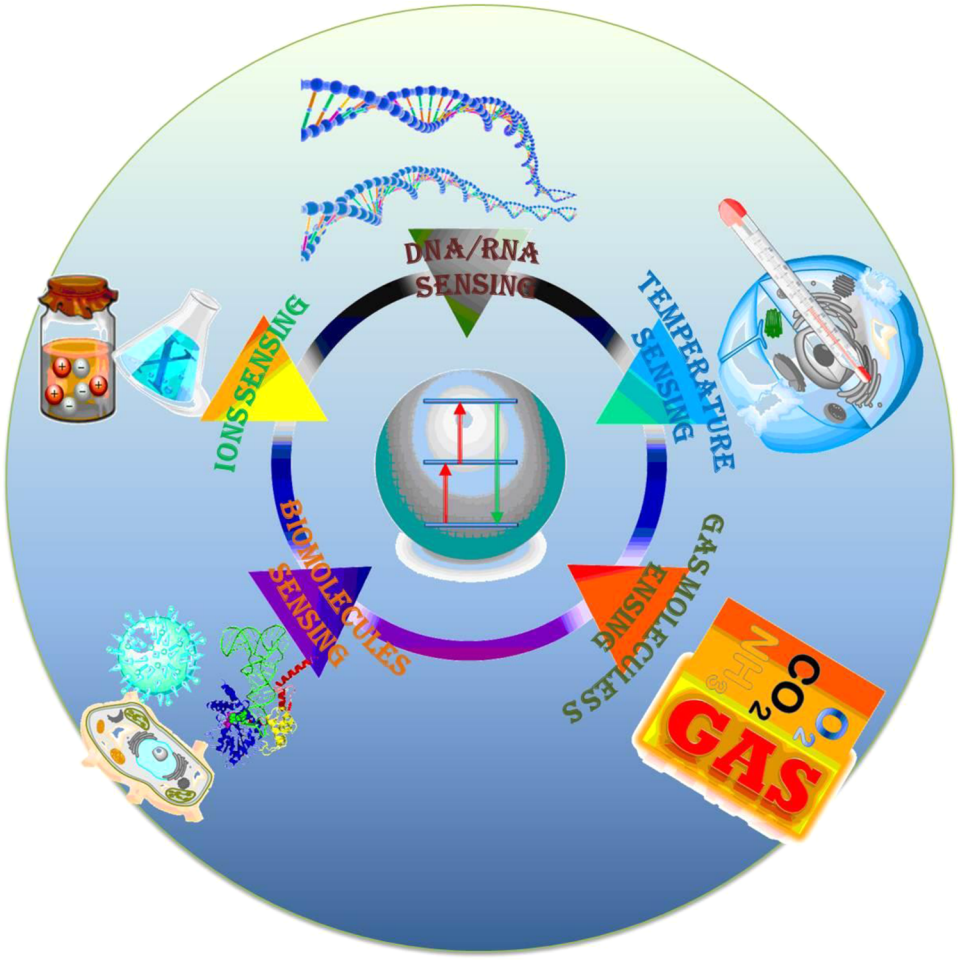


**Figure 18.** Schematic illustration of biosensing and bioassay applications of UCNPs in diverse fields.

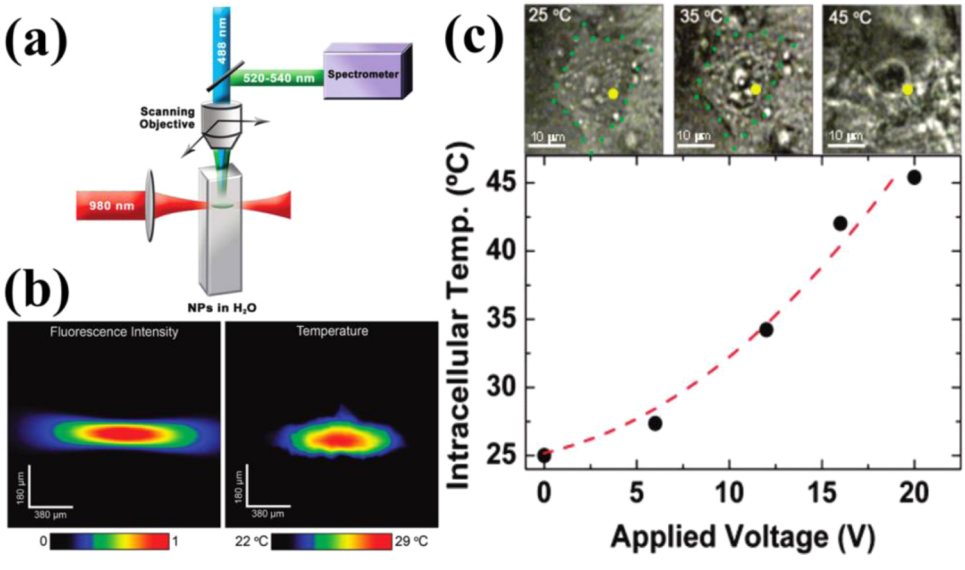


**Figure 19.** (A) Schematic of nanothermometer used to monitor the temperature profile created by heating a colloidal solution of $NaYF_4$:$Er^{3+}$,$Yb^{3+}$ UCNPs in water with a NIR diode laser (980 nm, pump beam) and scanned with an $Ar^+$ laser (488 nm, probe beam). (B) Confocal image of all of the visible upconverted luminescence under 980 nm excitation (left). Thermal image of the spot created by the 980 nm pump beam (right). (C) Optical transmission images of an individual HeLa cell at different temperatures and temperature-dependent property of the HeLa cell determined by UCNPs as a function of the applied voltage. The voltage determines the heating temperature of plate under the cells. Reprinted with permission from ref 351. Copyright 2010 American Chemical Society.


dx.doi.org/10.1021/cr400425h | *Chem. Rev.* 2014, 114, 5161−5214

directly related to any biochemical property of a system except for temperature. Therefore, to be useful in a biochemical recognition process (the fundamental process in chemical sensing), UCNPs have to be used in combination with suitable recognition elements such as indicator dyes. The recognition element of a biosensor may consist of an enzyme, an antibody, a polynucleotide, or even living cells. Next, the process of biochemical recognition has to be transduced into an optical signal given by the UCNPs. The transduction was generally implemented by a FRET and/or LRET mechanism. In the following, we summarized UCNP-based in vitro temperature sensing, detection of ions (cyanide, mercury, etc.), sensing of small gas molecules (oxygen, carbon dioxide, ammonia, etc.), as well as UCNP-based bioassays for biomolecules (avidin, ATP, DNA, RNA, etc.) (see Figure 18).

### 6.1. Temperature Sensing in Cells

Temperature is a fundamental parameter that plays an important role for numerous applications and scientific researches. An accurate and noninvasive determination of this parameter is also of particular importance for biology, for example, the investigation of enzyme reactions or metabolism in a single live cell. It is known that the PL intensity ratio between the emissions of $Er^{3+}$ ions at 520 nm from the $^2H_{11/2} \rightarrow {}^4I_{15/2}$ transition and at 550 nm from the $^4S_{3/2} \rightarrow {}^4I_{15/2}$ transition is very sensitive to the temperature; the populations in the $^4S_{3/2}$ and $^2H_{11/2}$ levels approximately follow the Boltzmann Distribution Law under steady-state excitations.[351] In this case, the ratio of the two intensities $I_{520}$ and $I_{550}$ can be related to the temperature through the following equation:

$$\frac{I_{520}}{I_{550}} = A \exp\left(-\frac{\Delta E}{K_b T}\right) \quad (4)$$

where $K_b$ is the Boltzmann constant, $\Delta E$ is the energy gap between the two excited levels, and $A$ is a constant depending on the two levels lifetimes. Therefore, the ratio ($I_{520}/I_{550}$) will increase with temperature increase, which is very valuable for temperature evaluation.

As a result, based on this feature, the first UC nanothermometer in live cell was designed by Capobianco et al. using water-dispersed PEI-coated $NaYF_4:Er^{3+}/Yb^{3+}$ UCNPs (Figure 19).[351] The nanothermometers are able to record thermal gradient images of liquids based on the thermal profiles in a water solution of $NaYF_4:Er^{3+}/Yb^{3+}$ nanoparticles. Moreover, after incubation with HeLa cervical cancer cells, the fluorescent nanothermometers were used to measure the internal temperature of the living cell from 25 °C to the thermally induced death at 45 °C (Figure 19). In addition, Wolfbeis et al. reported on the temperature sensing using UCNPs of varying size, dopant concentration, and core/shell structure.[352] It is found that the core−shell structured hexagonal ($NaYF_4$:20%$Yb^{3+}$,2%$Er^{3+}$)@$NaYF_4$ UCNPs are more suitable for temperature sensing due to the higher brightness; they have the ability to resolve temperature differences of less than 0.5 °C in the physiological range between 20 and 45 °C.[352]

### 6.2. Biosensing of Metal Ions

Hazardous ions such as cyanide ions ($CN^-$) and mercuric ions ($Hg^{2+}$) are extremely toxic to mammals; detecting and evaluation of the concentration of these, therefore, are of particular interests and importance for the lives. Sensing ions using UCNPs have been shown to be highly sensitive in living cells.[233,353] As the UC effect is inert to the interested ions, UCNPs have to be used in collaboration with suitable organic indicator that has a recognition capability of the targeted ions. As discussed in section 3.8, the FRET and/or LRET process between a UCNP and a dye can be utilized to excite fluorescent organic dyes. The same mechanisms are utilized here to construct sensors involving organic indicator of metal ions. The biochemical recognition will then modulate the PL intensity, displaying a colorimetric change in solution that even can be discerned by naked eyes.[354] Zhang et al. developed a kind of energy transfer sensor to determine $Hg^{2+}$ in aqueous media in which a $NaYF_4:Yb^{3+}/Tm^{3+}$ UCNP is employed as energy donor, while the SYBR Green, a DNA intercalating dye functions, is used as an energy acceptor.[355] By monitoring the ratio of the acceptor emission to the donor emission, they can quantitatively detect the presence of the mercuric ions with a limit of detection (LOD) of 0.06 nM. Li et al. reported on a highly selective water-soluble probe for UC luminescence sensing of intracellular $Hg^{2+}$ ions where chromophoric ruthenium complex (N719) was labeled on the surface of $NaYF_4$:20 mol % $Yb^{3+}$,1.6 mol % $Er^{3+}$,0.4 mol % $Tm^{3+}$ nanoparticles.[354] The N719-UCNPs can be applied for bioimaging for $Hg^{2+}$ ion in living cells. The LOD of $Hg^{2+}$ ions in water is reported to be down to 1.95 ppb (parts per billion), which is even lower than the maximum level (2 ppb) of $Hg^{2+}$ in drinking water set by the United States Environmental Protection Agency. Wolfbeis et al. reported on sensing of heavy metal ions such as $Cu^{II}$, $Hg^{II}$, $Pb^{II}$, $Cd^{II}$, $Co^{II}$, $Ag^{I}$, $Fe^{III}$, $Zn^{II}$ through evaluation of quenching of the luminescence of UCNPs by heavy metal ions based on the Stern−Volmer relationship. Optical sensing of the Cu(II),[356] Ce(IV),[309] as well as Na(I) and Ca(II)[357] has also been reported based on UCNPs.

### 6.3. Biosensing of Gas Molecules

Determination of the concentration of gas molecules such as oxygen, carbon dioxide, ammonia, and many others in aqueous samples or biological fluids has great significance in analytical biochemistry, clinical medical diagnosis, and bioprocess monitoring.[358,359] The use of UCNPs for gas molecules sensing has attracted extensive interest because of their outstanding properties. The first oxygen sensor based on UCNPs was presented by Wolfbeis's group, in which $NaYF_4:Yb^{3+}/Tm^{3+}$ UCNPs as nanolamps and iridium(III) complexes as oxygen indicators were both incorporated in an ethyl cellulose thin film.[360] The fluorescence of iridium(III) complex, produced by FRET and/or LRET from UCNPs, is sensitive to molecular oxygen concentration, which can quantify the content of oxygen molecules. Liu et al. developed a novel multifunctional nanocomposite sensor, which involves $NaYF_4:Yb^{3+}/Tm^{3+}$ UCNPs, oxygen indicator of Ru(II) complex, and biocompatible silica shell. It can precisely determine the concentration of $O_2$ from 0 to 100%.[361]However, until now, detection of oxygen is limited to oxygen molecules in gas environment. Quantification of molecular oxygen in physiological environment will be of much more importance and interest, which is essential for investigations of cellular respiration, adenosine triphosphate (ATP) generation during oxidative phosphorylation, as well as for the investigation of hemoglobin.

Molecular carbon dioxide and ammonia are toxic to many aquatic organisms at low concentrations; optical detection of them is nontrivial. It is known that they can interact with water molecules and thus vary the pH value of biological fluids. This


dx.doi.org/10.1021/cr400425h | Chem. Rev. 2014, 114, 5161−5214

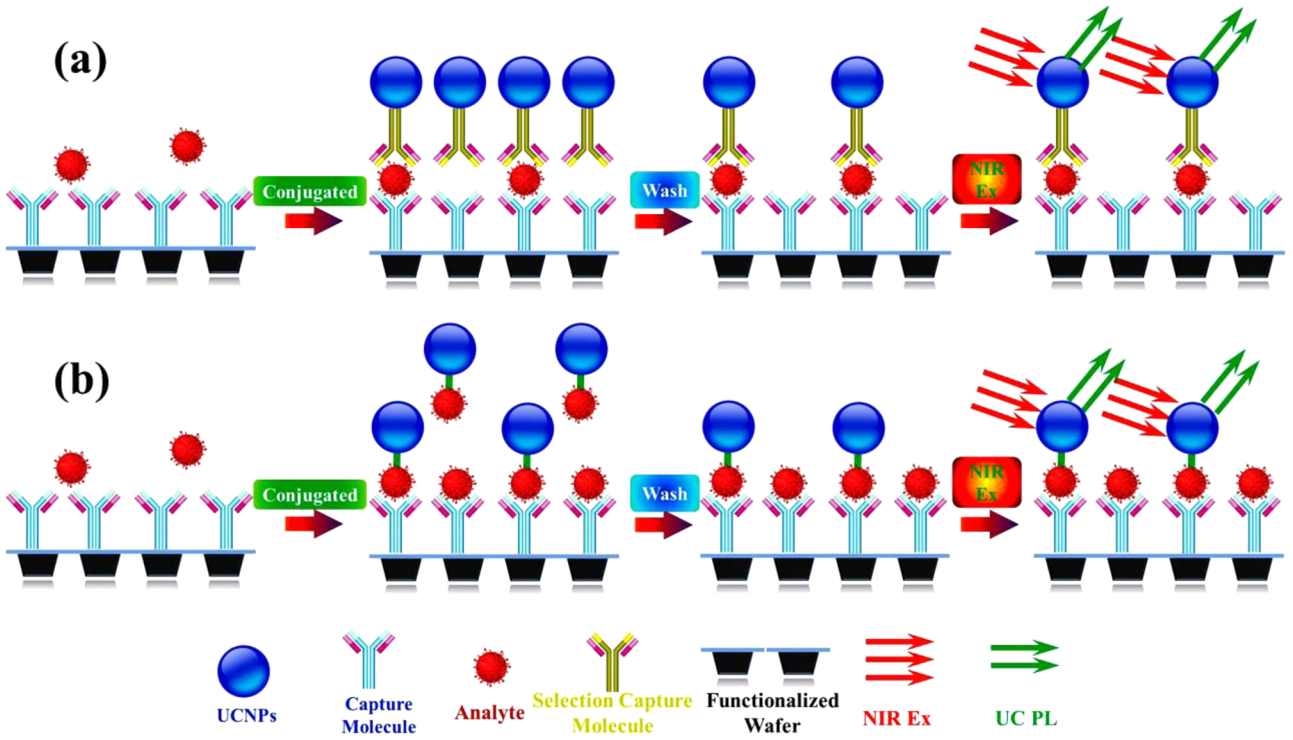


**Figure 20.** Schematic illustration of typical heterogeneous assays based on UCNPs: (a) sandwich-type assay; the optical response is proportional to the concentration of an analyte; and (b) competitive assay; the optical response is inversely proportional to the concentration of an analyte.

provides an opportunity to quantify their concentration through optical evaluations of the pH variations. Inspired by the first optical pH sensor based on UCNPs,[362] the pertinent colorimetrics or fluorometrics have been developed to meet this need. Wolfbeis et al. reported on a $CO_2$ optical sensor utilizing the $NaYF_4$:$Yb^{3+}$/$Er^{3+}$ UCNPs in combination with a long-wavelength absorption pH probe bromothymol blue (BTB).[363] The LOD is measured to be about 0.11% for the concentration of $CO_2$. According to a similar principle, they also designed an ammonia sensor utilizing the combination of $NaYF_4$:$Yb^{3+}$/$Er^{3+}$ nanoparticles and a pH probe of the phenol red, which are both immobilized in a polystyrene matrix. The ratiometric change of the intensities of the green to the red UC emission of the nanoparticles can determine the content of ammonia reaching a LOD as low as 400 $\mu$M.[364]

## 6.4. Bioassays

A bioassay is a biochemical test that measures the presence or concentration of a biomolecules (antibody, immunoglobulin, etc.), often referred to as an "analyte", in a solution. It plays a vital role in point-of-care theranostics; for example, the highly sensitive detection of cancerous biomarkers in human fluid samples is important for early cancer diagnostics, which can increase patient survival. The bioassay consists of two categories: (i) heterogeneous assay and (ii) homogeneous assay. A heterogeneous assay is performed in multiple steps with analytes being added, washed, and separated at different points in the assay, while a homogeneous assay is carried out simply by mixing the analytes and the sample and then making an optical measurement. The use of UCNPs in assays provides several advantages: (i) Because of the unique nature of UC, there is no background luminescence from the carrier fluid or the assay biochemistry, significantly decreasing the LOD that is unavailable from conventional assays. (ii) The optical properties of UCNPs are inert to the environment (e.g., buffer chemistry and assay temperature). As a result, the detection process is unaffected by the sampled fluid and is robust with respect to a large variety of environmental sampling conditions.

**6.4.1. Heterogeneous Assay.** Heterogeneous assay platform utilizes biofunctionalized molecules (capture molecule) that are immobilized on a solid substrate to detect target analytes with the assistance of UCNPs. As illustrated in Figure 20, the heterogeneous assay can be divided into two categories: (i) The first is sandwich (or noncompetitive) assay. The sandwich assay utilizes the capture molecule immobilized on the substrate to catch an analyte, which can then seize reactant-molecule-labeled UCNPs. In analogy to a capture molecule, a reactant molecule is also able to specifically bind to the analyte. After washing off excess unbound reactant-molecule-labeled UCNPs, measurement of UC PL can determine the concentration of the reactant-molecule-labeled UCNPs, which equals that of the analyte. In the sandwich assay, the measured UC PL intensity is proportional to the analyte concentration. (ii) The second is competitive assays. Unlike sandwich assays, the competitive assays utilize the competition process between an analyte and an analyte-labeled UCNP to anchor on the capture molecules immobilized on the substrate. Without the presence of the analyte, the system displays the highest UC PL. With the increase of the analyte concentration, a decreased UC PL is observed resulting from the less analyte-labeled UCNPs on the substrate. A calibration between the concentration of the analyte and the UC PL intensity is needed to quantify the analyte in the test sample. It is worth mentioning that a sandwich heterogeneous assay is often applied to detect large biomolecules that have multiple binding sites, while a competitive assay is generally applied to detect small biomolecules.

The first heterogeneous bioassay based on UC particles was reported by Zijlmans and co-workers for the detection of


dx.doi.org/10.1021/cr400425h | *Chem. Rev.* 2014, 114, 5161−5214

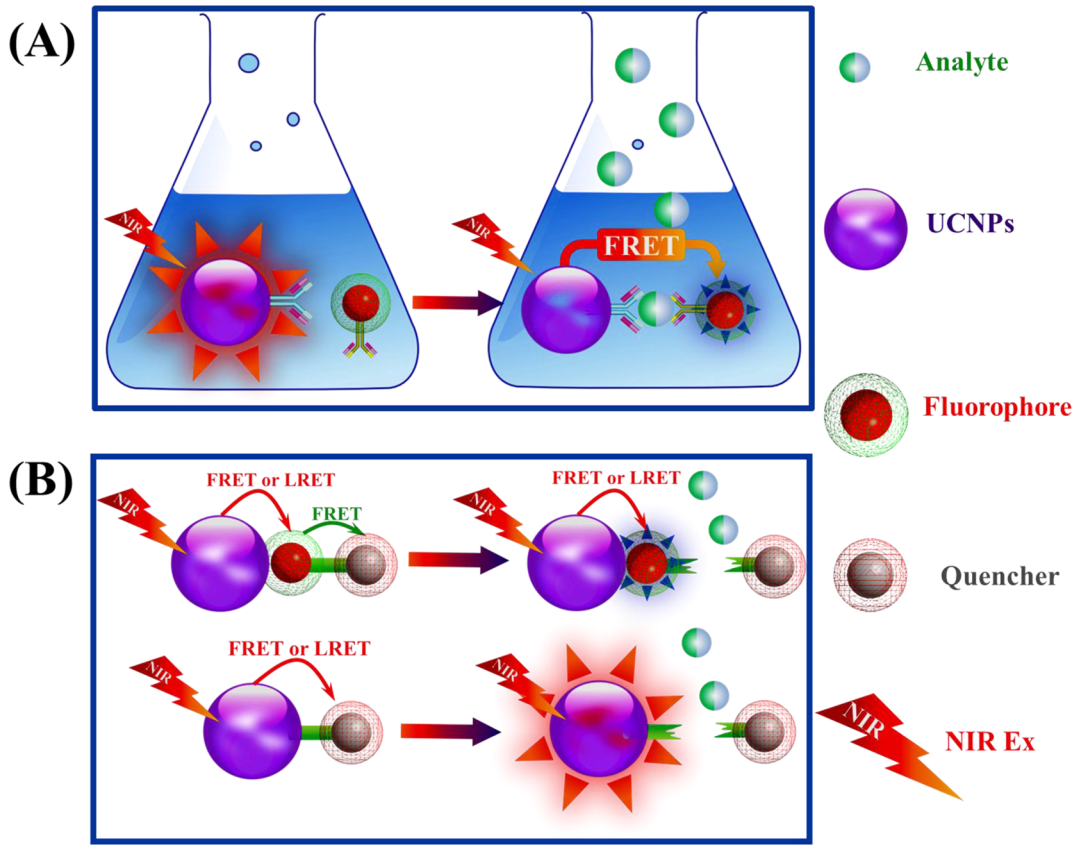


**Figure 21.** Schematic illustration of typical homogeneous assays based on UCNPs. (a) Assays utilizing a sandwich-type structure. These systems involve the use of UCNPs as energy donors and strong-absorbing materials as energy acceptors. The donors and acceptors are brought into close proximity by analytes. (b) Assays utilizing the inhibition of energy transfer process. (b, upper) The fluorophore utilized as the energy donor of UCNPs is initially deactivated by a linked quencher through a FRET process. The linkage between the fluorophore and the quencher can be cut off by an analyte (generally, an enzyme), restoring the PL of the fluorophore. (b, lower) The PL of UCNP, quenched by FRET or LRET to a quencher, can be recovered by analyte-induced separation of the quencher from the UCNP or elimination of quenchers' strong absorption.

prostate-specific antigen (PSA) in human prostate tissue in 1999.[365] Since then, numerous efforts have been made to use UC particles for diverse heterogeneous bioassays to detect analytes ranging from human chorionic gonadotropin,[366] a drug of abuse panel,[367] DNA detection,[368] bacterial pathogen (*Streptococcus pneumoniae*),[369] to nuleic acids.[370] The UC heterogeneous assay has shown significantly improved LOD over conventional assays due to the elimination of autofluorescence. For example, a detection limit of 10 pg of human chorionic gonadotropin in a lateral flow (LF) immunochromatographic UC assay format has been accomplished, which is an about 10-fold improvement in detection sensitivity as compared to conventional assays based on gold nanoparticles or colored latex beads.[366] Moreover, it has been shown by Niedbala et al. that an LF-based UC strip assay is able to provide simultaneous detection of amphetamine, methamphetamine, phencyclidine, and opiates in saliva by using multicolor UC particles. However, most heterogeneous assays reported before are based on submicrometer-sized UC particles that are not stable in colloidal solution. Smaller UCNPs with an improved stability and a decreased number of probe molecules per particle should result in better target-to-reporter ratios and improved assay kinetics.[371,372] A sandwich-hybridization assay for the ultrasensitive detection of DNA using sub-50 nm $NaYF_4$:$Yb^{3+}$/$Er^{3+}$ UCNPs has been attempted by Li et al., displaying an impressive detection limit of 10 nM without polymerase chain reaction (PCR) amplification.[76]

**6.4.2. Homogeneous Assay.** Homogeneous UC assays take advantage of the distance-dependent energy transfer between an energy donor (UCNPs) and a nearby acceptor molecule through long-range dipole−dipole interactions to detect analytes in the solution. Unlike heterogeneous assays involving multisteps of tedious separation and washing, homogeneous assay can be implemented easily in one mixing step, tending to be faster, simpler, and more automatic. When a UCNP and an energy acceptor are placed in a close proximity and the absorption of the acceptor and the emission of UCNP are overlapped, the excitation of UCNP can excite the energy acceptor via FRET or LRET, which then emits PL at a given wavelength. This well-established FRET or LRET mechanism has been previously utilized to tune UC PL (see section 3.8). Homogeneous UC assays generally utilize a sandwich structure to detect an analyte in which a UCNP and an acceptor molecule are both labeled with the capture molecule that can specifically seize the analyte. Generally, the capture-molecule-labeled UCNPs and the capture-molecule-labeled acceptor molecules are far from each in the solution, producing no detectable signal (either the quenching of UC PL or the fluorescence of acceptor molecule). Only the presence of analytes can bring the UCNPs and the acceptor molecules into close proximity to establish a FRET or LRET process that gives birth to the binding-modulated signal.

The application of UC particles in homogeneous assay dates back to the work by Mitchell and Morgan in 2007,[373] and


dx.doi.org/10.1021/cr400425h | *Chem. Rev.* 2014, 114, 5161−5214

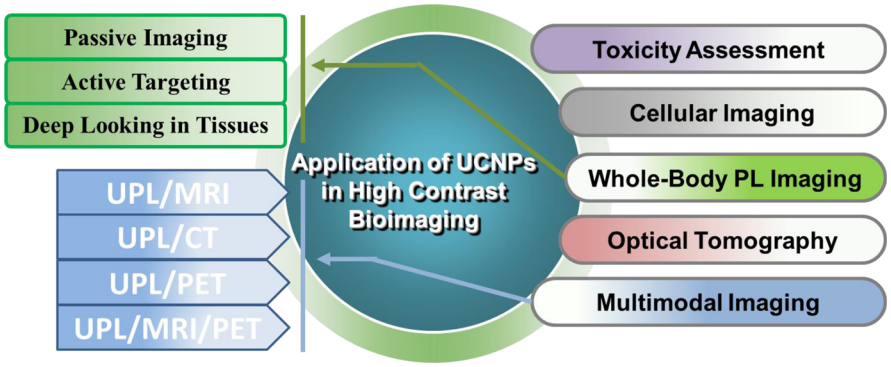


**Figure 22.** Schematic illustration of applications of UCNPs in high contrast bioimaging.

subsequently by Kuningas and co-workers who utilized the streptavidin conjugated UC particles as donors and biotinylated phycobiliprotein (biotin-BPE) as the acceptor.[374] Simultaneous detection of multiple analytes by using multipeak emission profiles of UC particle donors has also been reported by Rantanen et al.[315] However, these works involve the use of large-sized UC particles as energy donors. Because only emitting lanthanide dopants located near the particle surfaces can participate in the LRET or FRET, a considerably large fraction of emissive ions embedded in the core structures produces signals only through nonproximity-based reabsorptive energy transfer, limiting the detection sensitivity.[52,334,375,376] Later, Zhang and co-workers demonstrated that the small-sized oligonucleotide-modified UCNPs can be used as a sensitive biosensor to detect target-DNA reaching a LOD down to 1.3 nM.[338] They also revealed that oligonucleotide-modified UCNPs can distinguish target DNAs with single-base mismatches.[337,339] In addition, Li and co-workers developed a sensitive DNA sensor using streptavidin-functionalized small-sized $NaYF_4$:$Yb^{3+}$/$Er^{3+}$ UCNPs as the energy donors and reporter-DNA-TAMRA as the energy acceptor to detect a trace amount of target-DNA with a nonoptimized LOD ranging from 10 to 60 nM.[66]

Besides organic dyes, metallic nanoparticles like gold nanoparticles and graphene oxide have also been frequently investigated as superior quenchers of UC donors in homogeneous assays. It is anticipated that the combination of the large extinction coefficient of gold nanoparticles and graphene oxide and the uniqueness of UCNPs can result in increased detection sensitivity and decreased LOD. For instance, highly sensitive UC homogeneous biosensors employing $NaYF_4$:$Yb^{3+}$/$Er^{3+}$ UCNPs as the energy donors and gold nanoparticles as the energy acceptors have been accomplished for detection of avidin and rabbit antigoat IgG,[227,344] yielding a very low LOD of 0.5 nM for avidin and 0.88 $\mu$g/mL for goat antigoat IgG, respectively. The efficient energy transfer from UCNPs to graphene oxide has been shown in GO-$NaYF_4$:Yb/Er nanocomposite prepared by a one-step facile method,[377] which was then utilized to construct a novel biosensing platform to detect glucose in serum samples and other biomolecules.[336]

The inhibition of energy transfer process (FRET or LRET) between the UCNPs and the acceptor molecule has also been investigated to detect a trace amount of the analytes under NIR light excitation (see Figure 21b). It generally involves two ways: (i) The fluorescence of the acceptor dye evoked by the FRET or LRET is initially quenched by another quencher linked to the acceptor dye. The linkage can be cut off by the analyte, thus recovering the fluoresence of the acceptor dye. On the basis of this idea, an intriguing fluorescence-quenching-based enzyme activity assay has been developed, in which an Alexa Fluor 680 (AF680) fluorophore is utilized as the energy acceptor to receive the upconverted energy from UCNPs, and is quenched by the Blackberry Quencher 650 (BBQ650) that is linked to AF680 through a single-stranded oligonucleotide sequence. The oligonucleotide can be cut into shorter fragments upon an enzymatic reaction catalyzed by benzonase endonuclease, which led to the fluorescence recovery of AF680. It was found that this assay offers an 8-fold increase in signal-to-background ratio as compared to the conventional method relying on direct excitation into AF680 at 655 nm. (ii) The FRET or LRET process is deactivated by separation of the UCNPs and the acceptor dye, thus recovering the UC PL of UCNPs. This type of assay can be illustrated by the rapid detection of glutathione in aqueous solutions and living cells, whereby the UC PL of UCNPs, quenched by the linked manganese dioxide ($MnO_2$) nanosheets, is recovered by adding a small amount of glutathione to the solutions, which reduces $MnO_2$ into $Mn^{2+}$.[378] Similarly, an assay for detection of metalloproteinase-2 (MMP-2, important biomarker in blood) has been developed by utilizing PEI-modified $NaYF_4$:$Yb^{3+}$/$Er^{3+}$ UCNPs (energy donors) linked through a polypeptide chain to carbon nanoparticles (energy acceptors). The addition of MMP-2 in solution can scissor the substrate peptide between the UCNPs and the carbon nanoparticles and recover the UC PL of UCNPs, creating a LOD as low as 10 pg/mL for this homogeneous assay.[379]

### 6.5. Future Opportunities for Biosensing and Bioassays

UCNPs-based biosensing and bioassays are emerging as a new thrust in the theranostic field. The utilization of unique optical properties of UCNPs did push the LOD of these systems down to about 1 order of magnitude or more when compared to that of conventional methods involving latex particles, gold nanoparticles, and organic dyes. However, the efficiency of UCNPs still restrains the LOD of these systems; development of more efficient UCNPs can further increase the detection limit. In addition, multiplexed detections of a variety of analytes or multiplexed sensing of biochemical entities using the multicolor emissions of UCNPs will be an important area to explore in the coming years. Furthermore, the present bioassays are manually performed in a slow running manner. Flow cytometry is a laser-based biophysical technology that can be employed in biomarker detection, allowing simultaneous multiparametric analysis of the physical characteristics of up to thousands of particles per second. The incorporation of


dx.doi.org/10.1021/cr400425h | Chem. Rev. 2014, 114, 5161−5214

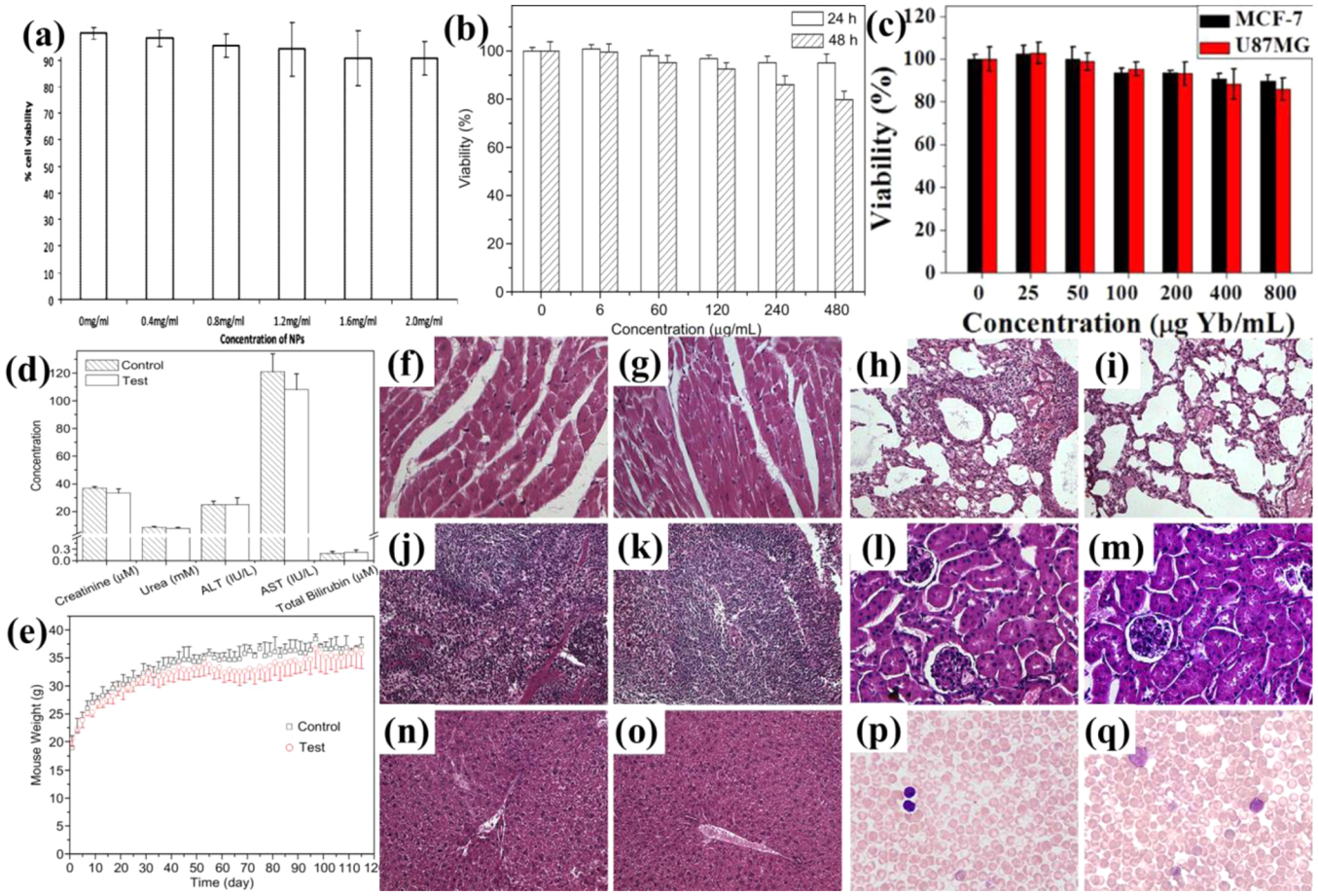


**Figure 23.** Cell viabilities of (a) human pancreatic cancer Panc 1 cells (ref 300), (b) human nasopharyngeal epidermal carcinoma cells (KB cells) (ref 48), and (c) human glioblastoma U87MG cells and human breast cancer MCF-7 cells incubated with UCA-RGD of different concentrations (ref 380). (d) Serum biochemistry results obtained from mice injected with PAA-UCNPs 115 days postinjection (dose = 15 mg/kg, test) and mice receiving no injection (control). (e) Change in body weight obtained from mice injected with PAA-UCNPs (dose = 15 mg/kg, test) and without injection (control). These findings did not indicate a trend of toxicity. (f–q) Hematoxylin and eosin-stained tissue sections from mice injected with PAA-UCNPs 115 days postinjection (f, j, n, h, l, and p) and mice receiving no injection (g, k, o, i, m, and q). Tissues were harvested from heart (f, g), spleen (h, i), liver (m, k), lung (l, m), kidney (n, o), and blood smear (p, q) (ref 48). Reprinted with permission from refs 300, 48, and 380. Copyright 2008 American Chemical Society, 2010 Elsevier B.V., and 2013 Nature Publishing Group.

UCNPs with flow cytometer might be an appealing direction in the future, allowing a faster and automatic detection, and thus providing opportunities for point-of-care theranostics.

## 7. HIGH CONTRAST BIOIMAGING

PL imaging plays an important role in biomedical research, being extremely useful for early detection, screening, and image-guided therapy of life-threatening diseases.[17] However, conventional Stokes-shifted fluorophores (organic fluorophores, fluorescent proteins, and metal complexes) or quantum dots are not ideal for bioimaging mainly due to the fact that the excitation is in the UV or visible range, which has limited light penetration and evokes strong imaging background (strong autofluorescence and light scattering).[17,85] Although NIR-excited nonlinear materials (two-photon dyes, quantum dots, gold nanorods, and second-harmonic-generation nanoparticles) overcome this limitation for bioimaging, the low efficiency of the nonlinear process and the needed high excitation density that requires an expensive pulsed excitation source severely limit their applications.[17,40] The "optical transparency window" of the biological tissues in the NIR range (750–1100 nm) not only allows for deeper light penetration, but also results in lower autofluorescence and reduced light scattering. Therefore, highly efficient imaging contrasts, with excitation and/or emission both in this NIR window, are ideal for bioimaging. UCNPs have emerged as a new generation of promising bioimaging nanomaterials for these endeavors. Figure 22 illustrates the use of UCNPs in various fields for high contrast bioimaging.

### 7.1. In Vitro and In Vivo Toxicity Assessment

The toxicity of UCNPs has been investigated with reference to in vitro cytotoxic activity and long-term in vivo toxicity.[48,326,372] MTT (methyl thiazolyl tetrazolium), MTS ((3-(4,5-dimethylthiazol-2-yl)-5-(3-carboxymethoxyphenyl)-2-(4-sulfophenyl)-2*H*-tetrazolium, sodium salts), and CCK-8 mitochondrial metabolic activity assays have been utilized to evaluate a large variety of cells such as human pancreatic cancer Panc 1 cells, human nasopharyngeal epidermal carcinoma cells (KB cells), human glioblastoma U87MG cells, and human breast cancer MCF-7 cells (Figure 23 a-c).[48,300,380] After incubation with UCNPs for at least 24 h, the cellular viabilities were estimated to be generally greater than 90% at high doses, concluding the low cytotoxicity of UCNPs.[48,300,380] It is worth mentioning that


dx.doi.org/10.1021/cr400425h | *Chem. Rev.* 2014, 114, 5161–5214

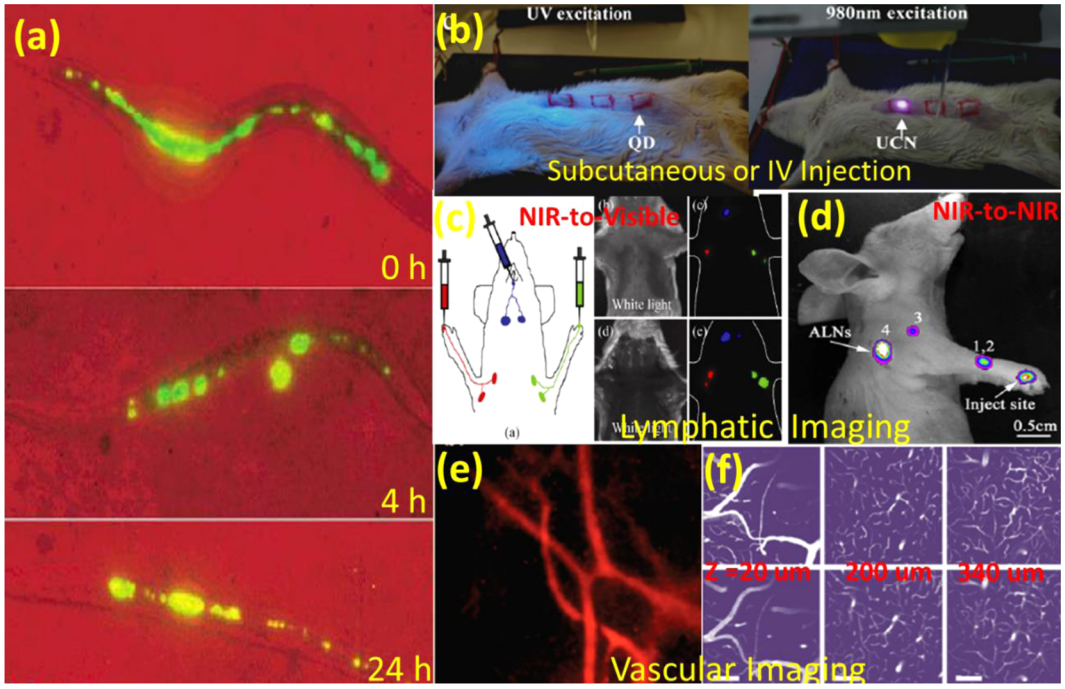


**Figure 24.** (a) Pseudo color images of *C. elegans* after being deprived of food over various periods of time: the red color represents the brightfield and green for the UC emission of $Y_2O_3$:$Yb^{3+}$/$Er^{3+}$ UCNPs (ref 384). (b) Comparison of mouse imaging after subcutaneous injection of (left) green-emitting QDs under UV excitation and (right) green-emitting $NaYF_4$:$Yb^{3+}$/$Er^{3+}$ UCNPs under NIR excitation (ref 387). (c) Multicolor sentinel lymph node imaging of a mouse using NIR-to-blue UCNPs of $NaY_{0.78}Yb_{0.2}Tm_{0.02}F_4$, NIR-to-green UCNPs of $NaY_{0.78}Yb_{0.2}Er_{0.02}F_4$, and NIR-to-red UCNPs of $NaY_{0.78}Yb_{0.3}Er_{0.01}F_4$.(ref 329). (d) Sentinel lymph node imaging of a mouse using NIR-to-NIR UCNPs of $LaF_3$:Yb/Tm (ref 331). (e) PL imaging of blood vessels in the mouse ear following tail vein injection of $Y_2O_3$:$Yb^{3+}$/$Er^{3+}$ UCNPs using NIR excitation at 980 nm (ref 403). (f) High-resolution cortical vasculature imaging using NIR-to-green dendritic UCNPs at various depths under cw NIR laser diode excitation (ref 404). Reprinted with permission from refs 384, 387, 329, 331, 403, and 404. Copyright 2006 American Chemical Society, 2008 Elsevier B.V., 2010 Springer, 2011 Elsevier B.V., 2013 Elsevier B.V., 2009 Royal Society of Chemistry Publishing, and 2012 National Academy of Sciences.

the effects of surface charge of UCNPs on the cell viability have also been investigated, displaying a negligible difference.[381]

The in vivo toxicity of UCNPs is one of the most important characteristics regarding theranostic applications of UCNPs. Until now, in vivo toxicity of hydrophilic UCNPs has been systematically investigated in mice,[48,56,382] *Caenorhabditis elegans* (*C. elegans*) worms,[383−385] and zebrafish embryos.[386] The results of these investigations all indicate no obvious toxicity of UCNPs. In particular, Li et al. have systematically investigated the long-term toxicity of PAA-coated UCNPs in mice through behavior observation, body weight measurement, histology and hematology analysis, and serum biochemistry assays. No abnormal behaviors and body weight fluctuations were observed (Figure 23e) with an administration of a dose of 15 mg/kg of PAA-coated UCNPs for about 3 months. The structures of the organs (heart, lung, liver, spleen, and kidney) of the exposed mice were normal and nearly identical to those of the control group, indicating no tissue damage, inflammation, and lesions (Figure 23f,g). Blood smear analysis indicated that the number and shape of red blood cells, platelet, and white blood cells were normal. Furthermore, established serum biochemistry assays indicated that the three important hepatic indicators (alanine aminotransferase, aspartate aminotransferase, and total bilirubin) and two indicators for kidney functions (creatinine and urea) were at similar levels for the mice exposed to PAA-UCNPs and for the control mice (Figure 23d). These results suggested no toxicity of PAA-UCNPs in mice over a long exposure time of 115 days. However, the in vivo toxic evaluation is limited to small animals like mice that are probably different from the human body. Future toxic investigations on nonhuman primates might provide useful information for their clinical translation. Moreover, the investigations of the clearance properties of UCNPs remain rather limited until now, which deserves attention.

### 7.2. Cellular Imaging

High contrast cellular imaging has been widely reported in recent years using NIR-to-visible (blue, green, red) and NIR-to-NIR UCNPs. One of the first demonstrations of UCNPs as two-photon excited fluorescence imaging probes was reported in 2008 by Zhang et al. who demonstrated that PEI-coated $NaYF_4$:$Yb^{3+}$/$Er^{3+}$ UCNPs conjugated with folic acid could be used to target human HT29 adenocarcinoma cells and human OVCAR3 ovarian carcinoma cells that have high levels of folate receptors on cell surface.[387] It is found that strong UC PL is observed with an absence of background autofluoresence under NIR excitation at 980 nm. Because their inherent high photon conversion efficiency and nonblinking emission behavior, UCNPs have been shown to enable reliable single-molecule imaging with long-time tracking capability.[388−391] Nonfunctionalized UCNPs have been utilized to image a variety of cell lines through cellular endocytosis, such as breast cancer cells (SK-BR-3 and MCF-7),[389] HeLa cells,[118,303,392−395] NIH 3T3 mouse embryonic fibroblasts,[388] ovarian cancer cells,[176,396] KB cells,[308] AB12 mouse mesothelioma cells,[397] HepG2 cells,[398] Huh-7 liver cancer cells,[399] MB49 bladder cancer cell lines,[189] and Panc 1 cells.[300] Importantly, Wong et al. showed that the surface charge of UCNPs largely determines their cellular uptake efficiency; the positively charged PEI-coated UCNPs have greater cellular uptake than their neutral and negative


dx.doi.org/10.1021/cr400425h | *Chem. Rev.* 2014, 114, 5161−5214

counterparts through a clathrin-mediated endocytosis way in HeLa Cells.[381]

In contrast, several works investigated targeted imaging of tumor cells using UCNPs that are functionalized with biomolecular recognition moieties (see section 5.7). A range of targeting molecules have been reported such as folic acid for targeting folate receptors overexpressed on various cancer cells (such as HeLa cells, human HT29 adenocarcinoma cells, human OVCAR3 ovarian carcinoma cells, human colon cancer cells),[53,348,387,400−402] rabbit anti-CEA8 antibodies for targeting carcinoembryonic antigen (CEA) on HeLa cells,[50,345] the anti-Claudin 4 and antimesothelin antibodies for the antigen receptor on Panc 1 cells,[55] and the RGD peptide for the $\alpha v\beta 3$ integrin receptor overexpressed on U87MG cells (human glioblastom).[49,349] Importantly, high contrast multicolor targeted cellular imaging has been demonstrated using $NaYbF_4$ UCNPs doped with $Er^{3+}$, $Tm^{3+}$, and $Ho^{3+}$ ions that emit different colors.[345] This provides possibilities of using UCNPs to image multiplexed macromolecules or organelles in a single cell to probe the cellular activities within this cell, or to image multiplexed cells to investigate cell differentiation or cell−cell interactions. It was found that in all of these works, using targeting molecules for specific binding can lead to an efficient cellular uptake and enhanced imaging within the cell walls and organelles. The ability of UCNPs to target cancerous cells provides opportunities to diagnose the tumors inside the bodies.

Despite that the reported cellular imaging has a high contrast, a low optical imaging resolution is obtained even with a customized confocal microscope. This arises from the long rise and decay time of the luminescence of UCNPs, as well as from the saturation effect that results in lowered spatial confinement effect (for the saturation effect, please consult eq 1). The saturation effect can be expected in confocal microscope imaging, as the excitation density in the focus plane can reach $\sim 10^6$ W/cm$^2$,[162] which is high enough to induce a saturation effect in most UCNPs that have a typical saturation threshold in the range of $10^1-10^3$ W/cm$^2$.[58] Engineering UCNPs with short luminescence rise time and lifetime as well as with an increased saturation threshold can accomplish cell imaging with both high resolution and high contrast.

### 7.3. Whole-Body Photoluminescent Imaging

**7.3.1. Passive Imaging.** Passive PL imaging has been investigated to demonstrate the potential capability of UCNPs for various types of small animal imaging and the biodistribution and/or biocompatibility behaviors of UCNPs, providing convenient information for biocompatibility evaluation as well as for theranostic applications. Ways of subcutaneous or tail vein injection have been generally employed to administrate the UCNPs into small animals to implement in vivo UC PL imaging. In addition, lymphatic imaging, high-resolution vascular imaging, multiplexed imaging, and real-time cellular trafficking have all been successfully demonstrated using surface-engineered UCNPs under cw NIR laser diode excitations.

The biocompatibility and imaging capability of UCNPs in live organism were pioneered by Lim et al.,[54] who inoculated $Y_2O_3$:$Yb^{3+}$/$Er^{3+}$ nanoparticles in the size range of 50−150 nm into live nematode *C. elegans* worms. Upon excitation at 980 nm, the statistical distribution of the nanoparticles in the intestines can be clearly visualized (Figure 24a). Importantly, the nanoparticles have shown good biocompatibility as the worms do not exhibit unusual behavior in feeding. In a recent work, they also prepared sub-10-nm $Y_2O_3$:$Yb^{3+}$/$Er^{3+}$ nanoparticles, which hold promise for staining ultrafine structures in biological systems.[385] Zhang et al. first showed the advantages of using NIR-to-green UCNPs in small animal imaging under NIR cw laser excitation,[387] including absence of photodamage to living organisms, very low autofluorescence, high detection sensitivity, and high light penetration depth in biological tissues. A higher imaging depth using UCNPs than QDs is shown in Figure 24b. Biocompatibility assessment and advantages of imaging using UCNPs have also been investigated by several other works, which clearly point out the importance of UCNPs for small animal imaging.[48,405,406] In vivo trafficking of transplanted myoblast cells and mesenchymal stem cells that are labeled with UCNPs has also been investigated, providing real-time observation of the interaction between the transplanted cells and the living body.[407,408] Such trafficking ability is essential for evaluation of therapeutic effectiveness of cell transplant that are emerging as an attractive treatment modality for various diseases.

Local lymphatic drainage is an important route for the metastasis of cancer cells. Thus, identification of sentinel lymph nodes or evaluation of the lymphatic system is important for cancer diagnostics and therapy. Kobayashi et al. have first demonstrated that NIR and green-emitting UCNPs can be utilized for two-color imaging of mouse lymph nodes without autofluorescence.[409] Liu et al. utilized three different kinds of UCNPs with multicolor emissions (blue, green, and red) for multiplexed lymphangiography of three groups of lymph nodes (Figure 24c).[329] Li et al. reported on the use of NIR-to-NIR amine-functionalized $LaF_3$:$Yb^{3+}$/$Tm^{3+}$ UCNPs for the lymphatic bioimaging of a mouse with high SNR (Figure 24d).[331] Importantly, in a recent report, they also showed that NIR-to-NIR $NaLuF_4$:$Yb^{3+}$/$Tm^{3+}$ UCNPs allow for real-time lymphatic imaging in vivo under ambient light illumination.[410]

It is worth noting that Figure 24c also illustrates the potential multiplexed imaging capability of UCNPs for simultaneous recognition and tracking of different organisms using engineered multicolor emissions (see section 3). Autofluorescence-free in vivo multicolor imaging using fluoride UCNPs with selected lanthanide dopants and designed cross-relaxations has been demonstrated by Tian et al.[411] Organic dye-loaded or QDs-loaded $NaYF_4$:$Yb^{3+}$/$Er^{3+}$ (or $Tm^{3+}$) nanocomposites with a broad range of colors produced by LRET or FRET from UCNPs to dyes or QDs have also been reported for in vivo multicolor UC PL imaging by spectral unmixing the emissions of different probes.[232,225] Moreover, Wang et al. reported on $NaYF_4$:$Yb^{3+}$/$Er^{3+}$/$La^{3+}$ nanorods as probes for deep tissue sensitive multicolor imaging in vivo.[412] The output color approximately indicated the depth of the nanorods in the tissues.

Changes in vascularization and vascular malfunction are associated with many diseases such as cardiovascular and kidney diseases as well as various types of cancers. Vascular imaging provides direct information about the number and configurations of vessels, permeability of the vasculature, and functional abnormalities of the vessels. An interesting development toward this regard has been demonstrated by Hilderbrand et al., who carried out in vivo vascular imaging of nude mice using $Y_2O_3$:$Yb^{3+}$/$Er^{3+}$ nanoparticles coated with PEG polymer (Figure 24e).[403] The polymer coating minimizes nonspecific tissue binding and prolongs the circulation half-lives of the particles in the blood. Importantly, as seen in Figure 24e, the


dx.doi.org/10.1021/cr400425h | *Chem. Rev.* 2014, 114, 5161−5214

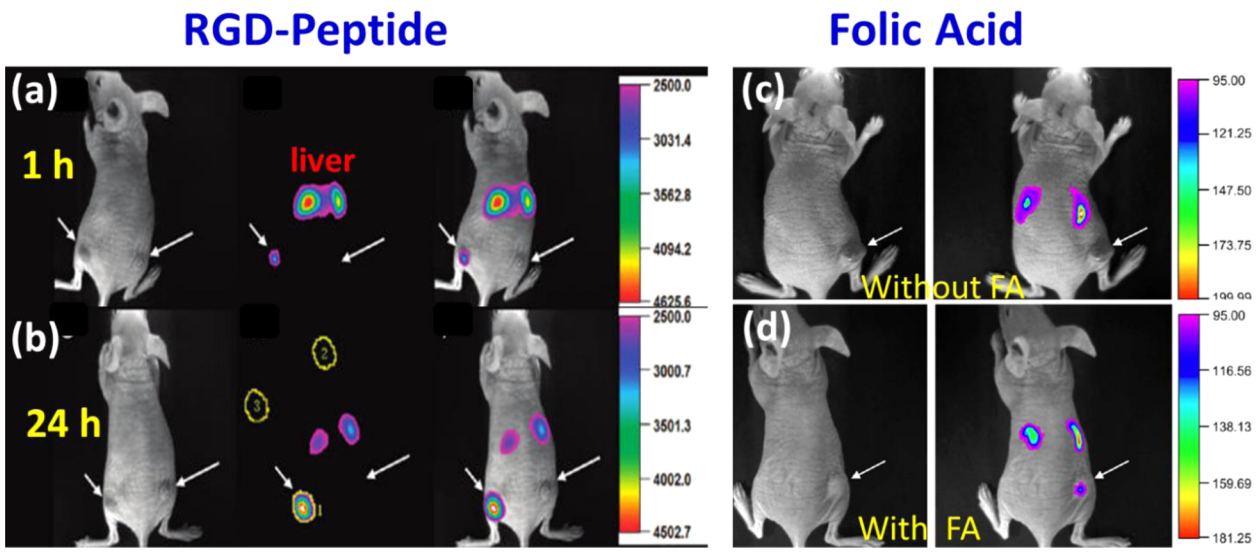


**Figure 25.** (a,b) In vivo UC PL imaging of subcutaneous U87MG tumor (left hind leg, indicated by short arrows) and MCF-7 tumor (right hind leg, indicated by long arrows) bearing mice after intravenous injection of RGD-conjugated $NaYF_4$:$Yb^{3+}$/$Tm^{3+}$ nanoparticles for (a) 1 h and (b) 24 h. The left, middle, and right columns are bright-field, UC PL, and overlay images, respectively. Intense UC PL signal was observed in the U87MG tumor, whereas no obvious signal was seen in the MCF-7 tumor. In vivo SNR = $(I_{ROI1} - I_{ROI3})/(I_{ROI2} - I_{ROI3})$ where ROI 1 represents specific uptake region of interest; ROI 2 is nonspecific uptake region of interest; and ROI 3 is background region of interest (Figure 25 b) (ref 49). (c,d). In vivo UC PL imaging of subcutaneous HeLa tumor-bearing athymic nude mice (right hind leg, pointed by white arrows) after intravenous injection of UCNPs-$NH_2$ without FA (c) and UCNPs-FA (d), respectively. The left and right columns represent the bright-field images as well as the overlay of bright and UC PL images, respectively (ref 348). Reprinted with permission from refs 49 and 348. Copyright 2009 American Chemical Society and 2009 Elsevier B.V.

UCNPs are sufficiently bright to enable in situ vascular imaging of the mouse ear following a tail vein injection. Moreover, a new type of surface-engineered dendritic upconverting nanoparticles, developed by Vinogradov et al., enabled in vivo multiphoton microscopic vascular imaging with low-power CW laser sources.[404] High-resolution mapping of the cortical vasculature down to 400 $\mu$m under the tissue surface can be accomplished (Figure 24f).

**7.3.2. Active Targeting.** Targeted imaging of the tumor is important for cancer diagnosis and therapy, in which the important target-specific recognition capability is enabled by the ligand−receptor and antigen−antibody interactions. In this kind of application, bioconjugation chemistry (section 5.7) plays vital roles to introduce specific recognition biomolecules onto the surface of UCNPs. Recently, more attention has been placed to target imaging of specific structures in vivo. Although in vitro target imaging involving a broad spectrum of recognition biomolecules has been reported (see section 7.2), in vivo target imaging has been limited to UCNPs conjugated with FA and RGD peptides.

It is well-known that the RGD peptide has a high affinity for the $\alpha_v\beta_3$ integrin receptor, which plays a pivotal role in tumor angiogenesis. On the basis of this, Li et al. have linked RGD to the surface of $NaYF_4$:$Yb^{3+}$/$Tm^{3+}$ nanoparticles for targeted imaging of nude mouse bearing human glioblastoma U87MG tumors with overexpressed $\alpha_v\beta_3$ integrin (Figure 25a and b).[49] Time-dependent sequence of UCPL in vivo imaging has been investigated, showing clear targeted imaging of tumors 1 h postinjection, and can be retained for 24 h. Importantly, region of interest (ROI) analysis of the UC luminescence signal in vivo showed that UC imaging achieved a high signal-to-noise ratio (SNR) of ~24 between the tumor and the background (Figure 25b), which generally cannot be obtained in single-photon or two-photon fluorescence imaging. In addition, it has also been reported that neurotoxin-conjugated $NaYF_4$:$Yb^{3+}$/$Er^{3+}$/$Ce^{3+}$ UCNPs could directly target and visualize tumors in living animals and produce high-contrast images based on highly specific tumor binding of the polypeptide neurotoxins.[341]

FA as a targeting agent has high stability, nonimmunogenic character, and the ability to conjugate with a wide variety of biomolecules on cancer cells. Moreover, folate receptors are overexpressed in a large variety of human cancerous cells but not in normal cells. FA-modified UCNPs have been investigated for cellular targeted imaging (see section 7.2). Recently, FA-functionalized UCNPs were prepared through the reaction of 6-aminohexanoic acid-coated $NaYF_4$:$Yb^{3+}$/$Er^{3+}$ UCNPs with the carboxylic acid-activated FA through the EDC chemistry described in section 5.7.[348] It was found that, at 24 h after intravenous injection, a strong UC PL signal at 650 nm was observed at the tumor, whereas no obvious UC PL was observed in the tumor for the control mouse, which was injected with amine-functionalized UCNPs (Figure 25c and d). The UC PL signal in the tumor can also be inhibited by 10 mg/kg dose of FA, further substantiating the specific tumor targeting.

**7.3.3. Deep Tissue Imaging.** Although the NIR excitation light for UCNPs has strong penetration ability, the UV/visible UC emissions can still be strongly absorbed by biomolecules, which can limit their applications in deep tissue imaging. For small-animal in vivo imaging, the $NIR_{in}$−$NIR_{out}$ UCNPs is very well suited for whole-body read out because the optical transparency window favorable for light penetration is in NIR wavelengths (700−1000 nm) for deep imaging of animal tissues. The feature of $NIR_{in}$−$NIR_{out}$ UCNPs allows high contrast in vivo optical bioimaging, as both light attenuation and scattering are significantly reduced in the NIR spectral range and the autofluorescence of tissues is absent under the


dx.doi.org/10.1021/cr400425h | Chem. Rev. 2014, 114, 5161−5214

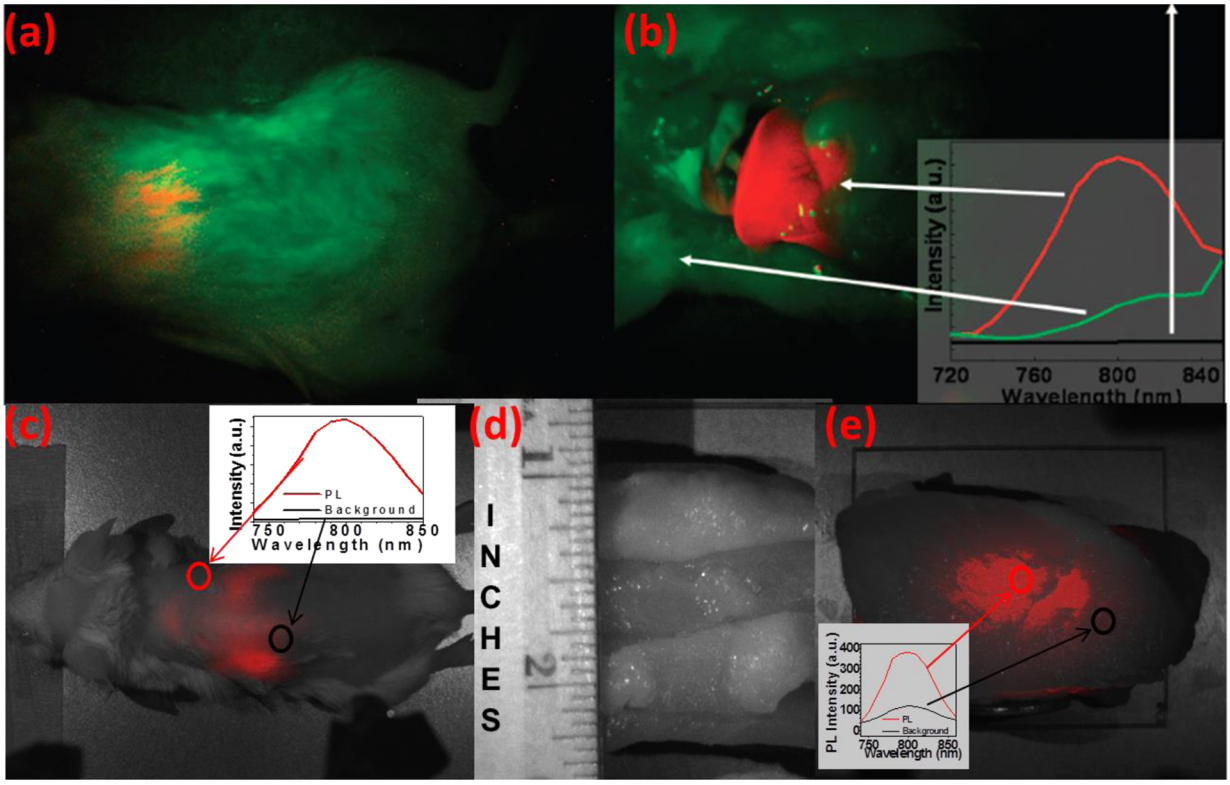


**Figure 26.** Whole-body images of mouse injected with $NaYF_4$:$Yb^{3+}$/$Tm^{3+}$ UCNPs; intact mouse (a), same mouse after dissection (b). The red color indicates emission from UCNPs; green and black show background as indicated by the arrows. The inset presents the PL spectra corresponding to the spectrally unmixed components of the multispectral image obtained with the Maestro system (ref 300). (c) Whole-body images of a BALB/c mouse injected via tail vein with the hyaluronic acid-coated $\alpha$-($NaYbF_4$:0.5% $Tm^{3+}$)/$CaF_2$ core/shell UCNPs. (d) Bright-field image of the pork tissue (side view), displaying the imaging depth; (e) UC PL image of the cuvette containing $\alpha$-($NaYbF_4$:0.5% $Tm^{3+}$)/$CaF_2$ core/shell UCNPs covered with a pork tissue. The insets in (c) and (e) show the spectra of the NIR UC PL and background taken from the circled area (ref 38). Reprinted with permission from refs 300 and 38. Copyright 2008 American Chemical Society and 2012 American Chemical Society.

conditions of UC excitation and emission. The strong two-photon NIR UC PL between 750 and 850 nm (the transition from $^3H_4 \rightarrow {}^3H_6$) from $Tm^{3+}$ ions, when excited at 980 nm, is particularly suitable for this purpose. Prasad et al. first reported high contrast in vivo bioimaging using $NIR_{in}$–$NIR_{out}$ UC PL $NaYF_4$:$Yb^{3+}$/$Tm^{3+}$ UCNPs (Figure 26a and b).[300] However, the weak PL that can only be detected by highly sensitive electron multiplied charge-coupled devices (EMCCD) is still a substantial limitation for improving the signal-to-background ratio (SBR) and the imaging depth. Li et al. reported on sub-10 nm citric acid-capped hexagonal $NaLuF_4$:$Gd^{3+}$/$Yb^{3+}$/$Tm^{3+}$ UCNPs for whole-body PL imaging of a mouse.[295] The UC quantum yield (800 nm) for these nanoparticles was measured to be about 0.47% under excitation density of 17.5 W/$cm^2$ at 980 nm. A high contrast UC PL imaging of the whole body of a mouse with a penetration depth of about 2 cm and an excellent detection limit of 50 cells can be achieved. More recently, Prasad et al. reported on the development of novel efficient core/shell $NIR_{in}$–$NIR_{out}$ ($NaYbF_4$:$Tm^{3+}$)/$CaF_2$ UCNPs, which were intravenously injected in BALB/c mice to perform whole-body imaging; a high SBR of 310 was achieved (Figure 26c).[38] The quantum yield can reach as high as 0.6% under imaging excitation conditions of 0.3 W/$cm^2$ at 980 nm. It is shown that the UCPL signal can be readily detected and imaged, with a low background, through a 3.2 cm thick pork tissue (Figure 26d and e).[38] The study provides a foundation for the development of 3-D imaging systems for the advanced whole-body optical imaging.

### 7.4. Optical Tomography

Fluorescence diffuse optical tomography (FDOT) is a form of computed tomography that creates a digital volumetric model of a fluorophore-sustained object by reconstructing images made from light scattered through an object. In a typical experiment, a highly scattering tissue medium is illuminated by a narrow collimated beam, and the luminescence from the sustained target that propagates through the medium is collected by an array of detectors attached to the tissue surface. The shape of the target can be reconstructed on the basis of the recorded optical data, which discern the target from the surrounding environment. FDOT is a compact, fast, and highly sensitive technique for three-dimensional deep-tissue imaging of fluorescent targets. These properties and the noninvasive nature of FDOT have made it very attractive for longitudinal studies of small animals, where it has been applied to follow the development in time of, for example, cancer tumors, proteases, Alzheimer's disease, and different drug effects.

The contrast agents used in FDOT are based on endogenous fluorophores such as hemoglobin, collagen, and elastin. The utilization of exogenous Stokes-shifted contrast agents such as molecular dyes or quantum dots can improve the detection sensitivity. However, autofluorescence and noise are still the nuisance for high contrast FDOT. Although much of the noise can be suppressed by employing low-noise equipment, the tissue autofluorescence remains to plague the measurements with traditional Stokes-shifted fluorophores. In addition, the linear power density dependence of the emission from these


dx.doi.org/10.1021/cr400425h | Chem. Rev. 2014, 114, 5161–5214

fluorophores results in poor spatial resolution in the reconstructed images, as sharp spatial features are inevitably smeared out during diffuse light propagation.

The use of UCNPs can completely eliminate the tissue autofluorescence because the emission from endogenous fluorophores is Stokes-shifted.[413] Hence, the UCNPs have been suggested as an alternative to fluorophores in FDOT. Xu et al. have recently demonstrated the use of $NaYF_4$:$Yb^{3+}$/$Tm^{3+}$ nanoparticles for DOT scanning in a controlled environment by using a gelatin-based tissue phantom.[414] The reconstructed optical data obtained from UCNPs showed a uniform and confined phosphor distribution (Figure 27a). In contrast, the reconstructed optical data obtained from the use of an organic fluorophore (Rhodamine 6G) showed severe artifacts at two ends of the fluorescent target (Figure 27b). In addition to the anti-Stokes shifted emission, it has been shown that the nonlinear power dependence of the UC emission can be further exploited to enhance both the quality and the contrast of the resulting images.[415] The experiments show that the spatial resolution of the FDOT reconstruction images can be significantly improved by the use of the synthesized $NaYF_4$:$Yb^{3+}$/$Tm^{3+}$@$NaYF_4$ UCNPs and break the current spatial resolution limits of FDOT images obtained from using conventional linear fluorophores as contrast agents (Figure 27c and d).[416] Although the advantages of UCNPs for FDOT imaging have been shown, the application of UCNPs for in vivo model or human tissue model remains unassessed. Further works of UCNPs on FDOT in either of these models will be essential to evaluate their potential for clinical practices.

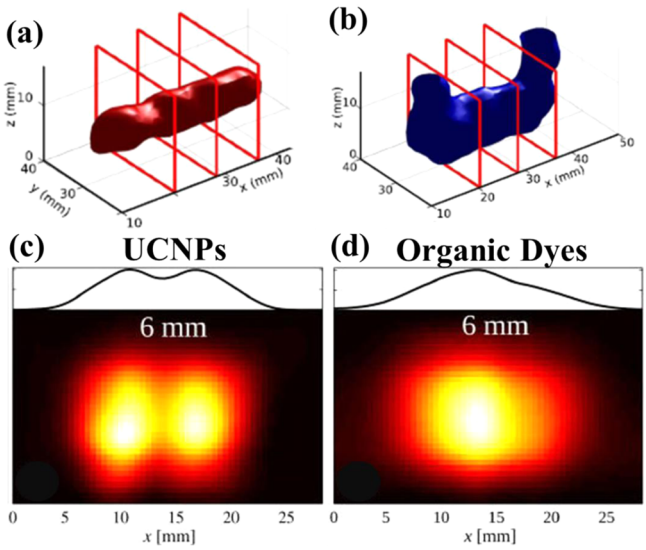


**Figure 27.** A comparison of $NaYF_4$:$Yb^{3+}$/$Tm^{3+}$ UCNPs (left column) and organic dyes (right column) in FDOT. (a,b) Three-dimensional rendering of the reconstructed fluorophores; the boxes indicate the position of the cross-sectional slices. (a) Reconstruction using UCNPs shows a smooth and uniform rendering. (b) Reconstruction using Rhodamine 6G shows several artifacts at the two ends of the fluorescent target (ref 414). (c,d) Two-dimensional plots of the FDOT reconstructions with (c) the quadratically power-dependent $NaYF_4$:$Yb^{3+}$/$Tm^{3+}$@$NaYF_4$ UCNPs as contrast agents and (d) the linearly power-dependent DY-781 fluorophores, and their corresponding intensity profiles (line plots). The true depth was $z$ = 7 mm, while the separation distance between the fluorescent tubes was set to 6 mm. The use of quadratic UCNPs clearly leads to reconstructions with higher spatial resolutions and qualities (ref 416). Reprinted with permission from refs 414 and 416. Copyright 2009 American Institute of Physics and 2012 American Chemical Society.

### 7.5. Multimodal Imaging

Current biomedical imaging techniques have been adopted in the development of imaging the structures and functions of biological systems. It includes all of the major radiological modalities, that is, magnetic resonance imaging (MRI), computed tomography (CT), and positron emission tomography (PET). These imaging technologies are expected to furnish anatomic, physiologic, molecular, and genomic information for accurate disease diagnosis, prediction of treatment response, and development of highly specific and sensitive drugs and imaging agents. However, none of the current imaging methods used in humans provides comprehensive medical imaging. To harness the strengths of different imaging methods, multimodal imaging has become an attractive strategy for in vivo studies. The advantages of UCNPs in optical bioimaging include high photostability, narrow emission lines, absence of blinking, large anti-Stokes shifts, and improved tissue penetration with NIR excitation. The considerable attention and rapid development of UCNPs offers possible opportunity for multimodal imaging. UC PL optical and radiological imaging methods have a symbiotic relationship that can be explored in a multimodality imaging framework, which, thus, is the focus of this section.

**7.5.1. Upconversion Photoluminescence and Magnetic Resonance Imaging (MRI).** To combine the merits of these imaging modalities, multimodal imaging based on $Ln^{3+}$-UCNPs have been developed and utilized as nanoprobes for in vitro and in vivo dual-modal UC PL and MRI imaging. $Gd^{3+}$ ion-based materials are promising for use as MRI contrast agents due to seven unpaired inner 4f electrons, which can efficiently change the spin−lattice relaxation of the protons of coordinated and/or nearby waters for $T_1$-weighted MRI imaging. The other main class of contrast agents is based on changing the spin−spin (or transverse) relaxation time for $T_2$-weighted MRI imaging. The commonly used superparamagnetic iron oxide belongs to this type of negative contrast agents, which can darken the image where the contrast agents have been accumulated.

The ability to incorporate $Gd^{3+}$ ions in a nanocrystalline matrix allows for a dramatic increase of $Gd^{3+}$ concentration in nanoscale, thus providing an efficient way to build up $T_1$-based MRI contrast agents on the well-established UCNPs.[417,418] There are two attractive strategies to construct UCPL/MRI functional probes: (i) Codoping $Yb^{3+}$, $Er^{3+}$, and/or $Tm^{3+}$ into $Gd^{3+}$-based host lattice to realize efficient UCPL and MRI; and (ii) the utilization of a core/shell structure with the core for UC PL and the shell of $Gd^{3+}$-based compound for MRI. On the basis of $Gd^{3+}$-based nanomaterials, a large variety of nanomaterials have been reported and used for in vitro or in vivo dual modal UCPL/MRI imaging. Nanomaterials constructed on the first strategy encompass $NaYF_4$:$Er^{3+}$/$Yb^{3+}$/$Gd^{3+}$,[44,55,417] $NaYF_4$:$Tm^{3+}$/$Yb^{3+}$/$Gd^{3+}$,[45,419] $NaGdF_4$:$Yb^{3+}$/$Er^{3+}$,[420] and $NaGdF_4$:$Yb^{3+}$/$Er^{3+}$/$Tm^{3+}$@$SiO_2$-Au@PEG5000.[60] The reported $T_1$ MR relaxation constant is in the range of 0.14−5.6 $mM^{-1}$ $s^{-1}$, and the highest one is reported in hydrophilic and carboxylic acid-functionalized $Yb^{3+}$/$Er^{3+}$/$Tm^{3+}$ codoped $NaGdF_4$ nanoparticles with NIR-to-NIR UC PL and high magnetic properties.[45] Representative nanomaterials constructed on the second strategy include $NaYF_4$:$Yb^{3+}$/$Er^{3+}$@$NaGdF_4$,[186,421] $NaYbF_4$:$Tm^{3+}$@$NaGdF_4$,[37] $NaLuF_4$:$Yb^{3+}$/


dx.doi.org/10.1021/cr400425h | Chem. Rev. 2014, 114, 5161−5214

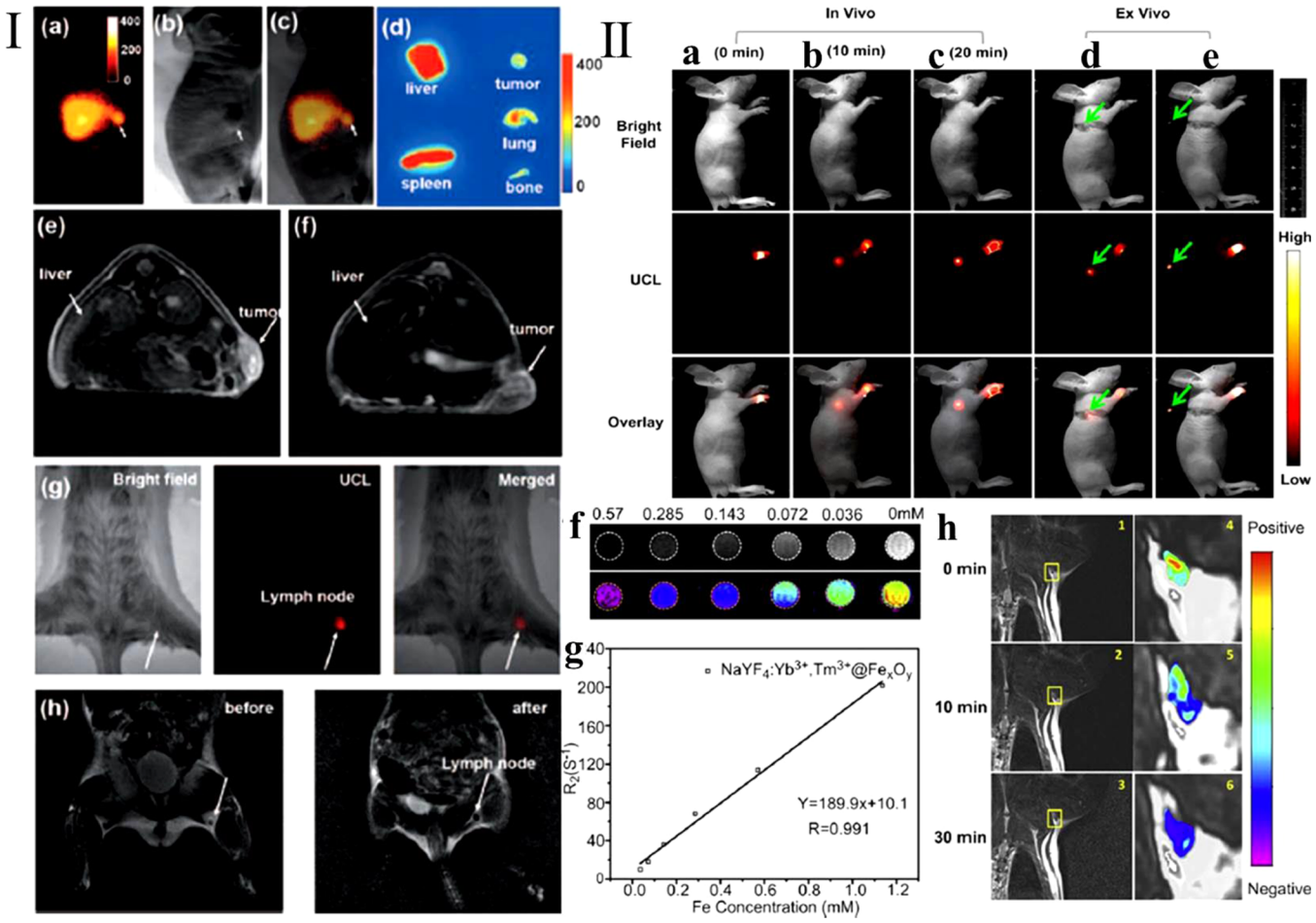


**Figure 28.** (I a–c) The UC PL (I a), bright-field (I b), and merged (I c) images of a KB tumor-bearing mouse 1 h after intravenous injection of PEGylated multifunctional nanoparticles. (I d) Ex vivo UCPL imaging showing accumulation of multifunctional nanoparticles in the liver, spleen, tumor, bone, and lung of the injected mouse at 24 h post injection. T2-weighted images of KB-tumor bearing nude mice with (I e) and without (I f) injection of multifunctional nanoparticles. Multimodal UC PL (I g) and T2MR (I h) imaging for in vivo lymphangiography mapping using multifunctional nanoparticles (ref 63). In vivo UCPL imaging of lymphatic system after injection with $NaYF_4:Yb^{3+}/Tm^{3+}@Fe_xO_y$ nanoparticles into a nude mouse at various time: (II a) 0 min, (II b) 10 min, and (II c) 20 min. (II f) T2-weighted and color-mapped MR images of various molar concentrations of $NaYF_4:Yb^{3+}/Tm^{3+}@Fe_xO_y$ nanoparticles. Deionized water (0 mg/mL) was the reference. (II g) Relaxation rate $R_2$ ($1/T_2$) versus various molar concentrations of hydrophilic $NaYF_4:Yb^{3+}/Tm^{3+}@Fe_xO_y$ nanoparticles at room temperature using a 3T MRI scanner. (II h) MR images of the armpit region after injection with $NaYF_4:Yb^{3+}/Tm^{3+}@Fe_xO_y$ nanoparticles and color-mapped coronal images of lymph node at various time (ref 425). These figures are adapted from refs 63 and 425. Copyright 2011 John Wiley and Sons and 2011 Elsevier B.V.

$Tm^{3+}@SiO_2$-GdDTPA,[422] $NaYF_4:Tm^{3+}/Yb^{3+}/Gd^{3+}@mSiO_2$,[423] $NaLuF_4:Gd^{3+}/Yb^{3+}/Tm^{3+}$,[424] and $NaYF_4$@Si-DTTA-$Gd^{3+}$.[319] The reported $T_1$MR relaxation constant is in the range of 0.48–6.8 $s^{-1}$ $mM^{-1}$, whereby the highest one is reported in silanized complex 3-aminopropyl(trimethoxysilyl)-diethylenetriamine tetraacetic acid (Si-DTTA)-$Gd^{3+}$ shell.[319] It is worth pointing out that these UCNPs, working as dual-modal imaging agents, can also be utilized for nanotheranostics by incorporation of therapeutic function. For example, $NaYF_4:Yb^{3+}/Er^{3+}@NaGdF_4$@mesoporous silica, containing cisplatin in the silica shell, can deliver cisplatin to tumors to implement synergistic chemo-/radiotherapy by radiosensitization of cisplatin, while having magnetic/luminescent dual-mode imaging.[421] It is out of note that the incorporation of $Mn^{2+}$ into the lattice of UCNPs is another promising route to construct $T_1$ MRI and UCPL imaging contrast agents. $Mn^{2+}$ ion has five unpaired d electrons and is capable of enhancing the longitudinal relaxation rate of water protons in tissues. In a recent work, Tan et al. have shown that sub-10 nm $NaMnF_3$ codoped with $Yb^{3+}/Er^{3+}$ or $Tm^{3+}$ nanoparticles can produce highly sensitive pure UC and $T_1$ MRI signal. The T1MR relaxation constant can reach as high as 12.687 $mM^{-1}$ $s^{-1}$.

Because of their large magnetic moment, superparamagnetic iron oxide ($Fe_3O_4$) nanoparticles have been combined with lanthanide doped-UCNPs for UC PL and $T_2$-enhanced MR imaging imaging. For example, Liu et al. developed multifunctional nanoparticles, $NaYF_4:Yb^{3+}/Er^{3+}@Fe_3O_4$@Au, which incorporated optical and magnetic properties useful for multimodality imaging (Figure 28, column I).[63] These multifunctional nanoparticles are synthesized via a simple layer-by-layer self-assembly strategy, which successively loads iron oxide nanoparticles and then gold nanoparticles onto the surface of UCNPs. The lymph node of the hind leg of a mouse is able to be simultaneously imaged in both UCPL mode or in $T_2$-weighted MRI mode, clearly showing the advantages of combined dual modal imaging. In addition, Li et al. reported seed-mediated synthesis of $NaYF_4:Yb^{3+}/Tm^{3+}@Fe_xO_y$ core/shell nanostructure as an imaging agent for T2MRI and UC PL bimodal lymphatic imaging (Figure 28, column II).[425] This work provides an imaging contrast candidate to guide clinical


dx.doi.org/10.1021/cr400425h | Chem. Rev. 2014, 114, 5161–5214

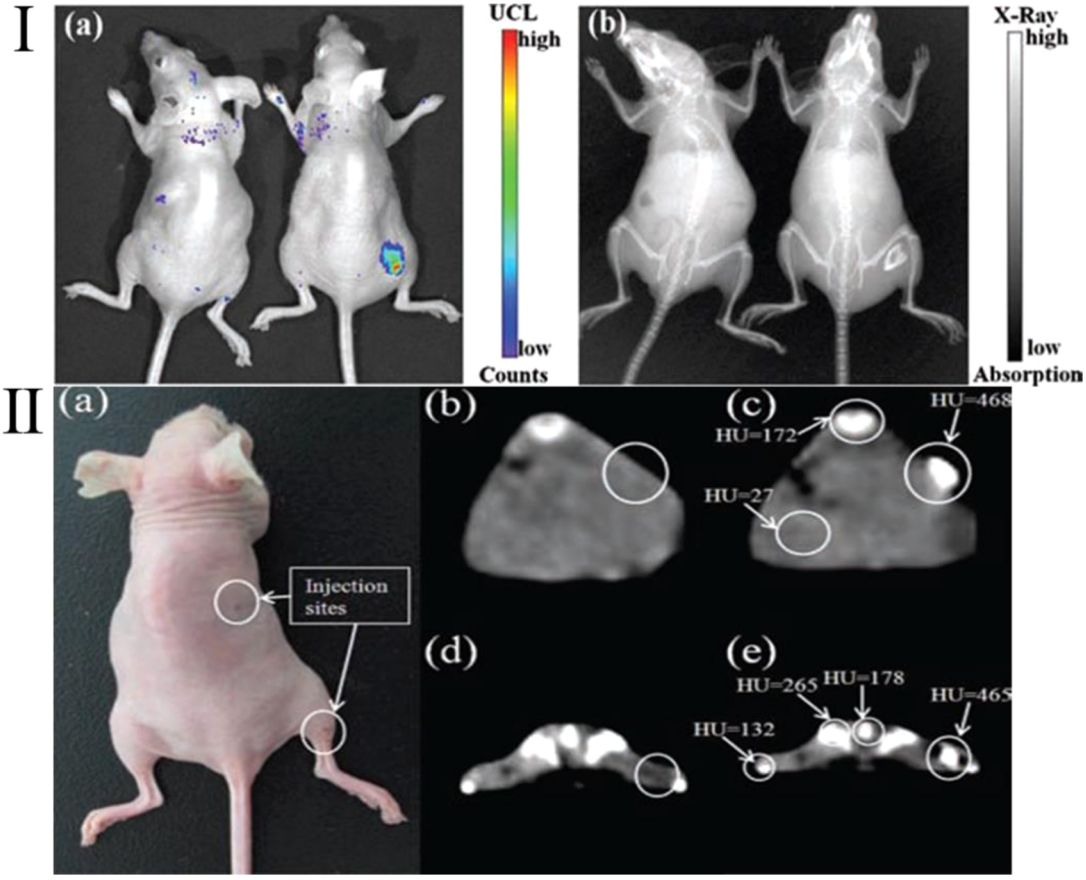


**Figure 29.** In vivo UC PL imaging (I a) and X-ray imaging (I b) of mice after subcutaneous injection (left) without and (right) with $NaGdF_4$:$Yb^{3+}$/$Er^{3+}$. In vivo CT images of mice after subcutaneous injection with lanthanide-doped $NaGdF_4$ UCNPs suspended in PBS. (II a) The photograph of the injected mouse; (II b,c) the transverse image of the back, the HU value of the injection site is 468; (II d,e) the transverse image of the buttock, the HU value of the injection site is 465. Reprinted with permission from ref 427. Copyright 2011 John Wiley and Sons.

lymph nodal study and diagnosis without skin surgery. By introducing the high UC luminescence quantum yield $NaLuF_4$ as a luminescent shell, Li et al. also designed and synthesized the core/shell upconversion-magnetic $Fe_3O_4$@$NaLuF_4$:$Yb^{3+}$/$Er^{3+}$/$Tm^{3+}$ nanostructure for UC PL and $T_2$MR imaging.[426]

**7.5.2. Upconversion Photoluminescence and X-ray Computed Tomography (CT).** X-ray computed tomography (CT) is an imaging procedure that uses computer-processed X-rays to produce tomographic images of specific areas of the body. These cross-sectional images are used for diagnostic and therapeutic purposes in various medical disciplines. Lanthanide elements have higher atomic numbers and K-edge values within the X-ray spectrum in medical use, thus providing an opportunity to create strong X-ray attenuation for enhanced CT. The combined use of lanthanide-doped UCNPs as CT and UC PL imaging contrast agents has attracted wide interests recently. For example, Cui et al. reported on lanthanide-doped $NaGdF_4$ UCNPS as effective contrast agents for dual-mode UC PL imaging and CT imaging in vivo, as can be seen in Figure 29.[427] Importantly, by optimizing the CT contrast elements in the UCNPs according to the fundamental principles of X-ray imaging, Lu et al. have synthesized several nanoparticulate CT contrast agents with excellent imaging performance.[428,429] For example, an $Yb^{3+}$-based $NaYbF_4$ agent provides enhanced contrast as compared to currently available CT contrast agents under normal operating conditions.[430] They also integrated both $Ba^{2+}$ and $Yb^{3+}$ with great differential in K-edge value into a single NP to yield the first example of binary contrast agents, which display much higher contrast than iodinated agents at different voltages and is highly suited to diagnostic imaging of various patients.[431] However, the developed NPs by Lu et al. are incapable of implementing simultaneous CT and UC PL imaging due to the lack of luminescent activators in the matrix. This drawback can be overcome by introducing $Tm^{3+}$- or $Er^{3+}$-dopants into $NaYbF_4$ and $BaYbF_5$ nanoparticles.[380,432] Interestingly, Shi et al. found that, in addition to CT and UC PL bioimaging, $BaYbF_5$:$Er^{3+}$ nanocubes can also work as irradiation dose enhancers in tumors during radiotherapy.[380] This provides a theranostic paradigm for UCNPs, whereby the precise positioning of tumor is entailed by their role in multimodal imaging, and tumor eradiating is implemented via radiotherapy through their role as irradiation enhancer. Varying types of heavy metal element in the host lattice of UCNPs to have a prominent radiotherapy enhancement effect will be an interesting area to explore.

**7.5.3. Upconversion Photoluminescence and Positron Emission Tomography (PET).** Positron emission tomography (PET) is a nuclear medicine imaging technique that produces a three-dimensional image in the body by detecting pairs of $\gamma$ rays emitted indirectly by a positron-emitting radionuclide in the imaging contrast agents. The development of a new imaging contrast agent that combines UC PL and PET is exciting because of the opportunity to obtain more anatomical and physiological details of living systems. In particular, PET imaging using $^{18}F$, which is the most widely used radionuclide, has become an established clinical tool for


dx.doi.org/10.1021/cr400425h | Chem. Rev. 2014, 114, 5161−5214

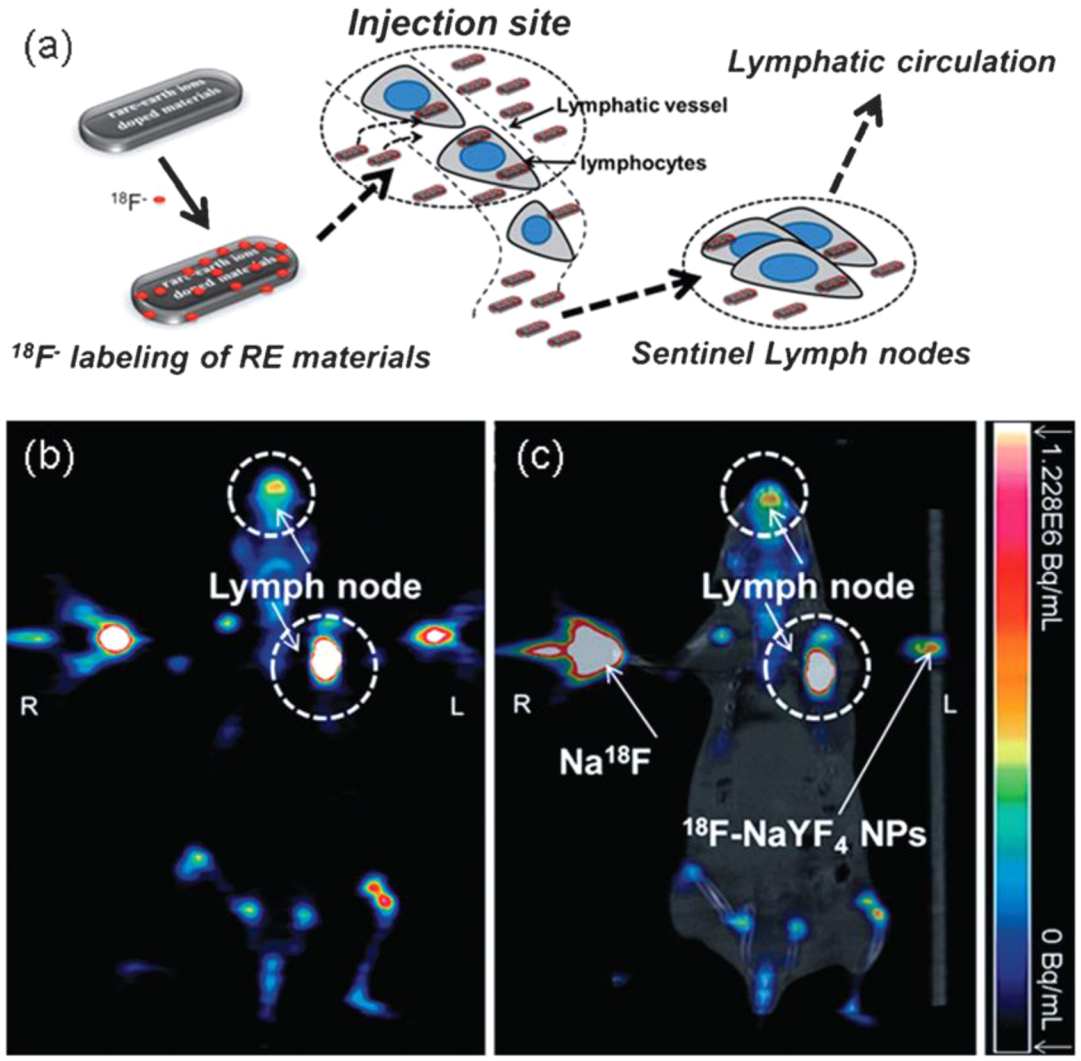


**Figure 30.** (a) Schematic representation of preparation of $^{18}$F-labeled rare-earth (RE) materials and lymph node imaging mechanism. The $^{18}$F-labeling is by virtue of a reaction between RE ions and $^{18}$F. Entrance of lymphotropic materials into lymph nodes is mainly via nonselective endothelial transcytosis into the lymph nodes via the lymphatic system. PET imaging (b) and PET/CT imaging (c) of lymph node 30 min after subcutaneous injection of $^{18}$F-UCNPs. Thirty minutes after subcutaneous injection of $^{18}$F-UCNPs into the left paw footpad, the signal in lymph node quickly reached the peak intensity and maintained up to 60 min post injection, while as control free $^{18}$F ions injected into the right paw showed no lymphatic imaging ability. Reprinted with permission from ref 62. Copyright 2011 Elsevier B.V.

whole-body imaging. Because of a short half-life of $^{18}$F, a quick coupling of $^{18}$F into the probe with a high reaction yield is of vital importance. Li et al. developed a simple, rapid, and efficient strategy (Figure 30a) to synthesize $^{18}$F-labeled UCNPs by immersion of UCNPs with $^{18}$F containing solution for five minutes.[62] The strong binding between $^{18}$F and lanthanide ions can attract $^{18}F^-$ onto the UCNPs surface in a convenient way. It is found that these $^{18}$F-labeled UCNPs could be used for PET imaging of their in vivo distribution giving applications in lymph monitoring (Figure 30b). Combining the application of UCL imaging in cells and tissue, $^{18}$F-labeled UCNPs become a useful contrast agent to provide both UCPL and PET imaging.

**7.5.4. Upconversion Photoluminescence, Magnetic Resonance Imaging (MRI), and Positron Emission Tomography (PET) or X-ray Computed Tomography (CT).** The combination of UCNPs with different properties can offer synergistic multifunctional nanomedical platforms with optical, magnetic, and radioactive properties, which make them possible to accomplish multimodal imaging. The incorporation of multimodal capability in UCNPs generally relies on the selection of appropriate lanthanide ions in the host lattice or the choice of proper surface treatment with desired imaging capability. For example, Li and co-workers developed a radioactive, magnetic UCNPs based on $^{18}$F-labeled $NaYF_4:Gd^{3+}/Yb^{3+}/Er^{3+}$ or $NaYF_4:Yb^{3+}/Tm^{3+}@NaGdF_4$, in which the $^{18}$F radionuclide on the treated nanoparticle surface enables the PET imaging, the $Gd^{3+}$ ions enable the MRI imaging, and the $Yb^{3+}/Er^{3+}$ provides the ability for UC PL imaging.[433] Another effective way to incorporate a set of imaging modalities in UCNPs is to employ a core/shell structure in which separate layers and nanoparticle surface parts are intended for different imaging modalities. The advantage of this strategy is that the different imaging modalities are spatially isolated, minimizing the interference between each other. For example, core−shell $Fe_3O_4@NaLuF_4:Yb^{3+}/Er^{3+}/Tm^{3+}$ nanostructure and $NaLuF_4:Yb^{3+}/Tm^{3+}@SiO_2$−GdDTPA have been reported as imaging probes for trimodality CT/MRI/UCPL imaging (see Figure 31).[422,426] $TaO_x$-decorated $NaYF_4:Yb^{3+}/Er^{3+}/Tm^{3+}@NaGdF_4$ core/shell UCNPs have also been reported by Shi et al. for in vivo CT/MR/UCL trimodal


dx.doi.org/10.1021/cr400425h | Chem. Rev. 2014, 114, 5161−5214

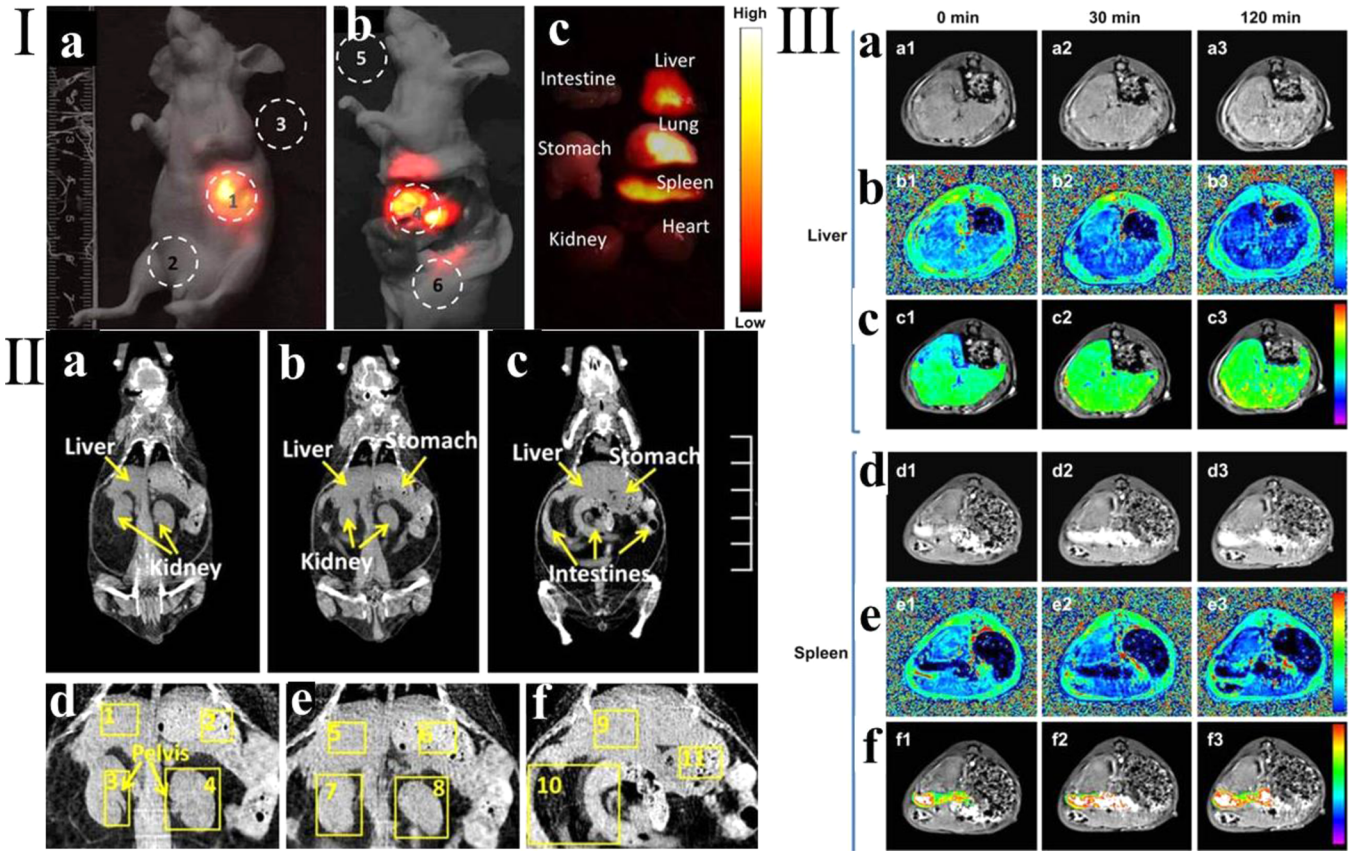


**Figure 31.** (I a) In vivo UC PL imaging of a nude mouse after injection with UCNP@$SiO_2$-GdDTPA for 10 min. (I b) Ex vivo UC PL imaging of the same but sacrificed nude mouse. (I c) Ex vivo UC PL image of main organs of the sacrificed nude mouse. (II a−c) Serials of coronal CT images of Kunming mouse at different layers after injection of UCNP@$SiO_2$-GdDTPA. (II e−g) Enlarged CT views of the abdomen. (III a,d) T1-weighted MRI images of liver (III a) and spleen (III d) at 0, 30, and 120 min after injection of UCNP@$SiO_2$-GdDTPA. (III b,e) T1 distribution images of liver (III b) and spleen (III e) at 0, 30, and 120 min after injection of UCNP@$SiO_2$-GdDTPA. (III c,f) Local colorized T1-weighted MR images of liver (III c) and spleen (III f) at 0, 30, and 120 min after injection of UCNP@$SiO_2$-GdDTPA. Reprinted with permission from ref 422. Copyright 2012 Elsevier B.V.

imaging.[434] More recently, $NaLuF_4$:Yb,Tm@$NaGdF_4$($^{153}$Sm) core/shell UCNPs have been reported for SPECT/CT/MR/UC PL four-modal bioimaging.[435] The essence to construct multimodal imaging nanoprobes is to utilize the paramagnetic properties of $Gd^{3+}$, $Fe_3O_4$, $TaO_x$ to realize MRI imaging, the high attenuation of X-ray of lanthanide ions (e.g., $Lu^{3+}$ or $Yb^{3+}$) to realize CT imaging, the $Yb^{3+}$, $Er^{3+}$/$Tm^{3+}$ lanthanide elements to realize the UC PL, and the radionuclide $^{153}$Sm for SPECT imaging or the $^{18}$F radionuclide for PET imaging. Multimodal imaging contrast agents of needs can be accomplished in particulate formulations by careful selections of a combination of lanthanide ions in well-defined hierarchical nanostructures with appropriately engineered nanoparticle surface. Moreover, multimodal UCNPs can conjugate with photoactivated platinum(IV) pro-drug to realize a multifunctional drug delivery system for imaging-guided cancer therapy, which incorporates UCPL/CT/MR trimodal imaging and NIR-activated platinum pro-drug delivery.[436]

### 7.6. Future Directions for High Contrast Bioimaging

UCNPs have been successfully used for high contrast in vitro, in vivo bioimaging as well as for multimodal imaging. The optical imaging depth can reach 3.2 cm in biological tissues (pork) using NIR-to-NIR UCNPs. However, there are still several interesting or important fields that need to be explored. Although the efficiency of UCNPs can play vital roles in all kinds of applications (see section 2.6), we will not include such discussion in the following, and instead we focus on imaging-related future directions.

(i) Despite few works on active target bioimaging, most investigations on PL or multimodal imaging are limited to passive bioimaging. Future work on targeted imaging needs to be explored. Using UCNPs in animal models to help solve practical biological or medical problems would be the next step.

(ii) Diffuse optical tomography using UCNPs has been limited to reconstruct 3-D images in tissue phantoms. Extensions of it into biological tissues, living biological bodies, or human tissues would be attractive.

(iii) Despite a few successful examples, the development of multifunctional nanoprobes based on UCNPs for multimodal imaging is still in its infancy. It remains a challenge to construct multimodial probes with compatible design. Development of a multifunctional nanoprobe for simultaneous bioimaging covering optical imaging, MRI, PET, SPECT, and CT monitoring would be an interesting topic.

(iv) Photoacoustic imaging is an emerging high-resolution imaging modality, which can work perfectly based on plasmonic nanostructures. Plasmonic UCNP nanostructures have been constructed to investigate plasmonic enhancement of UC PL (see section 2.3). The interaction of photoaccoustic imaging with UC PL imaging using plasmonic UCNP nanostructures will be an interesting topic to explore.


dx.doi.org/10.1021/cr400425h | *Chem. Rev.* 2014, 114, 5161−5214

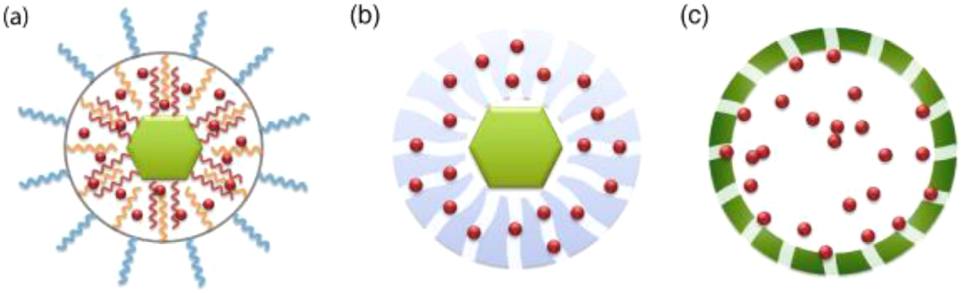


**Figure 32.** Schematic representation of current approaches to construct UCNP-based drug delivery systems: (a) hydrophobic pockets, (b) mesoporous silica shells, and (c) hollow mesoporous-coated spheres. Reprinted with permission from ref 99. Copyright 2013 Elsevier B.V.

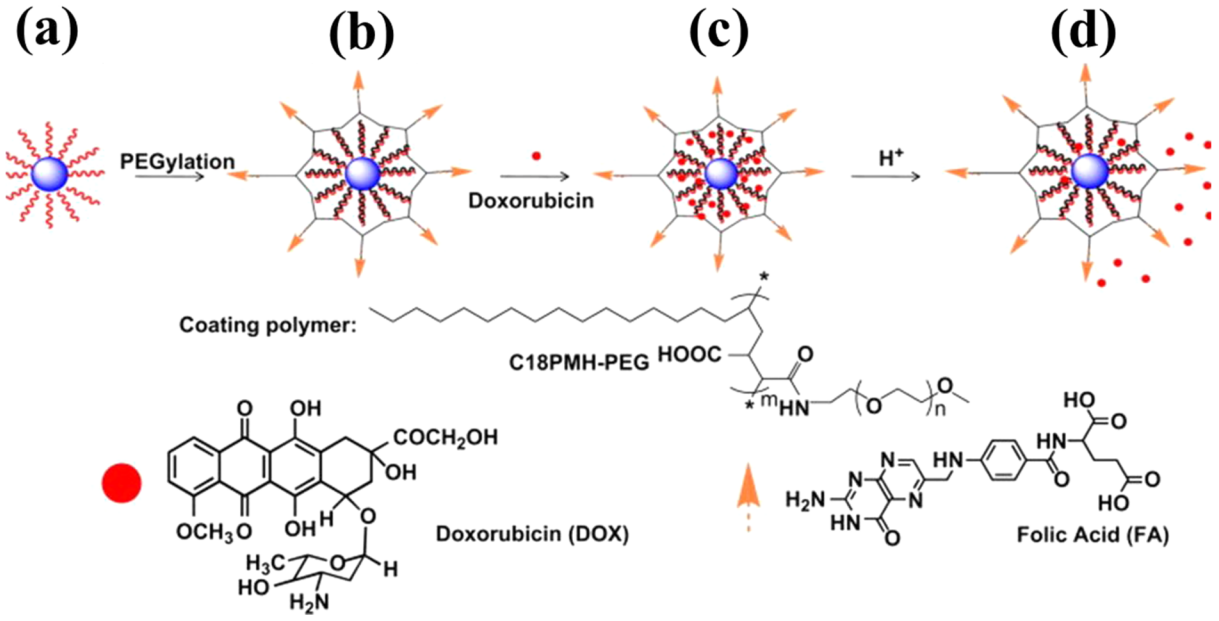


**Figure 33.** Schematic illustration of the UCNP-based drug delivery system. (a) As-synthesized oleic acid capped UCNPs; (b) C18PMH-PEG-FA functionalized UCNPs; (c) the loading of DOX on UCNPs; DOX molecules are physically adsorbed into the oleic acid layer on the nanoparticle surface by hydrophobic interactions; and (d) release of DOX from UCNPs triggered by decreasing pH. Reprinted with permission from ref 53. Copyright 2011 Elsevier B.V.

(v) Nanotoxicology studies in vitro and in vivo did not show the toxic effect of UCNPs. However, these conclusions based on small animals like mice and zebra fish are probably different from the human body. Future toxic investigations on nonhuman primates might provide useful information for their clinical translation.

(vi) Efficient UCNPs with clearable capability will be an appealing future direction. It requires a systematic optimization of present systems including the small size, the appropriate surface chemistry, the high efficiency, and the long circulation capability.

## 8. APPLICATION OF UPCONVERSION NANOPARTICLES IN DRUG DELIVERY AND THERAPY

The unique optical properties and high degree of tunability inherent in UCNPs make these particles highly attractive candidates for drug delivery and therapy applications. Their special features allow them to overcome various problems associated with conventional imaging probes and to provide versatility for creating nanoplatforms with both imaging and therapeutic modalities. Here, we survey the applications of UCNPs for drug delivery and therapy.

### 8.1. Drug Delivery

Drug delivery systems can enhance the efficacy of various pharmaceutical payloads and improve the solubility, stability, biodistribution, and pharmacokinetics of drugs.[13] There are three approaches in literature to build up UCNP-based systems for drug delivery: (i) hydrophobic pockets, (ii) mesoporous silica shells, and (iii) hollow spheres with mesoporous surface.

In the first method, hydrophobic drugs are encapsulated into "hydrophobic pockets" on the UCNP surface utilizing the hydrophobic−hydrophobic interaction between the hydrophobic ligand on the particle surface and the drugs. An example is PEGylated amphiphilic polymer onto the OA-capped $NaYF_4$:$Yb^{3+}$/$Er^{3+}$ UCNPs (see section 5.6), which creates a hydrophobic pocket on the particle surface whereby anticancer drug molecules of doxorubicin (DOX) could be partitioned (Figure 33a). The release of DOX was controlled by varying the pH of the solution, which has a higher rate at decreased pH. The result is favorable for controlled drug release in tumor cells.[53] Recently, a similar method was reported in the $NaYF_4$:$Yb^{3+}$/$Er^{3+}$ and iron oxide nanocomposites, which enables concurrent optical imaging and magnetic-targeted drug delivery.[437]


dx.doi.org/10.1021/cr400425h | Chem. Rev. 2014, 114, 5161−5214

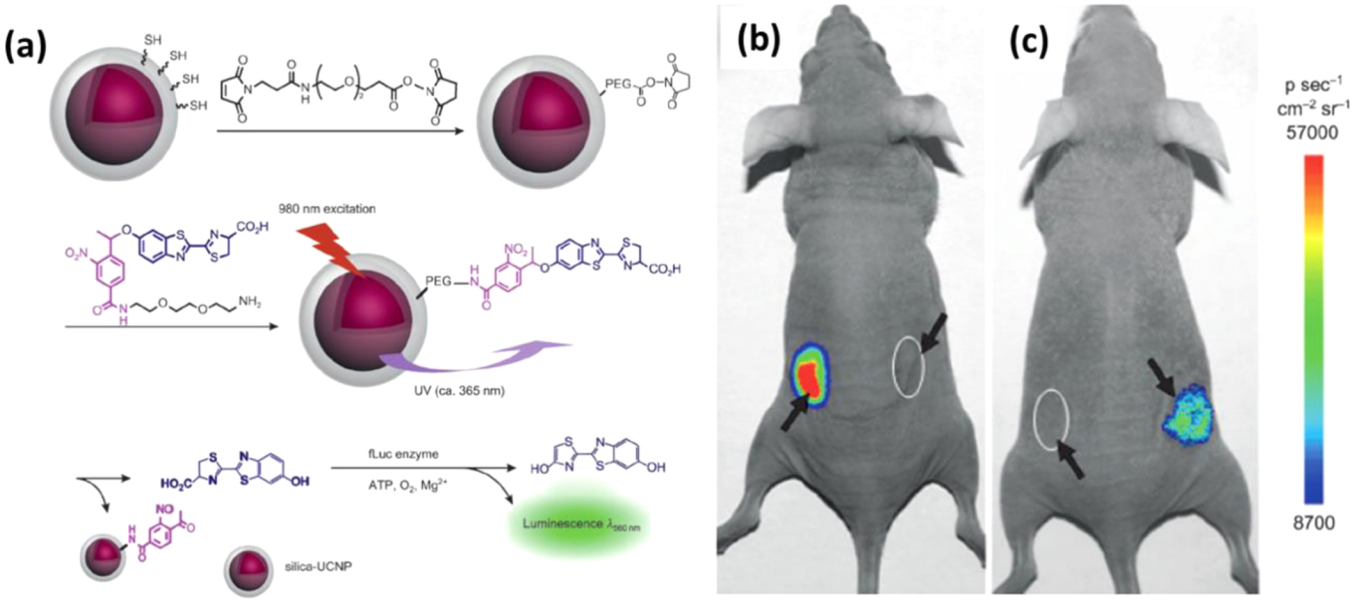


**Figure 34.** (a) Chemical design for uncaging D-luciferin and subsequent bioluminescence through the use of photocaged UCNPs. (b,c) Bioluminescent images of living mice that were treated with D-luciferin. (b) Left ellipse, injection with D-luciferin (20 mm, 20 mL); right ellipse, injection with photocaged nanoparticles without NIR light irradiation. (c) Left ellipse, injection with photocaged nanoparticles and irradiation with UV light for 10 min; right ellipse, injection with photocaged nanoparticles and irradiation with NIR light for 1 h. Comparison of (b) and (c) clearly indicates the NIR-induced release of D-luciferin in deep tissues. Reprinted with permission from ref 449. Copyright 2012 John Wiley and Sons.

In the second method, drugs are deposited in the pores of mesoporous silica shells coated onto the surface of UCNPs (Figure 33b). The mesopores in the silica shell have a high surface area and large pore volume, enabling it to accommodate large amount of drugs. For example, ibuprofen was added to mesoporous silica-coated $\beta$-$NaYF_4$:$Yb^{3+}$/$Er^{3+}$ UCNPs fibers, which were fabricated by an electrospinning process.[438] The ibuprofen-loading capability was further refined by the same researchers, who developed mesoporous silica-coated $\alpha$-$NaYF_4$:$Yb^{3+}$/$Er^{3+}$ nanospheres via a simple two-step sol−gel modification process. The ibuprofen load was modulated by varying the thicknesses of mesoporous $SiO_2$ layers.[325] Multifunctional nanocarriers based on the UC luminescent nanoparticles of $NaYF_4$:$Yb^{3+}$/$Er^{3+}$ core (UCNPs) and thermo/pH-coupling sensitive polymer poly[(*N*-isopropylacrylamide)-*co*-(methacrylic acid)] (P(NIPAm-*co*-MAA)) gated mesoporous silica shell are reported for cancer theranostics, including UC PL imaging, and for controlled drug release for therapy.[439]

In the third method, drugs are loaded into a hollow UCNP with a mesoporous shell (Figure 32c). The hollow structure enables adequate levels of drug loading while maintaining UC PL imaging ability. In this regard, Lin et al. reported on monodisperse core/shell structured upconverting Yb(OH)-$CO_3$@$YbPO_4$:$Er^{3+}$ hollow spheres as drug carriers for the anticancer drug of DOX.[440] It is found that DOX is shuttled into cells by core/shell hollow spheres carrier and released inside cells after endocytosis, and the DOX-loaded spheres exhibited much greater cytotoxicity than free DOX. Similarly, $Y_2O_3$:$Yb^{3+}$/$Er^{3+}$ hollow nanospheres have been synthesized for delivery of DOX into HeLa cells, which enable high contrast cellular and tissue imaging with no damage from radiation.[441] Importantly, a nanorattle system was recently developed through an ion-exchange process for magnetic-guided chemotherapy.[442] This nanorattle is a multifunctional mesoporous nanostructure, which consists of a hydrophilic lanthanide-doped $NaYF_4$ shell and an inner magnetic nanoparticle, and thus possesses both upconverting luminescent and magnetic properties. DOX was successfully loaded into the hollow volume of the nanorattle via the porous UCNP layer. In vivo experiments showed highly encouraging tumor shrinkage with doxorubicin and significantly enhanced tumor targeting in the presence of an applied magnetic field.

### 8.2. In Vitro and In Vivo Photoactivations

UV radiation-mediated photochemical reactions are of particular importance in advanced imaging, chemical biology, and drug-delivery systems. UV photons can manipulate the functions of biomolecules or mediate on-demand drug release in live systems via effective photoactivation. However, UV lamps or lasers produce an excessively large radiation area and have major drawbacks such as severe phototoxicity and significantly limited tissue penetrability. Hence, NIR-to-UV UCNPs play vital roles for these biomedical endeavors, which can spatiotemporally restrict photochemical reactions in the nanometer regime with minimal photodamage, have an excellent light penetration depth due to the use of NIR light excitation, and produce desired effects with a precise light control. These endeavors encompass two directions: (i) NIR light-induced photoswitching of molecular switches to toggle back and forth between two structurally and electronically different isomers; and (ii) NIR light-induced photoreleasing of molecular moieties or drugs.

In the first direction, Branda et al. designed a remote control of ring-opening or ring-closing of dithienylethene (DTE) photoswitches using two types of NIR-to-UV $\beta$-$NaYF_4$:$Yb^{3+}$/$Tm^{3+}$ and NIR-to-green $\beta$-$NaYF_4$:$Yb^{3+}$/$Tm^{3+}$ UCNPs that are both excited at 980 nm.[443] It is demonstrated that the UV UC emissions can close the opened DTE isomer, while the green UC emission can open the ring of the closed DTE isomer. However, these results are demonstrated separately in two thin films containing distinct types of UCNPs, limiting their applications in biomedcine. Later, the same group produced in situ photoswitching of DTE molecules using one type of


dx.doi.org/10.1021/cr400425h | *Chem. Rev.* 2014, 114, 5161−5214

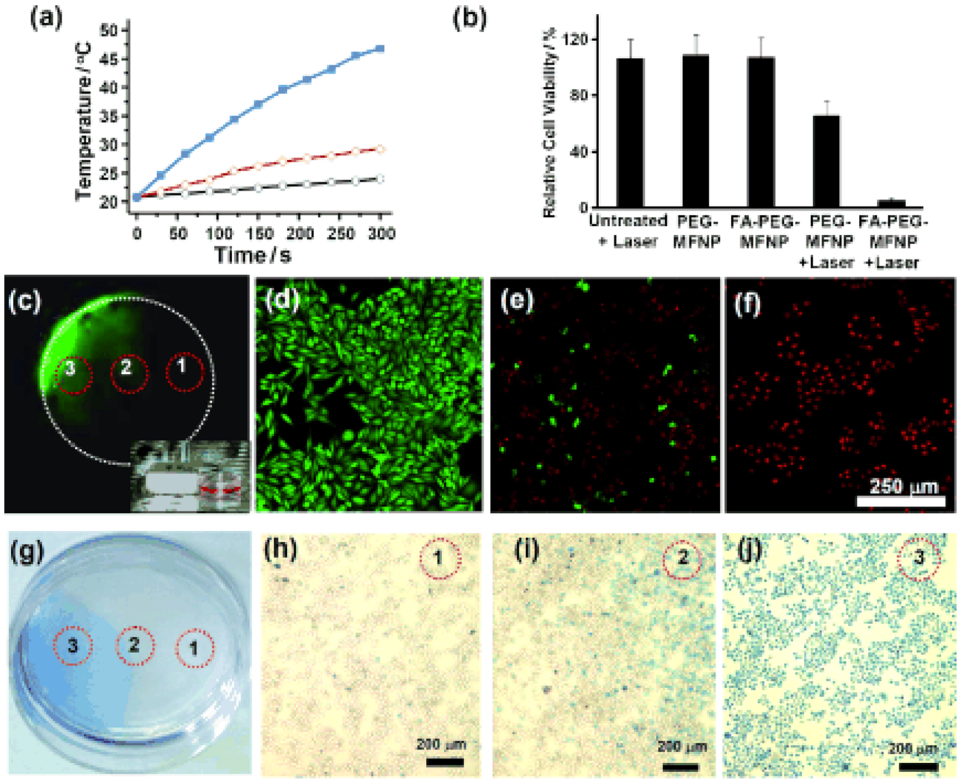


**Figure 35.** Dual-targeted photothermal ablation of cancer cells. (a) The heating curves of water (○), UCNP-iron oxide nanocomposite (◇), and multifunctional nanoparticles (MFNPs) under 808 nm laser irradiation. (b) Relative viabilities of PEG-MFNP or FA-PEG-MFNP treated KB cells with or without 808 nm laser irradiation. (c) A UCPL image of HeLa cells in a culture dish after incubation with PEG-MFNP in the presence of magnetic field taken by the Maestro in vivo imaging system (980 nm excitation). Inset: A photo showing the experimental setup. A magnet was placed close to the cell culture dish. (d–f) Confocal images of calcein AM (green, live cells) and propidium iodide (red, dead cells) costained cells after magnetic targeted PTT. Images were taken at different locations in the culture dish: (1) far from the magnet (d), (2) in the middle (e), and (3) close to the magnet (f). (g) A digital photo of the cell culture dish after magnetic targeted PTT and trypan blue staining. (h–j) Optical microscopy images of trypan blue stained cells after magnetic targeted PTT. Reprinted with permission from ref 63. Copyright 2011 John Wiley and Sons.

core–shell–shell $NaYF_4$ nanoparticles with $Er^{3+}/Yb^{3+}$ and $Tm^{3+}/Yb^{3+}$ ions doped into separate layers.[444] Because of the different dependence on the excitation density, the two-photon green UC in core–shell–shell UCNPs dominates at low density, while at high density the four-photon UV UC dominates. This feature provides a convenient way to photoswitch the DTE by merely adjusting the intensity of the 980 nm excitation light. However, the molecular switches and UCNPs have large distance in solution, which severely limits the energy transfer between the components, and thus increases the amount of irradiation time required for the photoreactions to occur. A more efficient way to implement photoswitching is to graft molecules onto the surface of UCNPs, which enables efficient FRET or LRET mechanism to trigger the ring-open or ring-close process. Capobianco et al. reported on the grafting of bis-spiropyran molecules onto the NIR-to-UV $LiYF_4:Yb^{3+}/Tm^{3+}$ UCNPs.[445] The transformation of the ring-closed bis-spiropyran form to the ring-open bis-merocyanine form takes only 3 min using this nanoplatform. It is worth pointing out that opposite to the use of UCNPs to manipulate the optical properties of molecule switches, the switched absorption peaks can be also be utilized to manipulate the color out of UCNPs either inside the film or in cell imaging by simply changing the irradiating lamp light wavelength.[446,447]

The second direction is of particular importance for the light-regulated release process in vitro and in vivo, such as the delivery of various molecules like proteins, peptides, nucleic acids, amino acids, and drugs into the desired sites of cells/animals. Light-sensitive functional groups are generally involved in the delivery system, which are cleavable upon UV light irradiation. On the basis of this simple idea, a range of systems have been developed. Zhang et al. reported on NIR-to-UV UCNPs for activating photocaged nucleic acids in much deeper tissues as compared to conventional systems.[448] Photocaged GFP-loaded UCNPs under the skin of mice and activated using the NIR laser have also been demonstrated. Xing et al. reported a system for the controlled uncaging of D-luciferin from D-luciferin-conjugated NIR-to-UV UCNPs. The released D-luciferin effectively conferred enhanced fluorescence and bioluminescence signals in vitro and in vivo with deep light penetration and low cellular damage (see Figure 34).[449] NIR light-induced siRNA release for RNA interference,[450] controllable drug delivery,[436,451,452] and rapid in situ photoactivation in live cells have also been presented recently using NIR-to-UV fluoride nanoparticles.[164] The chemistry of using the UV-photocleavable linkers to link the pertinent components onto the surface of UCNPs is quite important for these applications. Interestingly, UC PL of UCNPs can also trigger photoreactions of the NO precursor, iron/sulfur/nitrosyl cluster Roussin's black salt anion $Fe_4S_3(NO)_7^-$, to release NO into physiological targets.[453,454] Moreover, the disruption of UV-sensitive micelles,[455] hydrogels,[456] as well as UV-degradable polymer for theranostic drug release has also been presented using NIR-to-UV UCNPs.[457] Considering the wide interest in NIR light


dx.doi.org/10.1021/cr400425h | Chem. Rev. 2014, 114, 5161–5214

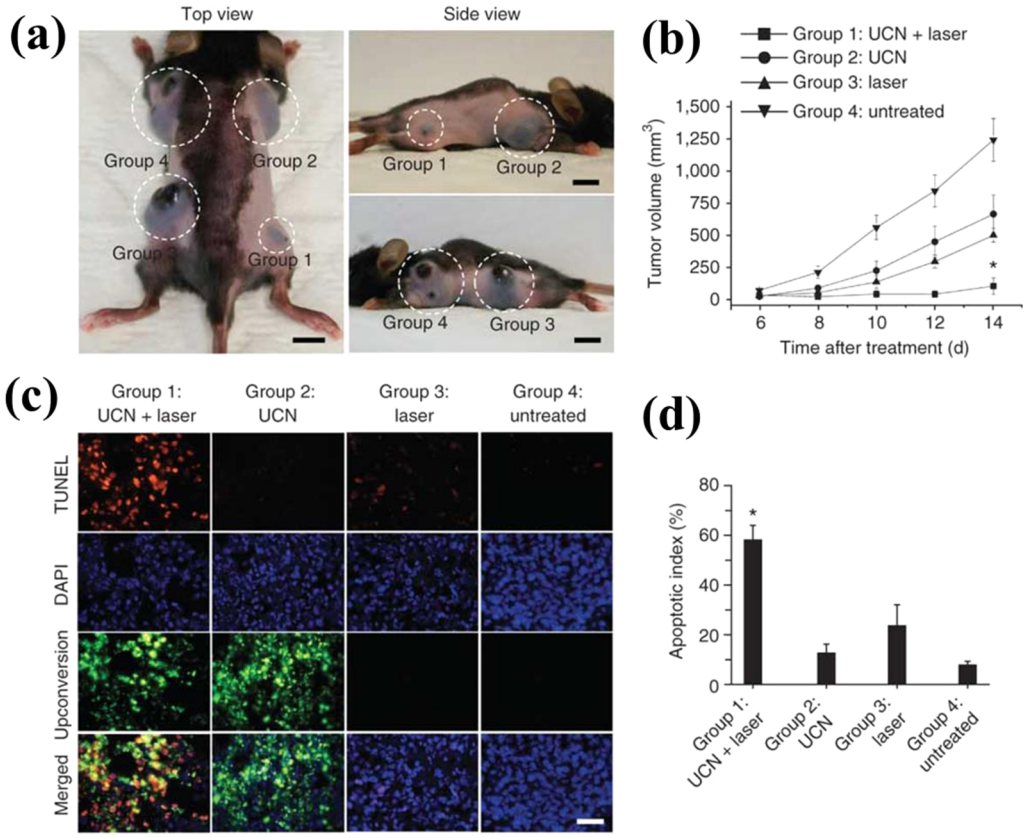


**Figure 36.** (a) Representative gross photos of a mouse showing tumors (highlighted by dashed white circles) at 14 d after treatment with the conditions described for groups 1−4. Scale bars, 10 mm. (b) Tumor volumes in the four treatment groups at 6, 8, 10, 12, and 14 d after treatment to determine the effectiveness of the treatment in terms of tumor cell growth inhibition. (c) TUNEL staining of tissue sections from the treatment groups at 24 h after treatment to determine the effectiveness of the treatment in terms of tumor cell death by apoptosis. DAPI counterstaining indicates the nuclear region, and upconversion fluorescence imaging indicates the position of the injected UCNP-labeled cell (×400 magnification). Scale bar, 20 $\mu$m. (d) The apoptotic index charted as the percentage of TUNEL-positive apoptotic nuclei divided by the total number of nuclei visualized by counterstaining with DAPI obtained from counts of randomly chosen microscopic fields. Reprinted with permission from ref 64. Copyright 2012 Nature Publishing Group.

activation for bioapplications, development of highly efficient NIR-to-UV UCNPs will be of great importance.

### 8.3. Upconversion-Guided Photothermal Therapy

Photothermal therapy (PTT) employs photoabsorbers to generate heat from light absorption, leading to thermal ablation of cancer cells. In recent years, PTT has emerged as an increasingly recognized alternative to classical cancer therapies such as surgery, radiotherapy, and chemotherapy.[19] Various nanomaterials with high optical absorbance have been highly successful in this application. Because of the low extinction coefficient of lanthanide ions, UCNPs generally have limited capability to convert light directly into heat. However, as mentioned in section 2.3, the UCNPs can be easily coupled to plasmonic nanoparticles that have strong extinction coefficient and are being actively used in PTT treatment of diseases. Indeed, multifunctional nanoparticles have been reported with combined upconverting luminescence, magnetic properties, and PTT function. Ultrasmall superparamagnetic $Fe_3O_4$ nanoparticles, created using layer-by-layer self-assembly, were coated on the surface of 200 nm sized $NaYF_4$:$Yb^{3+}$/$Er^{3+}$ UCNPs, on top of which a thin gold shell was formed by seed-induced reduction growth.[63] The layer of IONPs between UCNPs and the gold shell not only afforded magnetic properties but also reduced the luminescence quenching effects of the gold nanostructure to UCNPs. In addition, dual-targeted PTT ablation of cancer cells was successful at the cell culture level (Figure 35). Similarly, core−shell structured silver-coated $\beta$-$NaYF_4$:$Yb^{3+}$/$Er^{3+}$ nanoparticles have been utilized PTT experiments under excitation of a continuous 980-nm laser diode.[305] PTT was applied in vitro on HepG2 cells from human hepatic cancer and BCap-37 cells from human breast cancer, and the optimum mortality approached 95% with a power density of 1.5 W/cm$^2$, with much lower power than that reported for gold nanoshells and gold nanorods.[305] Moreover, by decorating ultrasmall plasmonic CuS nanoparticles onto the surface of silica-coated UCNPs, this kind of nanotheranostic agent not only entails effective PTT thermal ablation, but also enhances localized radiation dose to increase radiation therapy both in vitro and in vivo.[458]

### 8.4. Upconversion Photodynamic Therapy

Photodynamic therapy (PDT) is a clinical treatment that utilizes phototriggered chemical drugs (photosensitizers) to produce singlet oxygen ($^1O_2$) to kill tumors. Typical PDT treatments involve three components: the photosensitizer, the light source, and the oxygen within the tissue at the disease site.[17] Under appropriate light excitation (generally in the visible range), the photosensitizer can be excited from a ground singlet state to an excited singlet state, which undergoes intersystem crossing to a longer-lived triplet state and then reacts with a nearby oxygen molecule to produce highly


dx.doi.org/10.1021/cr400425h | Chem. Rev. 2014, 114, 5161−5214

cytotoxic $^1O_2$. PDT has been used for therapy in prostate, lung, head and neck, or skin cancers. However, conventional PDT is limited by the penetration depth of visible light needed for its activation.[19] NIR light in the "window of optical transparency" (750−1100 nm) of tissue can penetrate significantly deeper into tissues than the visible light, because absorbance and light scattering for most body constituents are minimal in this range.[17] Importantly, UCNPs can efficiently convert the deeply penetrating near-infrared light to visible wavelengths that can excite photosensitizer to produce cytotoxic $^1O_2$, promising their use in PDT treatment of pertinent located deeply tumors. The idea on UC PDT was first proposed by Prasad in his monograph entitled "*Introduction to Biophotonics*", which was later realized by Zhang et al. who incorporated the PDT with the most efficient $NaYF_4$:$Yb^{3+}$/$Er^{3+}$ UCNPs.[459] It is demonstrated that the viability of MCF-7/AZ bladder cancer cells can be significantly decreased using photosensitizer-impregnated UCNPs upon NIR light irradiation.

A large variety of UCNPs-photosensitizers systems have been established by taking advantage of FRET or LRET from (blue, green, and red) UCNPs to photosensitizers with appropriate absorption. For example, the photosensitizer of tris-(bipyridine)ruthenium(II) ($Ru(bpy)_3^{2+}$) has a maximum absorbance at ca. 450 nm, which is quite close to the blue emission of $Tm^{3+}$. In light of this, blue-emitting $NaYF_4$:$Yb^{3+}$/$Tm^{3+}$ nanoparticles coated by a silica shell containing $Ru(bpy)_3^{2+}$ have been reported to produce $^1O_2$.[460] The green-emitting $\beta$-$NaYF_4$:$Yb^{3+}$/$Er^{3+}$ UCNPs and meso-tetraphenylporphine photosensitizers have been utilized as a pair to kill 75% of HeLa cells.[461] In addition, on the basis of the red-emitting UCNPs, a new and efficient NIR photosensitizing nanoplatform for UC-PDT has been developed.[462] Three commonly used second-generation photosensitizers including Ce6, ZnPc, and MB were loaded into the $\alpha$-CD-functionalized UCNPs to produce effective treatment of cancer cells. However, the loading efficiency of photosensitizers on UCNPs as well as the luminescence efficiency of involved UCNPs remain rather poor, limiting the therapeutic efficacy of UC PDT. Strategies to increase payloads of photosensitizers or to employ more efficient core/shell UCNPs in the future will help improve the therapeutic efficacy of UC PDT.

The effectiveness of UC PDT has also worked in vivo. Recently, Liu et al. reported the pioneer work on in vivo UCNP-based PDT,[463] where the photosensitizing porphyrin derivative chlorine 6 (Ce6) is noncovalently incorporated into PEGylated amphiphilic polymer-coated $\beta$-$NaYF_4$:$Yb^{3+}$/$Er^{3+}$ nanoparticles. Upon directly injecting UCNP-Ce6 into the tumor sites and after 980 nm cw laser excitation, excellent tumor regression was observed.[463,464] However, the selectivity of UCNP-photosensitizer into tumor sites has not been shown in this work, which is important for UC PDT in vivo. The tumor-selectivity of UCNP-photosensitizer can be achieved by placing targeted ligands onto the UC nanoconstruct,[64,465] in which the targeted ligand allows high accumulation of UCNP−photosensitizer complex into tumor areas through specific recognition of the receptors on the cancer cell. Importantly, mesoporous silica-coated UCNPs with a tumor-targeting agent have been developed, which not only allows selective accumulation in tumor, but also permits a high loading of photosensitizers.[323] Moreover, as opposed to previous single photosensitizer approaches, the therapeutic function of UC-PDT was further enhanced by employing a combination of two different kinds of photosensitizers, which can strongly absorb both green and red dominant upconversion emissions of $NaYF_4$:$Yb^{3+}$/$Er^{3+}$ UCNPs. The combined use of two photosensitizers leads to a more efficient utilization of upconverted energy from UCNPs, thus producing greater PDT efficacy.[64] In vivo studies also showed tumor growth inhibition in PDT-treated mice by direct injection of UCNPs into melanoma tumors or intravenous injection of UCNPs conjugated with a tumor-targeting agent into tumor-bearing mice (Figure 36). Interestingly, UC-PDT has been extended to inactivation of viruses, suggesting a new type of promising antiviral approach with feasible applications in the treatment of virus-associated infections, lesions, and cancers.[466]

### 8.5. Future Directions for Therapeutics

UCNP-based therapeutic applications have shown promising results in drug delivery, light-regulated drug release, PTT, and PDT. However, most of the therapeutic results have been done in vitro with limited works in vivo. Therapeutic investigations of UCNPs in rodents will be an interesting exploration. To improve the chemotherapeutic efficacy, new designs of UCNPs-based therapeutic agents are important, which have a high payload of drugs and enable targeted release of therapeutic drugs. In addition, the treatment modalities of PDT and PTT are compatible with each other on the surface of UCNPs. The combined use of PDT and PTT in UCNPs might be able to result in an impressive therapeutic improvement. Moreover, theranostic agents for simultaneous medical diagnosis and therapy are needed in the future. An extensive exploration of imaging-guided delivery or therapy to treat cancers or malignant diseases will be appealing.

## 9. CONCLUDING REMARKS

In this Review, we have surveyed recent advancements in the design, nanochemistry, and theranostic applications of UCNPs. Indeed, these small-sized upconversion nanoparticles have attracted tremendous attention in theranostics due to their unique optical and chemical properties such as nonblinking, nonphotobleaching, absence of autofluorescence, low-toxicity, low photodamage to live cells, and their remarkable ability to penetrate light in tissues. They are now active in medical diagnostics and imaging, biosensing, drug delivery, photoactivation, and light-activated therapy. Multimodal UCNPs involving PL, MRI, PET, SPECT, and CT are emerging as a new set of theranostic nanoprobes for a broad spectrum of biomedical applications. However, practical applications of UCNPs set demanding requirements on their optical properties, their size and shape, their surface chemistry, their clinical prospects, as well as their ability to incorporate a number of imaging and therapy modalities to entail more accurate diagnostics and more effective therapeutics. New advancements in diverse aspects are needed to make rapid progress of this field toward this end. Although we have provided our opinions on future directions in each section of this Review on a particular aspect, here we would like to highlight some future directions that can produce pronounced effects in the field.

(1) The brightness of UCNPs is still unsatisfactory, in particular, under low excitation density of $10^{-2}$−$10^{-1}$ W/cm$^2$. This arises from two reasons: (i) the low quantum yield or low efficiency and (ii) the narrow and low extinction coefficient of UCNPs. Manipulation of local environment around the lanthanide dopants in UCNPs may be a promising direction to enhance the quantum yield. The drawback of low extinction coefficient of UCNPs is an intrinsic feature of 4f−4f optical


dx.doi.org/10.1021/cr400425h | *Chem. Rev.* 2014, 114, 5161−5214

transitions in lanthanide ions. An antenna effect from dyes, plasmons, quantum dots, or other doping elements with a strong absorption might be of great help to increase the brightness.

(2) The excitation wavelength of UCNPs is generally limited at ~980 nm (matching the absorption of sensitizer $Yb^{3+}$ ions). However, it overlaps with the absorption of water, which can cause damaging heating effect in biological tissues. The shift of the excitation wavelength to a more appropriate wavelength is appealing; for example, using $Nd^{3+}$ as a second sensitizer to sensitize the first sensitizer $Yb^{3+}$ can blue-shift the excitation wavelength to ~800 nm.[467−469] Dye-sensitized UCNPs will be another appealing approach to shift the excitation wavelength.

(3) The reported strategies to tune upconversion are often accompanied by a reduction of luminescent efficiency due to unwanted cross relaxations between different lanthanide ions. Tuning upconversion using core/shell structures and with minimized surface-related deactivations is promising, which can spatially isolate lanthanide ions in the core or the shell. The coupling of upconversion mechanisms in core/shell UCNPs with other types of emitters (like organic dyes) through FRET or LRET may open a totally new design criterion for achieving wide tunability of wavelengths but at higher efficiency. In addition, optical upconversion multiplexing or detection in the time domain will be an attractive new direction to explore.

(4) UCNPs are generally unable to biodegrade into biologically benign components. Thus, an efficient clearance of them is necessary, which requires their hydrodynamic size be less than 10 nm or even smaller. Hence, developing new or modified synthetic strategies to prepare sub-10 nm but efficient UCNPs is of crucial importance in the future. Moreover, surface engineering of these UCNPs to ensure prolonged stability in physiological buffers and long circulation in the blood for passive and/or active targeted delivery will be appealing for in vivo applications in the future.

(5) Biosensing and bioarrays using UCNPs can be a next thrust in this field, which provide numerous opportunities for point-of-care diagnostics without the need to refer to demanding clinical assessments.

(6) Development of a multifunctional nanoprobe to cover a broad spectrum of imaging modalities such as optical imaging, MRI, PET, SPECT, and CT would be an interesting topic. Moreover, nanotoxicology of UCNPs is currently limited to mouse and zebra fish investigations; future toxic investigations on nonhuman primates are necessary to provide useful information for their potential clinical translation.

(7) Under the guidance of UCPL-based imaging, the combined use of light-activated therapy (e.g., PDT and PTT) produced in UCNP nanostructure is a promising direction to enable more effective therapeutic effect in vitro and in vivo. Moreover, the integration of light-activated therapy with light-regulated drug delivery in UCNP nanoplatform can become a new direction for more efficient imaging-guided therapy.

## AUTHOR INFORMATION

### Corresponding Authors

*E-mail: guanying@buffalo.edu.
*E-mail: pnprasad@buffalo.edu.
*E-mail: shawn.chen@nih.gov.

### Notes

The authors declare no competing financial interest.

### Biographies

Guanying Chen received his B.S. and Ph.D. degrees in optics in 2004 and 2009, respectively, from Harbin Institute of Technology, P. R. China. He is a full professor at the School of Chemical Engineering and Technology, Harbin Institute of Technology, and a senior research scientist at the Institute for Lasers, Photonics, and Biophotonics, University at Buffalo, State University of New York. He was a postdoctoral fellow (2010−2011) at the Institute for Lasers, Photonics, and Biophotonics, University at Buffalo, State University of New York, and Department of Theoretical Chemistry & Biology, Royal Institute of Technology. He has published about 50 papers in *Chem. Soc. Rev.*, *Acc. Chem. Res.*, *ACS Nano*, *Small*, etc. His interests include lanthanide-doped nanomaterials, nanostructured solar cells, and nanoparticles-based diagnostics and therapeutics.

Hailong Qiu is pursuing his Ph.D. under Professors Guanying Chen and Chunhui Yang at the School of Chemical Engineering and Technology, Harbin Institute of Technology, P. R. China. He is a visiting research scholar at the Institute for Lasers, Photonics, and Biophotonics, University at Buffalo, State University of New York, supported by the fellowship of China Scholarship Council (CSC). His research focuses on lanthanide-doped nanoparticles in two directions: (1) chemical design and synthesis of lanthanide-doped inorganic nanoparticles; and (2) functionalization of lanthanide-doped nanoparticles for applications in bioimaging and solar cells.

Paras N. Prasad is a SUNY Distinguished Professor of Chemistry, Physics, Electrical Engineering and Medicine; the Samuel P. Capen Chair of Chemistry; the Executive Director of Institute for Lasers, Photonics, and Biophotonics, University at Buffalo, State University of New York; and the visiting Distinguished Professor at Korea University. He was named among the top 50 science and technology leaders in the world by Scientific American in 2005. He has published over 700 scientific and technical papers; four monographs (*Introduction to Nanomedicine and Nanobioengineering, Nanophotonics, Introduction to Biophotonics, Introduction to Nonlinear Optical Effects in Molecules and Polymers*); and eight edited books. He received many scientific awards and honors (Morley Medal; Schoellkopf Medal; Guggenheim Fellowship; Fellow of the APS, OSA, and SPIE, etc.). His interests include biophotonics, nanophotonics, nanomedicine, metamaterials, and solar cells.

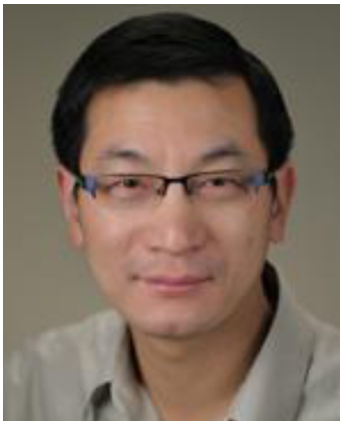

Xiaoyuan Chen earned his B.S. in 1993 and his M.S. in 1996 from Nanjing University, China. He then moved to the United States and obtained his Ph.D. in chemistry from the University of Idaho in 1999. After two quick postdocs at Syracuse University and Washington University in St. Louis, he joined the University of Southern California as an Assistant Professor of Radiology. He then moved to Stanford University in 2004. He was promoted to Associate Professor in 2008, and in the summer of 2009 he joined the intramural research program of the National Institute of Biomedical Imaging and Bioengineering (NIBIB), at the National Institutes of Health, as a senior investigator and chief of the Laboratory of Molecular Imaging and Nanomedicine (LOMIN). Dr. Chen has published over 400 papers, 4 books, and numerous book chapters. He is the founding editor of SCI journal "Theranostics", and sits on the editorial board of over 10 peer-reviewed journals.

## ACKNOWLEDGMENTS

This work was supported by the National Key Basic Research Program (973 Project) (2013CB733802, 2014CB744503), the Natural Science Foundation of China (No. 51102066, 81371596), the Program for Basic Research Excellent Talents in Harbin Institute of Technology (BRETIII 2012018), and the Intramural Research Program (IRP) of the National Institute of Biomedical Imaging and Bioengineering (NIBIB), National Institutes of Health (NIH).

## REFERENCES

(1) Chen, X.; Gambhir, S. S.; Cheon, J. *Acc. Chem. Res.* **2011**, *44*, 841.
(2) Jokerst, J. V.; Gambhir, S. S. *Acc. Chem. Res.* **2011**, *44*, 1050.
(3) Kircher, M. F.; Mahmood, U.; King, R. S.; Weissleder, R.; Josephson, L. *Cancer Res.* **2003**, *63*, 8122.
(4) McDonald, D. M.; Choyke, P. L. *Nat. Med.* **2003**, *9*, 713.
(5) Bunzli, J. C. G. *Chem. Rev.* **2010**, *110*, 2729.
(6) Bunzli, J. C. G.; Eliseeva, S. V. *Chem. Sci.* **2013**, *4*, 1939.
(7) Davis, M. E.; Zuckerman, J. E.; Choi, C. H. J.; Seligson, D.; Tolcher, A.; Alabi, C. A.; Yen, Y.; Heidel, J. D.; Ribas, A. *Nature* **2010**, *464*, 1067.
(8) Malek, A.; Merkel, O.; Fink, L.; Czubayko, F.; Kissel, T.; Aigner, A. *Toxicol. Appl. Pharmacol.* **2009**, *236*, 97.
(9) Jacobson, G. B.; Gonzalez-Gonzalez, E.; Spitler, R.; Shinde, R.; Leake, D.; Kaspar, R. L.; Contag, C. H.; Zare, R. N. *J. Pharm. Sci.* **2010**, *99*, 4261.
(10) Dolmans, D. E. J. G. J.; Fukumura, D.; Jain, R. K. *Nat. Rev. Cancer* **2003**, *3*, 380.
(11) Jain, P. K.; Huang, X. H.; El-Sayed, I. H.; El-Sayed, M. A. *Acc. Chem. Res.* **2008**, *41*, 1578.
(12) Lee, J. H.; Huh, Y. M.; Jun, Y.; Seo, J.; Jang, J.; Song, H. T.; Kim, S.; Cho, E. J.; Yoon, H. G.; Suh, J. S.; Cheon, J. *Nat. Med.* **2007**, *13*, 95.
(13) Xie, J.; Lee, S.; Chen, X. Y. *Adv. Drug Delivery Rev.* **2010**, *62*, 1064.
(14) Gao, X. H.; Cui, Y. Y.; Levenson, R. M.; Chung, L. W. K.; Nie, S. M. *Nat. Biotechnol.* **2004**, *22*, 969.
(15) Medintz, I. L.; Uyeda, H. T.; Goldman, E. R.; Mattoussi, H. *Nat. Mater.* **2005**, *4*, 435.
(16) Welsher, K.; Liu, Z.; Sherlock, S. P.; Robinson, J. T.; Chen, Z.; Daranciang, D.; Dai, H. J. *Nat. Nanotechnol.* **2009**, *4*, 773.
(17) Prasad, P. N. *Introduction to Biophotonics*; Wiley-Interscience: Hoboken, NJ, 2003.
(18) Prasad, P. N. *Nanophotonics*; Wiley-Interscience: Hoboken, NJ, 2004.
(19) Prasad, P. N. *Introduction to Nanomedicine and Nanobioengineering*; Wiley-Interscience: Hoboken, NJ, 2012.
(20) Zhang, J.; Campbell, R. E.; Ting, A. Y.; Tsien, R. Y. *Nat. Rev. Mol. Cell Biol.* **2002**, *3*, 906.
(21) Schrock, E.; duManoir, S.; Veldman, T.; Schoell, B.; Wienberg, J.; FergusonSmith, M. A.; Ning, Y.; Ledbetter, D. H.; BarAm, I.; Soenksen, D.; Garini, Y.; Ried, T. *Science* **1996**, *273*, 494.
(22) Liong, M.; Lu, J.; Kovochich, M.; Xia, T.; Ruehm, S. G.; Nel, A. E.; Tamanoi, F.; Zink, J. I. *ACS Nano* **2008**, *2*, 889.
(23) Radu, D. R.; Lai, C. Y.; Jeftinija, K.; Rowe, E. W.; Jeftinija, S.; Lin, V. S. Y. *J. Am. Chem. Soc.* **2004**, *126*, 13216.
(24) Sakamoto, Y.; Kaneda, M.; Terasaki, O.; Zhao, D. Y.; Kim, J. M.; Stucky, G.; Shim, H. J.; Ryoo, R. *Nature* **2000**, *408*, 449.
(25) Betzig, E.; Patterson, G. H.; Sougrat, R.; Lindwasser, O. W.; Olenych, S.; Bonifacino, J. S.; Davidson, M. W.; Lippincott-Schwartz, J.; Hess, H. F. *Science* **2006**, *313*, 1642.
(26) Nagai, T.; Ibata, K.; Park, E. S.; Kubota, M.; Mikoshiba, K.; Miyawaki, A. *Nat. Biotechnol.* **2002**, *20*, 87.
(27) Shaner, N. C.; Campbell, R. E.; Steinbach, P. A.; Giepmans, B. N. G.; Palmer, A. E.; Tsien, R. Y. *Nat. Biotechnol.* **2004**, *22*, 1567.
(28) Shaner, N. C.; Steinbach, P. A.; Tsien, R. Y. *Nat. Methods* **2005**, *2*, 905.

(29) Chithrani, B. D.; Ghazani, A. A.; Chan, W. C. W. *Nano Lett.* **2006**, *6*, 662.
(30) Huang, X. H.; El-Sayed, I. H.; Qian, W.; El-Sayed, M. A. *J. Am. Chem. Soc.* **2006**, *128*, 2115.
(31) Jiang, W.; Kim, B. Y. S.; Rutka, J. T.; Chan, W. C. W. *Nat. Nanotechnol.* **2008**, *3*, 145.
(32) Jaiswal, J. K.; Mattoussi, H.; Mauro, J. M.; Simon, S. M. *Nat. Biotechnol.* **2003**, *21*, 47.
(33) Kim, S.; Lim, Y. T.; Soltesz, E. G.; De Grand, A. M.; Lee, J.; Nakayama, A.; Parker, J. A.; Mihaljevic, T.; Laurence, R. G.; Dor, D. M.; Cohn, L. H.; Bawendi, M. G.; Frangioni, J. V. *Nat. Biotechnol.* **2004**, *22*, 93.
(34) Larson, D. R.; Zipfel, W. R.; Williams, R. M.; Clark, S. W.; Bruchez, M. P.; Wise, F. W.; Webb, W. W. *Science* **2003**, *300*, 1434.
(35) Wu, X. Y.; Liu, H. J.; Liu, J. Q.; Haley, K. N.; Treadway, J. A.; Larson, J. P.; Ge, N. F.; Peale, F.; Bruchez, M. P. *Nat. Biotechnol.* **2003**, *21*, 41.
(36) Chen, G. Y.; Ohulchanskyy, T. Y.; Kumar, R.; Agren, H.; Prasad, P. N. *ACS Nano* **2010**, *4*, 3163.
(37) Chen, G. Y.; Ohulchanskyy, T. Y.; Law, W. C.; Agren, H.; Prasad, P. N. *Nanoscale* **2011**, *3*, 2003.
(38) Chen, G. Y.; Shen, J.; Ohulchanskyy, T. Y.; Patel, N. J.; Kutikov, A.; Li, Z. P.; Song, J.; Pandey, R. K.; Agren, H.; Prasad, P. N.; Han, G. *ACS Nano* **2012**, *6*, 8280.
(39) Durr, N. J.; Larson, T.; Smith, D. K.; Korgel, B. A.; Sokolov, K.; Ben-Yakar, A. *Nano Lett.* **2007**, *7*, 941.
(40) Ohulchanskyy, T. Y.; Roy, I.; Yong, K. T.; Pudavar, H. E.; Prasad, P. N. *Nanomed. Nanobiotechnol.* **2010**, *2*, 162.
(41) Yong, K. T.; Qian, J.; Roy, I.; Lee, H. H.; Bergey, E. J.; Tramposch, K. M.; He, S. L.; Swihart, M. T.; Maitra, A.; Prasad, P. N. *Nano Lett.* **2007**, *7*, 761.
(42) Campagnola, P. J.; Loew, L. M. *Nat. Biotechnol* . **2003**, *21*, 1356.
(43) Pantazis, P.; Maloney, J.; Wu, D.; Fraser, S. E. *Proc. Natl. Acad. Sci. U.S.A.* **2010**, *107*, 14535.
(44) Zhou, J.; Yu, M. X.; Sun, Y.; Zhang, X. Z.; Zhu, X. J.; Wu, Z. H.; Wu, D. M.; Li, F. Y. *Biomaterials* **2011**, *32*, 1148.
(45) Zhou, J.; Sun, Y.; Du, X. X.; Xiong, L. Q.; Hu, H.; Li, F. Y. *Biomaterials* **2010**, *31*, 3287.
(46) Zhou, J.; Liu, Z.; Li, F. Y. *Chem. Soc. Rev.* **2012**, *41*, 1323.
(47) Zhang, F.; Braun, G. B.; Shi, Y. F.; Zhang, Y. C.; Sun, X. H.; Reich, N. O.; Zhao, D. Y.; Stucky, G. *J. Am. Chem. Soc.* **2010**, *132*, 2850.
(48) Xiong, L. Q.; Yang, T. S.; Yang, Y.; Xu, C. J.; Li, F. Y. *Biomaterials* **2010**, *31*, 7078.
(49) Xiong, L. Q.; Chen, Z. G.; Tian, Q. W.; Cao, T. Y.; Xu, C. J.; Li, F. Y. *Anal. Chem.* **2009**, *81*, 8687.
(50) Wang, M.; Mi, C. C.; Wang, W. X.; Liu, C. H.; Wu, Y. F.; Xu, Z. R.; Mao, C. B.; Xu, S. K. *ACS Nano* **2009**, *3*, 1580.
(51) Wang, F.; Liu, X. G. *Chem. Soc. Rev.* **2009**, *38*, 976.
(52) Wang, F.; Banerjee, D.; Liu, Y. S.; Chen, X. Y.; Liu, X. G. *Analyst* **2010**, *135*, 1839.
(53) Wang, C.; Cheng, L. A.; Liu, Z. A. *Biomaterials* **2011**, *32*, 1110.
(54) Lim, S. F.; Riehn, R.; Ryu, W. S.; Khanarian, N.; Tung, C. K.; Tank, D.; Austin, R. H. *Nano Lett.* **2006**, *6*, 169.
(55) Kumar, R.; Nyk, M.; Ohulchanskyy, T. Y.; Flask, C. A.; Prasad, P. N. *Adv. Funct. Mater.* **2009**, *19*, 853.
(56) Jalil, R. A.; Zhang, Y. *Biomaterials* **2008**, *29*, 4122.
(57) Haase, M.; Schafer, H. *Angew. Chem., Int. Ed.* **2011**, *50*, 5808.
(58) Auzel, F. *Chem. Rev.* **2004**, *104*, 139.
(59) He, G. S.; Markowicz, P. P.; Lin, T. C.; Prasad, P. N. *Nature* **2002**, *415*, 767.
(60) Xing, H. Y.; Bu, W. B.; Zhang, S. J.; Zheng, X. P.; Li, M.; Chen, F.; He, Q. J.; Zhou, L. P.; Peng, W. J.; Hua, Y. Q.; Shi, J. L. *Biomaterials* **2012**, *33*, 1079.
(61) Yang, Y.; Sun, Y.; Cao, T. Y.; Peng, J. J.; Liu, Y.; Wu, Y. Q.; Feng, W.; Zhang, Y. J.; Li, F. Y. *Biomaterials* **2013**, *34*, 774.
(62) Sun, Y.; Yu, M. X.; Liang, S.; Zhang, Y. J.; Li, C. G.; Mou, T. T.; Yang, W. J.; Zhang, X. Z.; Li, B. A.; Huang, C. H.; Li, F. Y. *Biomaterials* **2011**, *32*, 2999.
(63) Cheng, L.; Yang, K.; Li, Y. G.; Chen, J. H.; Wang, C.; Shao, M. W.; Lee, S. T.; Liu, Z. *Angew. Chem., Int. Ed.* **2011**, *50*, 7385.
(64) Idris, N. M.; Gnanasammandhan, M. K.; Zhang, J.; Ho, P. C.; Mahendran, R.; Zhang, Y. *Nat. Med.* **2012**, *18*, 1580.
(65) Bogdan, N.; Vetrone, F.; Ozin, G. A.; Capobianco, J. A. *Nano Lett.* **2011**, *11*, 835.
(66) Chen, Z. G.; Chen, H. L.; Hu, H.; Yu, M. X.; Li, F. Y.; Zhang, Q.; Zhou, Z. G.; Yi, T.; Huang, C. H. *J. Am. Chem. Soc.* **2008**, *130*, 3023.
(67) Judd, B. R. *Phys. Rev.* **1962**, *127*, 750.
(68) Ofelt, G. S. *J. Chem. Phys.* **1962**, *37*, 511.
(69) Chen, G. Y.; Somesfalean, G.; Liu, Y.; Zhang, Z. G.; Sun, Q.; Wang, F. P. *Phys. Rev. B* **2007**, *75*, 113114.
(70) Pollnau, M.; Gamelin, D. R.; Luthi, S. R.; Gudel, H. U.; Hehlen, M. P. *Phys. Rev. B* **2000**, *61*, 3337.
(71) Suyver, J. F.; Aebischer, A.; Garcia-Revilla, S.; Gerner, P.; Gudel, H. U. *Phys. Rev. B* **2005**, *71*, 125123.
(72) Chen, G. Y.; Liu, Y.; Zhang, Y. G.; Somesfalean, G.; Zhang, Z. G.; Sun, Q.; Wang, F. P. *Appl. Phys. Lett.* **2007**, *91*, 133103.
(73) Chen, G. Y.; Zhang, Y. G.; Somesfalean, G.; Zhang, Z. G.; Sun, Q.; Wang, F. P. *Appl. Phys. Lett.* **2006**, *89*, 163105.
(74) Chen, G. Y.; Somesfalean, G.; Zhang, Z. G.; Sun, Q.; Wang, E. P. *Opt. Lett.* **2007**, *32*, 87.
(75) Sun, Y. J.; Chen, Y.; Tian, L. J.; Yu, Y.; Kong, X. G.; Zhao, J. W.; Zhang, H. *Nanotechnology* **2007**, *18*, 275609.
(76) Wang, L. Y.; Li, Y. D. *Chem. Commun.* **2006**, *28*, 2557.
(77) Kramer, K. W.; Biner, D.; Frei, G.; Gudel, H. U.; Hehlen, M. P.; Luthi, S. R. *Chem. Mater.* **2004**, *16*, 1244.
(78) Wang, L. Y.; Li, Y. D. *Nano Lett.* **2006**, *6*, 1645.
(79) Suyver, J. F.; Aebischer, A.; Biner, D.; Gerner, P.; Grimm, J.; Heer, S.; Kramer, K. W.; Reinhard, C.; Gudel, H. U. *Opt. Mater.* **2005**, *27*, 1111.
(80) De la Rosa, E.; Salas, P.; Desirena, H.; Angeles, C.; Rodriguez, R. A. *Appl. Phys. Lett.* **2005**, *87*, 241912.
(81) Wang, G. F.; Peng, Q.; Li, Y. D. *J. Am. Chem. Soc.* **2009**, *131*, 14200.
(82) Wang, F.; Liu, X. G. *J. Am. Chem. Soc.* **2008**, *130*, 5642.
(83) Chen, G. Y.; Ohulchanskyy, T. Y.; Kachynski, A.; Agren, H.; Prasad, P. N. *ACS Nano* **2011**, *5*, 4981.
(84) Chen, D. Q.; Lei, L.; Yang, A. P.; Wang, Z. X.; Wang, Y. S. *Chem. Commun.* **2012**, *48*, 5898.
(85) Chen, G. Y.; Ohulchanskyy, T. Y.; Liu, S.; Law, W. C.; Wu, F.; Swihart, M. T.; Agren, H.; Prasad, P. N. *ACS Nano* **2012**, *6*, 2969.
(86) Chen, G. Y.; Liu, H. C.; Somesfalean, G.; Liang, H. J.; Zhang, Z. G. *Nanotechnology* **2009**, *20*, 385704.
(87) Rakov, N.; Maciel, G. S.; Sundheimer, M. L.; Menezes, S. L. D.; Gomes, A. S. L.; Messaddeq, Y.; Cassanjes, F. C.; Poirier, G.; Ribeiro, S. J. L. *J. Appl. Phys.* **2002**, *92*, 6337.
(88) Wang, L. L.; Qin, W. P.; Liu, Z. Y.; Zhao, D.; Qin, G. S.; Di, W. H.; He, C. F. *Opt. Express* **2012**, *20*, 7602.
(89) Liang, H. J.; Chen, G. Y.; Li, L.; Liu, Y.; Qin, F.; Zhang, Z. G. *Opt. Commun.* **2009**, *282*, 3028.
(90) Dwivedi, Y.; Thakur, S. N.; Rai, S. B. *Appl. Phys. B: Laser Opt.* **2007**, *89*, 45.
(91) Pushkar', A. A.; Uvarova, T. V.; Kiiko, V. V. *Opt. Spectrosc.* **2011**, *111*, 273.
(92) Chen, G.; Yang, C.; Prasad, P. N. *Acc. Chem. Res.* **2013**, *46*, 1474.
(93) Xu, C. T.; Zhan, Q.; Liu, H.; Somesfalean, G.; Qian, J.; He, S.; Andersson-Engels, S. *Laser Photonics Rev.* **2013**, *7*, 663.
(94) Chen, G.; Seo, J.; Yang, C.; Prasad, P. N. *Chem. Soc. Rev.* **2013**, *42*, 8304.
(95) Xue, X. J.; Wang, F.; Liu, X. G. *J. Mater. Chem.* **2011**, *21*, 13107.
(96) Liu, Y.; Tu, D.; Zhu, H.; Chen, X. *Chem. Soc. Rev.* **2013**, *42*, 6924.
(97) Chatterjee, D. K.; Gnanasammandhan, M. K.; Zhang, Y. *Small* **2010**, *6*, 2781.
(98) Wang, M.; Abbineni, G.; Clevenger, A.; Mao, C. B.; Xu, S. K. *J. Nanomed. Nanotechnol.* **2011**, *7*, 710.

(99) Shen, J.; Zhao, L.; Han, G. *Adv. Drug Delivery Rev.* **2013**, *65*, 744.
(100) Wang, G. F.; Peng, Q.; Li, Y. D. *Acc. Chem. Res.* **2011**, *44*, 322.
(101) Bouzigues, C.; Gacoin, T.; Alexandrou, A. *ACS Nano* **2011**, *5*, 8488.
(102) Li, C. X.; Lin, J. *J. Mater. Chem.* **2010**, *20*, 6831.
(103) Feng, W.; Han, C.; Li, F. *Adv. Mater.* **2013**, *25*, 5287.
(104) Gu, Z.; Yan, L.; Tian, G.; Li, S.; Chai, Z.; Zhao, Y. *Adv. Mater.* **2013**, *25*, 3758.
(105) Wang, C.; Cheng, L.; Liu, Z. *Theranostics* **2013**, *3*, 317.
(106) Liu, Y.; Tu, D.; Zhu, H.; Ma, E.; Chen, X. *Nanoscale* **2013**, *5*, 1369.
(107) Gnach, A.; Bednarkiewicz, A. *Nano Today* **2012**, *7*, 532.
(108) Martinez, A.; Morales, J.; Diaz-Torres, L. A.; Salas, P.; De la Rosa, E.; Oliva, J.; Desirena, H. *Mater. Sci. Eng., B* **2010**, *174*, 164.
(109) Patra, A.; Friend, C. S.; Kapoor, R.; Prasad, P. N. *Appl. Phys. Lett.* **2003**, *83*, 284.
(110) Ivaturi, A.; MacDougall, S. K. W.; Martín-Rodríguez, R.; Marta Quintanilla1, J. M. H.; Krämer, K. W.; Meijerink, A.; Richards, B. S. *J. Appl. Phys.* **2013**, *114*, 013505.
(111) Mialon, G.; Turkcan, S.; Dantelle, G.; Collins, D. P.; Hadjipanayi, M.; Taylor, R. A.; Gacoin, T.; Alexandrou, A.; Boilott, J. P. *J. Phys. Chem. C* **2010**, *114*, 22449.
(112) Kumar, G. A.; Pokhrel, M.; Martinez, A.; Dennis, R. C.; Villegas, I. L.; Sardar, D. K. *J. Alloys Compd.* **2012**, *513*, 559.
(113) Li, Y.; Wei, X. T.; Yin, M. *J. Alloys Compd.* **2011**, *509*, 9865.
(114) Chen, G. Y.; Liu, H. C.; Somesfalean, G.; Sheng, Y. Q.; Liang, H. J.; Zhang, Z. G.; Sun, Q.; Wang, F. P. *Appl. Phys. Lett.* **2008**, *92*, 113114.
(115) Bai, Y. F.; Wang, Y. X.; Yang, K.; Zhang, X. R.; Peng, G. Y.; Song, Y. L.; Pan, Z. Y.; Wang, C. H. *J. Phys. Chem. C* **2008**, *112*, 12259.
(116) Chen, G. Y.; Liu, H. C.; Liang, H. J.; Somesfalean, G.; Zhang, Z. G. *J. Phys. Chem. C* **2008**, *112*, 12030.
(117) Bai, Y. F.; Wang, Y. X.; Yang, K.; Zhang, X. R.; Song, Y. L.; Wang, C. H. *Opt. Commun.* **2008**, *281*, 5448.
(118) Bai, Y. F.; Yang, K.; Wang, Y. X.; Zhang, X. R.; Song, Y. L. *Opt. Commun.* **2008**, *281*, 2930.
(119) Wang, H. Q.; Nann, T. *ACS Nano* **2009**, *3*, 3804.
(120) Yang, D. M.; Li, C. X.; Li, G. G.; Shang, M. M.; Kang, X. J.; Lin, J. *J. Mater. Chem.* **2011**, *21*, 5923.
(121) Cheng, Q.; Sui, J. H.; Cai, W. *Nanoscale* **2012**, *4*, 779.
(122) Dou, Q. Q.; Zhang, Y. *Langmuir* **2011**, *27*, 13236.
(123) Li, Z. L.; Wang, B. S.; Xing, L. C.; Liu, S. L.; Tan, N.; Xiao, S. G.; Ding, J. W. *Chin. Opt. Lett.* **2012**, *10*, 081602.
(124) Huang, Q. M.; Yu, J. C.; Ma, E.; Lin, K. M. *J. Phys. Chem. C* **2010**, *114*, 4719.
(125) Hutter, E.; Fendler, J. H. *Adv. Mater.* **2004**, *16*, 1685.
(126) Haes, A. J.; Van Duyne, R. P. *J. Am. Chem. Soc.* **2002**, *124*, 10596.
(127) McFarland, A. D.; Van Duyne, R. P. *Nano Lett.* **2003**, *3*, 1057.
(128) Anker, J. N.; Hall, W. P.; Lyandres, O.; Shah, N. C.; Zhao, J.; Van Duyne, R. P. *Nat. Mater.* **2008**, *7*, 442.
(129) Maier, S. A.; Kik, P. G.; Atwater, H. A.; Meltzer, S.; Harel, E.; Koel, B. E.; Requicha, A. A. G. *Nat. Mater.* **2003**, *2*, 229.
(130) Xia, Y. N.; Li, W. Y.; Cobley, C. M.; Chen, J. Y.; Xia, X. H.; Zhang, Q.; Yang, M. X.; Cho, E. C.; Brown, P. K. *Acc. Chem. Res.* **2011**, *44*, 914.
(131) Hagglund, C.; Zach, M.; Kasemo, B. *Appl. Phys. Lett.* **2008**, *92*, 013113.
(132) Futamata, M.; Maruyama, Y.; Ishikawa, M. *J. Phys. Chem. B* **2003**, *107*, 7607.
(133) Singh, M. P.; Strouse, G. F. *J. Am. Chem. Soc.* **2010**, *132*, 9383.
(134) Zhao, J.; Jensen, L.; Sung, J. H.; Zou, S. L.; Schatz, G. C.; Van Duyne, R. P. *J. Am. Chem. Soc.* **2007**, *129*, 7647.
(135) Chen, Y.; Munechika, K.; Ginger, D. S. *Nano Lett.* **2007**, *7*, 690.
(136) Munechika, K.; Chen, Y.; Tillack, A. F.; Kulkarni, A. P.; Plante, I. J. L.; Munro, A. M.; Ginger, D. S. *Nano Lett.* **2010**, *10*, 2598.
(137) Noginov, M. A.; Zhu, G.; Belgrave, A. M.; Bakker, R.; Shalaev, V. M.; Narimanov, E. E.; Stout, S.; Herz, E.; Suteewong, T.; Wiesner, U. *Nature* **2009**, *460*, 1110.
(138) Luther, J. M.; Jain, P. K.; Ewers, T.; Alivisatos, A. P. *Nat. Mater.* **2011**, *10*, 361.
(139) Zhang, H.; Xu, D.; Huang, Y.; Duan, X. F. *Chem. Commun.* **2011**, *47*, 979.
(140) Saboktakin, M.; Ye, X. C.; Oh, S. J.; Hong, S. H.; Fafarman, A. T.; Chettiar, U. K.; Engheta, N.; Murray, C. B.; Kagan, C. R. *ACS Nano* **2012**, *6*, 8758.
(141) Xu, W.; Xu, S.; Zhu, Y. S.; Liu, T.; Bai, X.; Dong, B. A.; Xu, L.; Song, H. W. *Nanoscale* **2012**, *4*, 6971.
(142) Zhang, W. H.; Ding, F.; Chou, S. Y. *Adv. Mater.* **2012**, *24*, Op236.
(143) Paudel, H. P.; Zhong, L. L.; Bayat, K.; Baroughi, M. F.; Smith, S.; Lin, C. K.; Jiang, C. Y.; Berry, M. T.; May, P. S. *J. Phys. Chem. C* **2011**, *115*, 19028.
(144) Zhang, H.; Li, Y. J.; Ivanov, I. A.; Qu, Y. Q.; Huang, Y.; Duan, X. F. *Angew. Chem., Int. Ed.* **2010**, *49*, 2865.
(145) Liu, N.; Qin, W. P.; Qin, G. S.; Jiang, T.; Zhao, D. *Chem. Commun.* **2011**, *47*, 7671.
(146) Tu, N. N.; Wang, L. Y. *Chem. Commun.* **2013**, *49*, 6319.
(147) Schietinger, S.; Aichele, T.; Wang, H. Q.; Nann, T.; Benson, O. *Nano Lett.* **2010**, *10*, 134.
(148) Li, Z. Q.; Li, X. D.; Liu, Q. Q.; Chen, X. H.; Sun, Z.; Liu, C.; Ye, X. J.; Huang, S. M. *Nanotechnology* **2012**, *23*, 025402.
(149) Zhao, P.; Zhu, Y. H.; Yang, X. L.; Fan, K. C.; Shen, J. H.; Li, C. Z. *RSC Adv.* **2012**, *2*, 10592.
(150) Kannan, P.; Rahim, F. A.; Chen, R.; Teng, X.; Huang, L.; Sun, H. D.; Kim, D. H. *ACS Appl. Mater. Inter.* **2013**, *5*, 3508.
(151) Feng, W.; Sun, L. D.; Yan, C. H. *Chem. Commun.* **2009**, *7*, 4393.
(152) Sudheendra, L.; Ortalan, V.; Dey, S.; Browning, N. D.; Kennedy, I. M. *Chem. Mater.* **2011**, *23*, 2987.
(153) Xu, W.; Chen, B. T.; Yu, W.; Zhu, Y. S.; Liu, T.; Xu, S.; Min, X. L.; Bai, X.; Song, H. W. *Dalton Trans.* **2012**, *41*, 13525.
(154) Priyam, A.; Idris, N. M.; Zhang, Y. *J. Mater. Chem.* **2012**, *22*, 960.
(155) Deng, W.; Sudheendra, L.; Zhao, J. B.; Fu, J. X.; Jin, D. Y.; Kennedy, I. M.; Goldys, E. M. *Nanotechnology* **2011**, *22*, 325604.
(156) Ge, W.; Zhang, X. R.; Liu, M.; Lei, Z. W.; Knize, R. J.; Lu, Y. L. *Theranostics* **2013**, *3*, 282.
(157) Qian, L. P.; Zhou, L. H.; Too, H. P.; Chow, G. M. *J. Nanopart. Res.* **2011**, *13*, 499.
(158) Li, Z. Q.; Wang, L. M.; Wang, Z. Y.; Liu, X. H.; Xiong, Y. J. *J. Phys. Chem. C* **2011**, *115*, 3291.
(159) Liu, S.; Chen, G. Y.; Ohulchanskyy, T. Y.; Swihart, M. T.; Prasad, P. N. *Theranostics* **2013**, *3*, 275.
(160) Lakowicz, J. R. *Anal. Biochem.* **2001**, *298*, 1.
(161) Dulkeith, E.; Morteani, A. C.; Niedereichholz, T.; Klar, T. A.; Feldmann, J.; Levi, S. A.; van Veggel, F. C. J. M.; Reinhoudt, D. N.; Moller, M.; Gittins, D. I. *Phys. Rev. Lett.* **2002**, *89*, 203002.
(162) Zhao, J.; Jin, D.; Schartner, E. P.; Lu, Y.; Liu, Y.; Zvyagin, A. V.; Zhang, L.; Dawes, J. M.; Xi, P.; Piper, J. A.; Goldys, E. M.; Monro, T. M. *Nat. Nanotechnol.* **2013**, *8*, 729.
(163) Liang, H. J.; Zheng, Y. D.; Wu, L.; Liu, L. X.; Zhang, Z. G.; Cao, W. W. *J. Lumin.* **2011**, *131*, 1802.
(164) Shen, J.; Chen, G.; Ohulchanskyy, T. Y.; Kesseli, S. J.; Buchholz, S.; Li, Z.; Prasad, P. N.; Han, G. *Small* **2013**, *9*, 3213.
(165) Heer, S.; Kompe, K.; Gudel, H. U.; Haase, M. *Adv. Mater.* **2004**, *16*, 2102.
(166) Mahalingam, V.; Vetrone, F.; Naccache, R.; Speghini, A.; Capobianco, J. A. *Adv. Mater.* **2009**, *21*, 4025.
(167) Liang, L. F.; Wu, H.; Hu, H. L.; Wu, M. M.; Su, Q. *J. Alloys Compd.* **2004**, *368*, 94.
(168) Yin, A. X.; Zhang, Y. W.; Sun, L. D.; Yan, C. H. *Nanoscale* **2010**, *2*, 953.

(169) Wang, J.; Deng, R.; MacDonald, M. A.; Chen, B.; Yuan, J.; Wang, F.; Chi, D.; Hor, T. S. A.; Zhang, P.; Liu, G.; Han, Y.; Liu, X. *Nat. Mater.* **2013**, DOI: 10.1038/nmat3804.
(170) Wang, F.; Deng, R. R.; Wang, J.; Wang, Q. X.; Han, Y.; Zhu, H. M.; Chen, X. Y.; Liu, X. G. *Nat. Mater.* **2011**, *10*, 968.
(171) Johnson, N. J. J.; Veggel, F. C. J. M. v. *Nano Res.* **2013**, *6*, 547.
(172) Yi, G. S.; Chow, G. M. *Chem. Mater.* **2007**, *19*, 341.
(173) Mai, H. X.; Zhang, Y. W.; Sun, L. D.; Yan, C. H. *J. Phys. Chem. C* **2007**, *111*, 13721.
(174) Wang, Y.; Tu, L. P.; Zhao, J. W.; Sun, Y. J.; Kong, X. G.; Zhang, H. *J. Phys. Chem. C* **2009**, *113*, 7164.
(175) Johnson, N. J. J.; Korinek, A.; Dong, C. H.; van Veggel, F. C. J. M. *J. Am. Chem. Soc.* **2012**, *134*, 11068.
(176) Boyer, J. C.; Manseau, M. P.; Murray, J. I.; van Veggel, F. C. J. M. *Langmuir* **2010**, *26*, 1157.
(177) Boyer, J. C.; van Veggel, F. C. J. M. *Nanoscale* **2010**, *2*, 1417.
(178) Schafer, H.; Ptacek, P.; Zerzouf, O.; Haase, M. *Adv. Funct. Mater.* **2008**, *18*, 2913.
(179) Du, Y. P.; Sun, X.; Zhang, Y. W.; Yan, Z. G.; Sun, L. D.; Yan, C. H. *Cryst. Growth Des.* **2009**, *9*, 2013.
(180) Liu, Y. S.; Tu, D. T.; Zhu, H. M.; Li, R. F.; Luo, W. Q.; Chen, X. Y. *Adv. Mater.* **2010**, *22*, 3266.
(181) Wang, F.; Wang, J. A.; Liu, X. G. *Angew. Chem., Int. Ed.* **2010**, *49*, 7456.
(182) Wong, H. T.; Vetrone, F.; Naccache, R.; Chan, H. L. W.; Hao, J. H.; Capobianco, J. A. *J. Mater. Chem.* **2011**, *21*, 16589.
(183) Yi, G. S.; Peng, Y. F.; Gao, Z. Q. *Chem. Mater.* **2011**, *23*, 2729.
(184) Chen, G. Y.; Qiu, H. L.; Fan, R. W.; Hao, S. W.; Tan, S.; Yang, C. H.; Han, G. *J. Mater. Chem.* **2012**, *22*, 20190.
(185) Dong, C. H.; Korinek, A.; Blasiak, B.; Tomanek, B.; van Veggel, F. C. J. M. *Chem. Mater.* **2012**, *24*, 1297.
(186) Guo, H.; Li, Z. Q.; Qian, H. S.; Hu, Y.; Muhammad, I. N. *Nanotechnology* **2010**, *21*, 125602.
(187) Wang, Y. F.; Sun, L. D.; Xiao, J. W.; Feng, W.; Zhou, J. C.; Shen, J.; Yan, C. H. *Chem.—Eur. J.* **2012**, *18*, 5558.
(188) Lu, Q.; Li, A. H.; Guo, F. Y.; Sun, L.; Zhao, L. C. *Nanotechnology* **2008**, *19*, 145701.
(189) Li, Z. Q.; Guo, H. C.; Qian, H. S.; Hu, Y. *Nanotechnology* **2010**, *21*, 315105.
(190) Zhang, C.; Lee, J. Y. *ACS Nano* **2013**, *7*, 4393.
(191) Li, X. M.; Shen, D. K.; Yang, J. P.; Yao, C.; Che, R. C.; Zhang, F.; Zhao, D. Y. *Chem. Mater.* **2013**, *25*, 106.
(192) Abel, K. A.; Boyer, J. C.; van Veggel, F. C. J. M. *J. Am. Chem. Soc.* **2009**, *131*, 14644.
(193) Su, Q. Q.; Han, S. Y.; Xie, X. J.; Zhu, H. M.; Chen, H. Y.; Chen, C. K.; Liu, R. S.; Chen, X. Y.; Wang, F.; Liu, X. G. *J. Am. Chem. Soc.* **2012**, *134*, 20849.
(194) Zhang, F.; Che, R. C.; Li, X. M.; Yao, C.; Yang, J. P.; Shen, D. K.; Hu, P.; Li, W.; Zhao, D. Y. *Nano Lett.* **2012**, *12*, 2852.
(195) Vetrone, F.; Naccache, R.; Mahalingam, V.; Morgan, C. G.; Capobianco, J. A. *Adv. Funct. Mater.* **2009**, *19*, 2924.
(196) Ghosh, P.; Oliva, J.; De la Rosa, E.; Haldar, K. K.; Solis, D.; Patra, A. *J. Phys. Chem. C* **2008**, *112*, 9650.
(197) Zou, W. Q.; Visser, C.; Maduro, J. A.; Pshenichnikov, M. S.; Hummelen, J. C. *Nat. Photonics* **2012**, *6*, 560.
(198) Wilson, R.; Cossins, A. R.; Spiller, D. G. *Angew. Chem., Int. Ed.* **2006**, *45*, 6104.
(199) Finkel, N. H.; Lou, X.; Wang, C.; He, L. *Anal. Chem.* **2004**, *76*, 352A.
(200) Zhang, F.; Shi, Q. H.; Zhang, Y. C.; Shi, Y. F.; Ding, K. L.; Zhao, D. Y.; Stucky, G. D. *Adv. Mater.* **2011**, *23*, 3775.
(201) Gorris, H. H.; Wolfbeis, O. S. *Angew. Chem., Int. Ed.* **2013**, *52*, 3584.
(202) Meldal, M.; Christensen, S. F. *Angew. Chem., Int. Ed.* **2010**, *49*, 3473.
(203) Hardenbol, P.; Yu, F. L.; Belmont, J.; MacKenzie, J.; Bruckner, C.; Brundage, T.; Boudreau, A.; Chow, S.; Eberle, J.; Erbilgin, A.; Falkowski, M.; Fitzgerald, R.; Ghose, S.; Iartchouk, O.; Jain, M.; Karlin-Neumann, G.; Lu, X. H.; Miao, X.; Moore, B.; Moorhead, M.; Namsaraev, E.; Pasternak, S.; Prakash, E.; Tran, K.; Wang, Z. Y.; Jones, H. B.; Davis, R. W.; Willis, T. D.; Gibbs, R. A. *Genome Res.* **2005**, *15*, 269.
(204) Klostranec, J. M.; Xiang, Q.; Farcas, G. A.; Lee, J. A.; Rhee, A.; Lafferty, E. I.; Perrault, S. D.; Kain, K. C.; Chan, W. C. W. *Nano Lett.* **2007**, *7*, 2812.
(205) Suyver, J. F.; Grimm, J.; Kramer, K. W.; Gudel, H. U. *J. Lumin.* **2005**, *114*, 53.
(206) Chen, G. Y.; Yang, C. H.; Aghahadi, B.; Liang, H. J.; Liu, Y.; Li, L.; Zhang, Z. G. *J. Opt. Soc. Am. B* **2010**, *27*, 1158.
(207) Suyver, J. F.; Grimm, J.; van Veen, M. K.; Biner, D.; Kramer, K. W.; Gudel, H. U. *J. Lumin.* **2006**, *117*, 1.
(208) Boyer, J. C.; Vetrone, F.; Cuccia, L. A.; Capobianco, J. A. *J. Am. Chem. Soc.* **2006**, *128*, 7444.
(209) Ehlert, O.; Thomann, R.; Darbandi, M.; Nann, T. *ACS Nano* **2008**, *2*, 120.
(210) Chan, E. M.; Han, G.; Goldberg, J. D.; Gargas, D. J.; Ostrowski, A. D.; Schuck, P. J.; Cohen, B. E.; Milliron, D. J. *Nano Lett.* **2012**, *12*, 3839.
(211) Sarkar, S.; Meesaragandla, B.; Hazra, C.; Mahalingam, V. *Adv. Mater.* **2013**, *25*, 856.
(212) Vetrone, F.; Boyer, J. C.; Capobianco, J. A.; Speghini, A.; Bettinelli, M. *Chem. Mater.* **2003**, *15*, 2737.
(213) Mahalingam, V.; Naccache, R.; Vetrone, F.; Capobianco, J. A. *Chem. Commun.* **2011**, *47*, 3481.
(214) Kar, A.; Patra, A. *Nanoscale* **2012**, *4*, 3608.
(215) Qian, H. S.; Zhang, Y. *Langmuir* **2008**, *24*, 12123.
(216) Dou, Q. Q.; Idris, N. M.; Zhang, Y. *Biomaterials* **2013**, *34*, 1722.
(217) Niu, W. B.; Wu, S. L.; Zhang, S. F. *J. Mater. Chem.* **2010**, *20*, 9113.
(218) Niu, W. B.; Wu, S. L.; Zhang, S. F. *J. Mater. Chem.* **2011**, *21*, 10894.
(219) Bai, X.; Song, H. W.; Pan, G. H.; Lei, Y. Q.; Wang, T.; Ren, X. G.; Lu, S. Z.; Dong, B.; Dai, Q. L.; Fan, L. *J. Phys. Chem. C* **2007**, *111*, 13611.
(220) Li, Z. Q.; Zhang, Y. *Nanotechnology* **2008**, *19*, 345606.
(221) Ye, X. C.; Collins, J. E.; Kang, Y. J.; Chen, J.; Chen, D. T. N.; Yodh, A. G.; Murray, C. B. *Proc. Natl. Acad. Sci. U.S.A.* **2010**, *107*, 22430.
(222) Weiss, S. *Science* **1999**, *283*, 1676.
(223) Giepmans, B. N. G.; Adams, S. R.; Ellisman, M. H.; Tsien, R. Y. *Science* **2006**, *312*, 217.
(224) Li, Z. Q.; Zhang, Y.; Jiang, S. *Adv. Mater.* **2008**, *20*, 4765.
(225) Jeong, S.; Won, N.; Lee, J.; Bang, J.; Yoo, J.; Kim, S. G.; Chang, J. A.; Kim, J.; Kim, S. *Chem. Commun.* **2011**, *47*, 8022.
(226) Gorris, H. H.; Ali, R.; Saleh, S. M.; Wolfbeis, O. S. *Adv. Mater.* **2011**, *23*, 1652.
(227) Wang, L. Y.; Yan, R. X.; Hao, Z. Y.; Wang, L.; Zeng, J. H.; Bao, J.; Wang, X.; Peng, Q.; Li, Y. D. *Angew. Chem., Int. Ed.* **2005**, *44*, 6054.
(228) Liu, Y. S.; Zhou, S. Y.; Tu, D. T.; Chen, Z.; Huang, M. D.; Zhu, H. M.; Ma, E.; Chen, X. Y. *J. Am. Chem. Soc.* **2012**, *134*, 15083.
(229) Ju, Q.; Tu, D. T.; Liu, Y. S.; Li, R. F.; Zhu, H. M.; Chen, J. C.; Chen, Z.; Huang, M. D.; Chen, X. Y. *J. Am. Chem. Soc.* **2012**, *134*, 1323.
(230) Tu, D. T.; Liu, L. Q.; Ju, Q.; Liu, Y. S.; Zhu, H. M.; Li, R. F.; Chen, X. Y. *Angew. Chem., Int. Ed.* **2011**, *50*, 6306.
(231) Zheng, W.; Zhou, S.; Chen, Z.; Hu, P.; Liu, Y.; Tu, D.; Zhu, H.; Li, R.; Huang, M.; Chen, X. *Angew. Chem., Int. Ed.* **2013**, *52*, 6671.
(232) Cheng, L.; Yang, K.; Shao, M.; Lee, S.-T.; Liu, Z. *J. Phys. Chem. C* **2011**, *115*, 2686.
(233) Yao, L. M.; Zhou, J.; Liu, J. L.; Feng, W.; Li, F. Y. *Adv. Funct. Mater.* **2012**, *22*, 2667.
(234) Bogdan, N.; Vetrone, F.; Roy, R.; Capobianco, J. A. *J. Mater. Chem.* **2010**, *20*, 7543.
(235) Lu, Y.; Zhao, J.; Zhang, R.; Liu, Y.; Liu, D.; Goldys, E. M.; Yang, X.; Xi, P.; Sunna, A.; Lu, J.; Shi, Y.; Leif, R. C.; Huo, Y.; Shen, J.; Piper, J. A.; Robinson, J. P.; Jin, D. *Nat. Photonics* **2014**, *8*, 32.

(236) Zhao, J.; Lu, Z.; Yin, Y.; McRae, C.; Piper, J. A.; Dawes, J. M.; Jin, D.; Goldys, E. M. *Nanoscale* **2013**, *5*, 944.
(237) Mai, H. X.; Zhang, Y. W.; Si, R.; Yan, Z. G.; Sun, L. D.; You, L. P.; Yan, C. H. *J. Am. Chem. Soc.* **2006**, *128*, 6426.
(238) Zhan, Q. Q.; Qian, J.; Liang, H. J.; Somesfalean, G.; Wang, D.; He, S. L.; Zhang, Z. G.; Andersson-Engels, S. *ACS Nano* **2011**, *5*, 3744.
(239) Naccache, R.; Vetrone, F.; Mahalingam, V.; Cuccia, L. A.; Capobianco, J. A. *Chem. Mater.* **2009**, *21*, 717.
(240) Boyer, J. C.; Cuccia, L. A.; Capobianco, J. A. *Nano Lett.* **2007**, *7*, 847.
(241) Komban, R.; Klare, J. P.; Voss, B.; Nordmann, J.; Steinhoff, H. J.; Haase, M. *Angew. Chem., Int. Ed.* **2012**, *51*, 6506.
(242) Wang, J. A.; Wang, F.; Xu, J.; Wang, Y.; Liu, Y. S.; Chen, X. Y.; Chen, H. Y.; Liu, X. G. *C. R. Chim.* **2010**, *13*, 731.
(243) Zhou, H. P.; Zhang, Y. W.; Mai, H. X.; Sun, X.; Liu, Q.; Song, W. G.; Yan, C. H. *Chem.—Eur. J.* **2008**, *14*, 3380.
(244) Qiu, H. L.; Chen, G. Y.; Fan, R. W.; Cheng, C.; Hao, S. W.; Chen, D. Y.; Yang, C. H. *Chem. Commun.* **2011**, *47*, 9648.
(245) Zhang, Y. W.; Sun, X.; Si, R.; You, L. P.; Yan, C. H. *J. Am. Chem. Soc.* **2005**, *127*, 3260.
(246) Sun, X.; Zhang, Y. W.; Du, Y. P.; Yan, Z. G.; Si, R.; You, L. P.; Yan, C. H. *Chem.—Eur. J.* **2007**, *13*, 2320.
(247) Teng, X.; Zhu, Y. H.; Wei, W.; Wang, S. C.; Huang, J. F.; Naccache, R.; Hu, W. B.; Tok, A. I. Y.; Han, Y.; Zhang, Q. C.; Fan, Q. L.; Huang, W.; Capobianco, J. A.; Huang, L. *J. Am. Chem. Soc.* **2012**, *134*, 8340.
(248) Yi, G. S.; Chow, G. M. *Adv. Funct. Mater.* **2006**, *16*, 2324.
(249) Du, Y. P.; Zhang, Y. W.; Sun, L. D.; Yan, C. H. *J. Phys. Chem. C* **2008**, *112*, 405.
(250) Du, Y. P.; Zhang, Y. W.; Sun, L. D.; Yan, C. H. *J. Am. Chem. Soc.* **2009**, *131*, 3162.
(251) Si, R.; Zhang, Y. W.; Zhou, H. P.; Sun, L. D.; Yan, C. H. *Chem. Mater.* **2007**, *19*, 18.
(252) Cao, Y. C. *J. Am. Chem. Soc.* **2004**, *126*, 7456.
(253) Zhao, F.; Yuan, M.; Zhang, W.; Gao, S. *J. Am. Chem. Soc.* **2006**, *128*, 11758.
(254) Ding, Y.; Gu, J.; Ke, J.; Zhang, Y. W.; Yan, C. H. *Angew. Chem., Int. Ed.* **2011**, *50*, 12330.
(255) Ding, Y.; Gu, J.; Zhang, T.; Yin, A. X.; Yang, L.; Zhang, Y. W.; Yan, C. H. *J. Am. Chem. Soc.* **2012**, *134*, 3255.
(256) Wang, F.; Sun, L. D.; Gu, J.; Wang, Y. F.; Feng, W.; Yang, Y.; Wang, J. F.; Yan, C. H. *Angew. Chem., Int. Ed.* **2012**, *51*, 8796.
(257) Zhou, H. P.; Zhang, C.; Yan, C. H. *Langmuir* **2009**, *25*, 12914.
(258) Wang, H. Z.; Uehara, M.; Nakamura, H.; Miyazaki, M.; Maeda, H. *Adv. Mater.* **2005**, *17*, 2506.
(259) Shan, J.; Qin, X.; Yao, N.; Ju, Y. *Nanotechnology* **2007**, *18*, 445607.
(260) Shan, J. N.; Kong, W. J.; Wei, R.; Yao, N.; Ju, Y. G. *J. Appl. Phys.* **2010**, *107*, 054901.
(261) Shan, J. N.; Ju, Y. G. *Appl. Phys. Lett.* **2007**, *91*, 123103.
(262) Wang, F.; Han, Y.; Lim, C. S.; Lu, Y. H.; Wang, J.; Xu, J.; Chen, H. Y.; Zhang, C.; Hong, M. H.; Liu, X. G. *Nature* **2010**, *463*, 1061.
(263) Johnson, N. J. J.; Sangeetha, N. M.; Boyer, J. C.; van Veggel, F. C. J. M. *Nanoscale* **2010**, *2*, 771.
(264) Wang, J.; Wang, F.; Wang, C.; Liu, Z.; Liu, X. G. *Angew. Chem., Int. Ed.* **2011**, *50*, 10369.
(265) Zhang, Y.; Lin, J. D.; Vijayaragavan, V.; Bhakoo, K. K.; Tan, T. T. Y. *Chem. Commun.* **2012**, *48*, 10322.
(266) Wang, X.; Zhuang, J.; Peng, Q.; Li, Y. D. *Nature* **2005**, *437*, 121.
(267) He, M.; Huang, P.; Zhang, C. L.; Chen, F.; Wang, C.; Ma, J. B.; He, R.; Cui, D. X. *Chem. Commun.* **2011**, *47*, 9510.
(268) Li, P.; Peng, Q.; Li, Y. D. *Adv. Mater.* **2009**, *21*, 1945.
(269) Zhang, F.; Li, J.; Shan, J.; Xu, L.; Zhao, D. Y. *Chem.—Eur. J.* **2009**, *15*, 11010.
(270) Chen, D. Q.; Huang, P.; Yu, Y. L.; Huang, F.; Yang, A. P.; Wang, Y. S. *Chem. Commun.* **2011**, *47*, 5801.
(271) Nguyen, T. D.; Dinh, C. T.; Do, T. O. *ACS Nano* **2010**, *4*, 2263.
(272) Qiu, H. L.; Chen, G. Y.; Sun, L.; Hao, S. W.; Han, G.; Yang, C. H. *J. Mater. Chem.* **2011**, *21*, 17202.
(273) Yang, S. W.; Gao, L. *J. Am. Chem. Soc.* **2006**, *128*, 9330.
(274) Chen, D. Q.; Yu, Y. L.; Huang, F.; Huang, P.; Yang, A. P.; Wang, Y. S. *J. Am. Chem. Soc.* **2010**, *132*, 9976.
(275) Zhu, X. X.; Zhang, Q. H.; Li, Y. G.; Wang, H. Z. *J. Mater. Chem.* **2008**, *18*, 5060.
(276) Li, S. A.; Xie, T.; Peng, Q.; Li, Y. D. *Chem.—Eur. J.* **2009**, *15*, 2512.
(277) Chen, D. Q.; Yu, Y. L.; Huanga, F.; Wang, Y. S. *Chem. Commun.* **2011**, *47*, 2601.
(278) Chen, D. Q.; Lei, L.; Zhang, R.; Yang, A. P.; Xu, J.; Wang, Y. S. *Chem. Commun.* **2012**, *48*, 10630.
(279) Wang, G. F.; Peng, Q.; Li, Y. D. *Chem. Commun.* **2010**, *46*, 7528.
(280) Heer, S.; Lehmann, O.; Haase, M.; Gudel, H. U. *Angew. Chem., Int. Ed.* **2003**, *42*, 3179.
(281) Shi, F.; Wang, J. S.; Zhai, X. S.; Zhao, D.; Qin, W. P. *CrystEngComm* **2011**, *13*, 3782.
(282) Peng, Y.; Xing, M. M.; Luo, X. X.; Wang, L. Q. *Acta Phys. Sin* **2012**, *61*, 137201.
(283) Vetrone, F.; Mahalingam, V.; Capobianco, J. A. *Chem. Mater.* **2009**, *21*, 1847.
(284) Voorhees, P. W. *J. Stat. Phys.* **1985**, *38*, 231.
(285) Yang, T. S.; Sun, Y.; Liu, Q.; Feng, W.; Yang, P. Y.; Li, F. Y. *Biomaterials* **2012**, *33*, 3733.
(286) Zeng, J. H.; Su, J.; Li, Z. H.; Yan, R. X.; Li, Y. D. *Adv. Mater.* **2005**, *17*, 2119.
(287) Wang, L. Y.; Li, P.; Li, Y. D. *Adv. Mater.* **2007**, *19*, 3304.
(288) Yang, D. M.; Kang, X. J.; Shang, M. M.; Li, G. G.; Peng, C.; Li, C. X.; Lin, J. *Nanoscale* **2011**, *3*, 2589.
(289) Liu, Z. J.; Song, X. X.; Tang, Q. *Nanoscale* **2013**, *5*, 5073.
(290) Yan, R. X.; Li, Y. D. *Adv. Funct. Mater.* **2005**, *15*, 763.
(291) Lemyre, J. L.; Ritcey, A. M. *Chem. Mater.* **2005**, *17*, 3040.
(292) Li, C. X.; Yang, J.; Yang, P. P.; Lian, H. Z.; Lin, J. *Chem. Mater.* **2008**, *20*, 4317.
(293) Fu, Z. X.; Zheng, H. R.; He, E. J.; Gao, W.; Li, G. A. *Sci. China: Phys., Mech. Astron.* **2013**, *56*, 928.
(294) Zhang, F.; Wan, Y.; Yu, T.; Zhang, F. Q.; Shi, Y. F.; Xie, S. H.; Li, Y. G.; Xu, L.; Tu, B.; Zhao, D. Y. *Angew. Chem., Int. Ed.* **2007**, *46*, 7976.
(295) Liu, Q.; Sun, Y.; Yang, T. S.; Feng, W.; Li, C. G.; Li, F. Y. *J. Am. Chem. Soc.* **2011**, *133*, 17122.
(296) Li, C. X.; Quan, Z. W.; Yang, P. P.; Yang, J.; Lian, H. Z.; Lin, J. *J. Mater. Chem.* **2008**, *18*, 1353.
(297) Longmire, M.; Choyke, P. L.; Kobayashi, H. *Nanomedicine (London, U.K.)* **2008**, *3*, 703.
(298) Choi, H. S.; Liu, W.; Misra, P.; Tanaka, E.; Zimmer, J. P.; Ipe, B. I.; Bawendi, M. G.; Frangioni, J. V. *Nat. Biotechnol.* **2007**, *25*, 1165.
(299) Cheng, L.; Wang, C.; Liu, Z. *Nanoscale* **2013**, *5*, 23.
(300) Nyk, M.; Kumar, R.; Ohulchanskyy, T. Y.; Bergey, E. J.; Prasad, P. N. *Nano Lett.* **2008**, *8*, 3834.
(301) Zhang, Q. B.; Song, K.; Zhao, J. W.; Kong, X. G.; Sun, Y. J.; Liu, X. M.; Zhang, Y. L.; Zeng, Q. H.; Zhang, H. *J. Colloid Interface Sci.* **2009**, *336*, 171.
(302) Chen, Q. T.; Wang, X.; Chen, F. H.; Zhang, Q. B.; Dong, B.; Yang, H.; Liu, G. X.; Zhu, Y. M. *J. Mater. Chem.* **2011**, *21*, 7661.
(303) Cao, T. Y.; Yang, T. S.; Gao, Y.; Yang, Y.; Hu, H.; Li, F. Y. *Inorg. Chem. Commun.* **2010**, *13*, 392.
(304) Shen, J.; Sun, L. D.; Zhang, Y. W.; Yan, C. H. *Chem. Commun.* **2010**, *46*, 5731.
(305) Dong, B. A.; Xu, S.; Sun, J. A.; Bi, S.; Li, D.; Bai, X.; Wang, Y.; Wang, L. P.; Song, H. W. *J. Mater. Chem.* **2011**, *21*, 6193.
(306) Dong, A. G.; Ye, X. C.; Chen, J.; Kang, Y. J.; Gordon, T.; Kikkawa, J. M.; Murray, C. B. *J. Am. Chem. Soc.* **2011**, *133*, 998.
(307) Bogdan, N.; Rodriguez, E. M.; Sanz-Rodriguez, F.; de la Cruz, M. C. I.; Juarranz, A.; Jaque, D.; Sole, J. G.; Capobianco, J. A. *Nanoscale* **2012**, *4*, 3647.

(308) Hu, H.; Yu, M. X.; Li, F. Y.; Chen, Z. G.; Gao, X.; Xiong, L. Q.; Huang, C. H. *Chem. Mater.* **2008**, *20*, 7003.
(309) Zhou, H. P.; Xu, C. H.; Sun, W.; Yan, C. H. *Adv. Funct. Mater.* **2009**, *19*, 3892.
(310) Dai, Y. L.; Yang, D. M.; Ma, P. A.; Kang, X. J.; Zhang, X.; Li, C. X.; Hou, Z. Y.; Cheng, Z. Y.; Lin, J. *Biomaterials* **2012**, *33*, 8704.
(311) Sukhorukov, G. B.; Donath, E.; Lichtenfeld, H.; Knippel, E.; Knippel, M.; Budde, A.; Mohwald, H. *Colloids Surf., A* **1998**, *137*, 253.
(312) Bao, Y.; Luu, Q. A. N.; Lin, C. K.; Schloss, J. M.; May, P. S.; Jiang, C. Y. *J. Mater. Chem.* **2010**, *20*, 8356.
(313) Sivakumar, S.; Diamente, P. R.; van Veggel, F. C. *Chem.—Eur. J.* **2006**, *12*, 5878.
(314) Li, Z. Q.; Zhang, Y. *Angew. Chem., Int. Ed.* **2006**, *45*, 7732.
(315) Rantanen, T.; Jarvenpaa, M. L.; Vuojola, J.; Arppe, R.; Kuningas, K.; Soukka, T. *Analyst* **2009**, *134*, 1713.
(316) Liu, Z. Y.; Yi, G. S.; Zhang, H. T.; Ding, J.; Zhang, Y. W.; Xue, J. M. *Chem. Commun.* **2008**, *14*, 694.
(317) Hu, H.; Xiong, L. Q.; Zhou, J.; Li, F. Y.; Cao, T. Y.; Huang, C. H. *Chem.—Eur. J.* **2009**, *15*, 3577.
(318) Das, G. K.; Heng, B. C.; Ng, S. C.; White, T.; Loo, J. S. C.; D'Silva, L.; Padmanabhan, P.; Bhakoo, K. K.; Selvan, S. T.; Tan, T. T. Y. *Langmuir* **2010**, *26*, 8959.
(319) Li, Z. Q.; Zhang, Y.; Shuter, B.; Idris, N. M. *Langmuir* **2009**, *25*, 12015.
(320) Wang, L.; Zhao, W. J.; Tan, W. H. *Nano Res.* **2008**, *1*, 99.
(321) Roy, I.; Ohulchanskyy, T. Y.; Bharali, D. J.; Pudavar, H. E.; Mistretta, R. A.; Kaur, N.; Prasad, P. N. *Proc. Natl. Acad. Sci. U.S.A.* **2005**, *102*, 279.
(322) Yang, J. P.; Deng, Y. H.; Wu, Q. L.; Zhou, J.; Bao, H. F.; Li, Q.; Zhang, F.; Li, F. Y.; Tu, B.; Zhao, D. Y. *Langmuir* **2010**, *26*, 8850.
(323) Qian, H. S.; Guo, H. C.; Ho, P. C. L.; Mahendran, R.; Zhang, Y. *Small* **2009**, *5*, 2285.
(324) Yang, Y. F.; Qu, Y. Q.; Zhao, J. W.; Zeng, Q. H.; Ran, Y. Y.; Zhang, Q. B.; Kong, X. G.; Zhang, H. *Eur. J. Inorg. Chem* . **2010**, 5195.
(325) Kang, X. J.; Cheng, Z. Y.; Li, C. X.; Yang, D. M.; Shang, M. M.; Ma, P. A.; Li, G. G.; Liu, N. A.; Lin, J. *J. Phys. Chem. C* **2011**, *115*, 15801.
(326) Gai, S. L.; Yang, P. P.; Li, C. X.; Wang, W. X.; Dai, Y. L.; Niu, N.; Lin, J. *Adv. Funct. Mater.* **2010**, *20*, 1166.
(327) Xu, Z. H.; Li, C. X.; Ma, P. A.; Hou, Z. Y.; Yang, D. M.; Kang, X. J.; Lin, J. *Nanoscale* **2011**, *3*, 661.
(328) Jiang, G. C.; Pichaandi, J.; Johnson, N. J. J.; Burke, R. D.; van Veggel, F. C. J. M. *Langmuir* **2012**, *28*, 3239.
(329) Cheng, L. A.; Yang, K.; Zhang, S. A.; Shao, M. W.; Lee, S. T.; Liu, Z. A. *Nano Res.* **2010**, *3*, 722.
(330) Budijono, S. J.; Shan, J. N.; Yao, N.; Miura, Y.; Hoye, T.; Austin, R. H.; Ju, Y. G.; Prud'homme, R. K. *Chem. Mater.* **2010**, *22*, 311.
(331) Cao, T. Y.; Yang, Y.; Gao, Y. A.; Zhou, J.; Li, Z. Q.; Li, F. Y. *Biomaterials* **2011**, *32*, 2959.
(332) Nichkova, M.; Dosev, D.; Gee, S. J.; Hammock, B. D.; Kennedy, I. M. *Anal. Chem.* **2005**, *77*, 6864.
(333) Cui, S. S.; Chen, H. Y.; Gu, Y. Q. *J. Phys.: Conf. Ser.* **2011**, *277*, 012006.
(334) Rantanen, T.; Pakkila, H.; Jamsen, L.; Kuningas, K.; Ukonaho, T.; Lovgren, T.; Soukka, T. *Anal. Chem.* **2007**, *79*, 6312.
(335) Rantanen, T.; Jarvenpaa, M. L.; Vuojola, J.; Kuningas, K.; Soukka, T. *Angew. Chem., Int. Ed.* **2008**, *47*, 3811.
(336) Zhang, C. L.; Yuan, Y. X.; Zhang, S. M.; Wang, Y. H.; Liu, Z. H. *Angew. Chem., Int. Ed.* **2011**, *50*, 6851.
(337) Kumar, M.; Guo, Y.; Zhang, P. *Biosens. Bioelectron.* **2009**, *24*, 1522.
(338) Zhang, P.; Rogelj, S.; Nguyen, K.; Wheeler, D. *J. Am. Chem. Soc.* **2006**, *128*, 12410.
(339) Kumar, M.; Zhang, P. *Langmuir* **2009**, *25*, 6024.
(340) Zhou, J.; Yao, L. M.; Li, C. Y.; Li, F. Y. *J. Mater. Chem.* **2010**, *20*, 8078.
(341) Yu, X. F.; Sun, Z. B.; Li, M.; Xiang, Y.; Wang, Q. Q.; Tang, F. F.; Wu, Y. L.; Cao, Z. J.; Li, W. X. *Biomaterials* **2010**, *31*, 8724.
(342) Wang, M.; Mi, C. C.; Liu, J. L.; Wu, X. L.; Zhang, Y. X.; Hou, W.; Li, F.; Xu, S. K. *J. Alloys Compd.* **2009**, *485*, L24.
(343) Chen, J.; Guo, C. R.; Wang, M.; Huang, L.; Wang, L. P.; Mi, C. C.; Li, J.; Fang, X. X.; Mao, C. B.; Xu, S. K. *J. Mater. Chem.* **2011**, *21*, 2632.
(344) Wang, M.; Hou, W.; Mi, C. C.; Wang, W. X.; Xu, Z. R.; Teng, H. H.; Mao, C. B.; Xu, S. K. *Anal. Chem.* **2009**, *81*, 8783.
(345) Wang, M.; Mi, C. C.; Zhang, Y. X.; Liu, J. L.; Li, F.; Mao, C. B.; Xu, S. K. *J. Phys. Chem. C* **2009**, *113*, 19021.
(346) Jiang, S.; Zhang, Y. *Langmuir* **2010**, *26*, 6689.
(347) Jiang, S.; Zhang, Y.; Lim, K. M.; Sim, E. K. W.; Ye, L. *Nanotechnology* **2009**, *20*, 155101.
(348) Xiong, L. Q.; Chen, Z. G.; Yu, M. X.; Li, F. Y.; Liu, C.; Huang, C. H. *Biomaterials* **2009**, *30*, 5592.
(349) Zako, T.; Nagata, H.; Terada, N.; Utsumi, A.; Sakono, M.; Yohda, M.; Ueda, H.; Soga, K.; Maeda, M. *Biochem. Biophys. Res. Commun.* **2009**, *381*, 54.
(350) Ryu, J.; Park, H. Y.; Kim, K.; Kim, H.; Yoo, J. H.; Kang, M.; Im, K.; Grailhe, R.; Song, R. *J. Phys. Chem. C* **2010**, *114*, 21077.
(351) Vetrone, F.; Naccache, R.; Zamarron, A.; de la Fuente, A. J.; Sanz-Rodriguez, F.; Maestro, L. M.; Rodriguez, E. M.; Jaque, D.; Sole, J. G.; Capobianco, J. A. *ACS Nano* **2010**, *4*, 3254.
(352) Sedlmeier, A.; Achatz, D. E.; Fischer, L. H.; Gorris, H. H.; Wolfbeis, O. S. *Nanoscale* **2012**, *4*, 7090.
(353) Chen, J.; Zhao, J. X. *Sensors* **2012**, *12*, 2414.
(354) Liu, Q.; Peng, J. J.; Sun, L. N.; Li, F. Y. *ACS Nano* **2011**, *5*, 8040.
(355) Kumar, M.; Zhang, P. *Biosens. Bioelectron.* **2010**, *25*, 2431.
(356) Zhang, J.; Li, B.; Zhang, L. M.; Jiang, H. *Chem. Commun.* **2012**, *48*, 4860.
(357) Xie, L. X.; Qin, Y.; Chen, H. Y. *Anal. Chem.* **2012**, *84*, 1969.
(358) Borisov, S. M.; Nuss, G.; Klimant, I. *Anal. Chem.* **2008**, *80*, 9435.
(359) Borisov, S. M.; Papkovsky, D. B.; Ponomarev, G. V.; DeToma, A. S.; Saf, R.; Klimant, I. *J. Photochem. Photobiol., A* **2009**, *206*, 87.
(360) Achatz, D. E.; Meier, R. J.; Fischer, L. H.; Wolfbeis, O. S. *Angew. Chem., Int. Ed.* **2011**, *50*, 260.
(361) Liu, L.; Li, B.; Ying, J.; Wu, X.; Zhao, H.; Ren, X.; Zhu, D.; Su, Z. *Nanotechnology* **2008**, *19*, 495709.
(362) Sun, L. N.; Peng, H. S.; Stich, M. I. J.; Achatz, D.; Wolfbeis, O. S. *Chem. Commun.* **2009**, *7*, 5000.
(363) Ali, R.; Saleh, S. M.; Meier, R. J.; Azab, H. A.; Abdelgawad, I. I.; Wolfbeis, O. S. *Sens. Actuators, B: Chem.* **2010**, *150*, 126.
(364) Mader, H. S.; Wolfbeis, O. S. *Anal. Chem.* **2010**, *82*, 5002.
(365) Zijlmans, H. J. M. A. A.; Bonnet, J.; Burton, J.; Kardos, K.; Vail, T.; Niedbala, R. S.; Tanke, H. J. *Anal. Biochem.* **1999**, *267*, 30.
(366) Hampl, J.; Hall, M.; Mufti, N. A.; Yao, Y. M. M.; MacQueen, D. B.; Wright, W. H.; Cooper, D. E. *Anal. Biochem.* **2001**, *288*, 176.
(367) Niedbala, R. S.; Feindt, H.; Kardos, K.; Vail, T.; Burton, J.; Bielska, B.; Li, S.; Milunic, D.; Bourdelle, P.; Vallejo, R. *Anal. Biochem.* **2001**, *293*, 22.
(368) Corstjens, P.; Zuiderwijk, M.; Brink, A.; Li, S.; Feindt, H.; Neidbala, R. S.; Tanke, H. *Clin. Chem.* **2001**, *47*, 1885.
(369) Zuiderwijk, M.; Tanke, H. J.; Niedbala, R. S.; Corstjens, P. L. A. M. *Clin. Biochem.* **2003**, *36*, 401.
(370) van de Rijke, F.; Zijlmans, H.; Li, S.; Vail, T.; Raap, A. K.; Niedbala, R. S.; Tanke, H. J. *Nat. Biotechnol.* **2001**, *19*, 273.
(371) Corstjens, P. L.; Li, S.; Zuiderwijk, M.; Kardos, K.; Abrams, W. R.; Niedbala, R. S.; Tanke, H. J. *IEEE Proc. Nanobiotechnol.* **2005**, *152*, 64.
(372) Ukonaho, T.; Rantanen, T.; Jamsen, L.; Kuningas, K.; Pakkila, H.; Lovgren, T.; Soukka, T. *Anal. Chim. Acta* **2007**, *596*, 106.
(373) Morgan, C. G.; Mitchell, A. C. *Biosens. Bioelectron.* **2007**, *22*, 1769.
(374) Kuningas, K.; Rantanen, T.; Ukonaho, T.; Lovgren, T.; Soukka, T. *Anal. Chem.* **2005**, *77*, 7348.
(375) Kuningas, K.; Ukonaho, T.; Pakkila, H.; Rantanen, T.; Rosenberg, J.; Lovgren, T.; Soukka, T. *Anal. Chem.* **2006**, *78*, 4690.

(376) Kuningas, K.; Pakkila, H.; Ukonaho, T.; Rantanen, T.; Lovgren, T.; Soukka, T. *Clin. Chem.* **2007**, *53*, 145.
(377) Wei, W.; He, T. C.; Teng, X.; Wu, S. X.; Ma, L.; Zhang, H.; Ma, J.; Yang, Y. H.; Chen, H. Y.; Han, Y.; Sun, H. D.; Huang, L. *Small* **2012**, *8*, 2271.
(378) Deng, R. R.; Xie, X. J.; Vendrell, M.; Chang, Y. T.; Liu, X. G. *J. Am. Chem. Soc.* **2011**, *133*, 20168.
(379) Wang, Y. H.; Shen, P.; Li, C. Y.; Wang, Y. Y.; Liu, Z. H. *Anal. Chem.* **2012**, *84*, 1466.
(380) Xing, H. Y.; Zheng, X. P.; Ren, Q. G.; Bu, W. B.; Ge, W. Q.; Xiao, Q. F.; Zhang, S. J.; Wei, C. Y.; Qu, H. Y.; Wang, Z.; Hua, Y. Q.; Zhou, L. P.; Peng, W. J.; Zhao, K. L.; Shi, J. L. *Sci. Rep. (U.K.)* **2013**, *3*, 1751.
(381) Jin, J. F.; Gu, Y. J.; Man, C. W. Y.; Cheng, J. P.; Xu, Z. H.; Zhang, Y.; Wang, H. S.; Lee, V. H. Y.; Cheng, S. H.; Wong, W. T. *ACS Nano* **2011**, *5*, 7838.
(382) Cheng, L.; Yang, K.; Shao, M.; Lu, X.; Liu, Z. *Nanomedicine (London, U.K.)* **2011**, *6*, 1327.
(383) Zhou, J. C.; Yang, Z. L.; Dong, W.; Tang, R. J.; Sun, L. D.; Yan, C. H. *Biomaterials* **2011**, *32*, 9059.
(384) Lim, S. F.; Riehn, R.; Ryu, W. S.; Khanarian, N.; Tung, C. K.; Tank, D.; Austin, R. H. *Nano Lett.* **2006**, *6*, 169.
(385) Lim, S. F.; Riehn, R.; Tung, C. K.; Ryu, W. S.; Zhuo, R.; Dalland, J.; Austin, R. H. *Nanotechnology* **2009**, *20*, 405701.
(386) Wang, K.; Ma, J.; He, M.; Gao, G.; Xu, H.; Sang, J.; Wang, Y.; Zhao, B.; Cui, D. *Theranostics* **2013**, *3*, 258.
(387) Chatteriee, D. K.; Rufalhah, A. J.; Zhang, Y. *Biomaterials* **2008**, *29*, 937.
(388) Wu, S. W.; Han, G.; Milliron, D. J.; Aloni, S.; Altoe, V.; Talapin, D. V.; Cohen, B. E.; Schuck, P. J. *Proc. Natl. Acad. Sci. U.S.A.* **2009**, *106*, 10917.
(389) Park, Y. I.; Kim, J. H.; Lee, K. T.; Jeon, K. S.; Bin Na, H.; Yu, J. H.; Kim, H. M.; Lee, N.; Choi, S. H.; Baik, S. I.; Kim, H.; Park, S. P.; Park, B. J.; Kim, Y. W.; Lee, S. H.; Yoon, S. Y.; Song, I. C.; Moon, W. K.; Suh, Y. D.; Hyeon, T. *Adv. Mater.* **2009**, *21*, 4467.
(390) Nam, S. H.; Bae, Y. M.; Park, Y. I.; Kim, J. H.; Kim, H. M.; Choi, J. S.; Lee, K. T.; Hyeon, T.; Suh, Y. D. *Angew. Chem., Int. Ed.* **2011**, *50*, 6093.
(391) Ostrowski, A. D.; Chan, E. M.; Gargas, D. J.; Katz, E. M.; Han, G.; Schuck, P. J.; Milliron, D. J.; Cohen, B. E. *ACS Nano* **2012**, *6*, 2686.
(392) Zhang, Y. J.; Zheng, F.; Yang, T. L.; Zhou, W.; Liu, Y.; Man, N.; Zhang, L.; Jin, N.; Dou, Q. Q.; Zhang, Y.; Li, Z. Q.; Wen, L. P. *Nat. Mater.* **2012**, *11*, 817.
(393) Yu, L.; Lu, Y.; Man, N.; Yu, S. H.; Wen, L. P. *Small* **2009**, *5*, 2784.
(394) Vetrone, F.; Naccache, R.; Juarranz de la Fuente, A.; Sanz-Rodriguez, F.; Blazquez-Castro, A.; Rodriguez, E. M.; Jaque, D.; Sole, J. G.; Capobianco, J. A. *Nanoscale* **2010**, *2*, 495.
(395) Dong, N. N.; Pedroni, M.; Piccinelli, F.; Conti, G.; Sbarbati, A.; Ramirez-Hernandez, J. E.; Maestro, L. M.; Iglesias-de la Cruz, M. C.; Sanz-Rodriguez, F.; Juarranz, A.; Chen, F.; Vetrone, F.; Capobianco, J. A.; Sole, J. G.; Bettinelli, M.; Jaque, D.; Speghini, A. *ACS Nano* **2011**, *5*, 8665.
(396) Dai, Y. L.; Ma, P. A.; Cheng, Z. Y.; Kang, X. J.; Zhang, X.; Hou, Z. Y.; Li, C. X.; Yang, D. M.; Zhai, X. F.; Lin, J. *ACS Nano* **2012**, *6*, 3327.
(397) Shan, J. N.; Chen, J. B.; Meng, J.; Collins, J.; Soboyejo, W.; Friedberg, J. S.; Ju, Y. G. *J. Appl. Phys.* **2008**, *104*, 094308.
(398) Das, G. K.; Chan, P. P. Y.; Teo, A.; Loo, J. S. C.; Anderson, J. M.; Tan, T. T. Y. *J. Biomed. Mater. Res., Part A* **2010**, *93A*, 337.
(399) Akiyama, H.; Tokuzen, K.; Otsuka, H.; Soga, K.; Tashiro, F. *J. Phys.: Conf. Ser.* **2010**, *232*, 012001.
(400) Liu, K.; Liu, X. M.; Zeng, Q. H.; Zhang, Y. L.; Tu, L. P.; Liu, T.; Kong, X. G.; Wang, Y. H.; Cao, F.; Lambrechts, S. A. G.; Aalders, M. C. G.; Zhang, H. *ACS Nano* **2012**, *6*, 4054.
(401) Lee, K. Y.; Seow, E.; Zhang, Y.; Lim, Y. C. *Biomaterials* **2013**, *34*, 4860.
(402) Chatterjee, D. K.; Yong, Z. *Nanomedicine (London, U.K.)* **2008**, *3*, 73.
(403) Hilderbrand, S. A.; Shao, F. W.; Salthouse, C.; Mahmood, U.; Weissleder, R. *Chem. Commun.* **2009**, *28*, 4188.
(404) Esipova, T. V.; Ye, X. C.; Collins, J. E.; Sakadzic, S.; Mandeville, E. T.; Murray, C. B.; Vinogradov, S. A. *Proc. Natl. Acad. Sci. U.S.A.* **2012**, *109*, 20826.
(405) Vinegoni, C.; Razansky, D.; Hilderbrand, S. A.; Shao, F. W.; Ntziachristos, V.; Weissleder, R. *Opt. Lett.* **2009**, *34*, 2566.
(406) Salthouse, C.; Hildebrand, S.; Weissleder, R.; Mahmood, U. *Opt. Express* **2008**, *16*, 21731.
(407) Wang, C.; Cheng, L.; Xu, H.; Liu, Z. *Biomaterials* **2012**, *33*, 4872.
(408) Idris, N. M.; Li, Z. Q.; Ye, L.; Sim, E. K. W.; Mahendran, R.; Ho, P. C. L.; Zhang, Y. *Biomaterials* **2009**, *30*, 5104.
(409) Kobayashi, H.; Kosaka, N.; Ogawa, M.; Morgan, N. Y.; Smith, P. D.; Murray, C. B.; Ye, X. C.; Collins, J.; Kumar, G. A.; Bell, H.; Choyke, P. L. *J. Mater. Chem.* **2009**, *19*, 6481.
(410) Han, G.; Chen, G. Y. *Theranostics* **2013**, *3*, 354.
(411) Tian, Z.; Chen, G. Y.; Li, X.; Liang, H. J.; Li, Y. S.; Zhang, Z. G.; Tian, Y. *Laser Med. Sci.* **2010**, *25*, 479.
(412) Yu, X. F.; Li, M.; Xie, M. Y.; Chen, L. D.; Li, Y.; Wang, Q. Q. *Nano Res.* **2010**, *3*, 51.
(413) Xu, C. T.; Svensson, N.; Axelsson, J.; Svenmarker, P.; Somesfalean, G.; Chen, G. Y.; Liang, H. J.; Liu, H. C.; Zhang, Z. G.; Andersson-Engels, S. *Appl. Phys. Lett.* **2008**, *93*, 171103.
(414) Xu, C. T.; Axelsson, J.; Andersson-Engels, S. *Appl. Phys. Lett.* **2009**, *94*, 251107.
(415) Liu, H. C.; Xu, C. T.; Andersson-Engels, S. *Opt. Lett.* **2010**, *35*, 718.
(416) Xu, C. T.; Svenmarker, P.; Liu, H. C.; Wu, X.; Messing, M. E.; Wallenberg, L. R.; Andersson-Engels, S. *ACS Nano* **2012**, *6*, 4788.
(417) Chen, F.; Bu, W. B.; Zhang, S. J.; Liu, X. H.; Liu, J. N.; Xing, H. Y.; Xiao, Q. F.; Zhou, L. P.; Peng, W. J.; Wang, L. Z.; Shi, J. L. *Adv. Funct. Mater.* **2011**, *21*, 4285.
(418) Chen, F.; Bu, W.; Zhang, S.; Liu, J.; Fan, W.; Zhou, L.; Peng, W.; Shi, J. *Adv. Funct. Mater.* **2013**, *23*, 298.
(419) Johnson, N. J. J.; Oakden, W.; Stanisz, G. J.; Prosser, R. S.; van Veggel, F. C. J. M. *Chem. Mater.* **2011**, *23*, 3714.
(420) Liu, C.; Gao, Z.; Zeng, J.; Hou, Y.; Fang, F.; Li, Y.; Qiao, R.; Shen, L.; Lei, H.; Yang, W.; Gao, M. *ACS Nano* **2013**, *7*, 7227.
(421) Fan, W.; Shen, B.; Bu, W.; Chen, F.; Zhao, K.; Zhang, S.; Zhou, L.; Peng, W.; Xiao, Q.; Xing, H.; Liu, J.; Ni, D.; He, Q.; Shi, J. *J. Am. Chem. Soc.* **2013**, *135*, 6494.
(422) Xia, A.; Chen, M.; Gao, Y.; Wu, D. M.; Feng, W.; Li, F. Y. *Biomaterials* **2012**, *33*, 5394.
(423) Liu, J. A.; Bu, W. B.; Zhang, S. J.; Chen, F.; Xing, H. Y.; Pan, L. M.; Zhou, L. P.; Peng, W. J.; Shi, J. L. *Chem.—Eur. J.* **2012**, *18*, 2335.
(424) Zeng, S. J.; Xiao, J. J.; Yang, Q. B.; Hao, J. H. *J. Mater. Chem.* **2012**, *22*, 9870.
(425) Xia, A.; Gao, Y.; Zhou, J.; Li, C. Y.; Yang, T. S.; Wu, D. M.; Wu, L. M.; Li, F. Y. *Biomaterials* **2011**, *32*, 7200.
(426) Zhu, X. J.; Zhou, J.; Chen, M.; Shi, M.; Feng, W.; Li, F. Y. *Biomaterials* **2012**, *33*, 4618.
(427) He, M.; Huang, P.; Zhang, C. L.; Hu, H. Y.; Bao, C. C.; Gao, G.; He, R.; Cui, D. X. *Adv. Funct. Mater.* **2011**, *21*, 4470.
(428) Liu, Y. L.; Ai, K. L.; Lu, L. H. *Acc. Chem. Res.* **2012**, *45*, 1817.
(429) Zhang, G.; Liu, Y. L.; Yuan, Q. H.; Zong, C. H.; Liu, J. H.; Lu, L. H. *Nanoscale* **2011**, *3*, 4365.
(430) Liu, Y. L.; Ai, K. L.; Liu, J. H.; Yuan, Q. H.; He, Y. Y.; Lu, L. H. *Angew. Chem., Int. Ed.* **2012**, *51*, 1437.
(431) Liu, Y. L.; Ai, K. L.; Liu, J. H.; Yuan, Q. H.; He, Y. Y.; Lu, L. H. *Adv. Healthcare Mater.* **2012**, *1*, 461.
(432) Xing, H.; Bu, W.; Ren, Q.; Zheng, X.; Li, M.; Zhang, S.; Qu, H.; Wang, Z.; Hua, Y.; Zhao, K.; Zhou, L.; Peng, W.; Shi, J. *Biomaterials* **2012**, *33*, 5384.
(433) Liu, Q.; Sun, Y.; Li, C. G.; Zhou, J.; Li, C. Y.; Yang, T. S.; Zhang, X. Z.; Yi, T.; Wu, D. M.; Li, F. Y. *ACS Nano* **2011**, *5*, 3146.
(434) Xiao, Q.; Bu, W.; Ren, Q.; Zhang, S.; Xing, H.; Chen, F.; Li, M.; Zheng, X.; Hua, Y.; Zhou, L.; Peng, W.; Qu, H.; Wang, Z.; Zhao, K.; Shi, J. *Biomaterials* **2012**, *33*, 7530.

(435) Sun, Y.; Zhu, X.; Peng, J.; Li, F. *ACS Nano* **2013**, *7*, 11290.
(436) Dai, Y.; Xiao, H.; Liu, J.; Yuan, Q.; Ma, P.; Yang, D.; Li, C.; Cheng, Z.; Hou, Z.; Yang, P.; Lin, J. *J. Am. Chem. Soc.* **2013**, *135*, 18920.
(437) Xu, H.; Cheng, L.; Wang, C.; Ma, X. X.; Li, Y. G.; Liu, Z. *Biomaterials* **2011**, *32*, 9364.
(438) Hou, Z. Y.; Li, C. X.; Ma, P. A.; Li, G. G.; Cheng, Z. Y.; Peng, C.; Yang, D. M.; Yang, P. P.; Lin, J. *Adv. Funct. Mater.* **2011**, *21*, 2356.
(439) Zhang, X.; Yang, P.; Dai, Y.; Ma, P. a.; Li, X.; Cheng, Z.; Hou, Z.; Kang, X.; Li, C.; Lin, J. *Adv. Funct. Mater.* **2013**, *23*, 4067.
(440) Xu, Z. H.; Ma, P. A.; Li, C. X.; Hou, Z. Y.; Zhai, X. F.; Huang, S. S.; Lin, J. *Biomaterials* **2011**, *32*, 4161.
(441) Dong, L.; An, D.; Gong, M.; Lu, Y.; Gao, H. L.; Xu, Y. J.; Yu, S. H. *Small* **2013**, *9*, 3235.
(442) Zhang, F.; Braun, G. B.; Pallaoro, A.; Zhang, Y. C.; Shi, Y. F.; Cui, D. X.; Moskovits, M.; Zhao, D. Y.; Stucky, G. D. *Nano Lett.* **2012**, *12*, 61.
(443) Carling, C. J.; Boyer, J. C.; Branda, N. R. *J. Am. Chem. Soc.* **2009**, *131*, 10838.
(444) Boyer, J. C.; Carling, C. J.; Gates, B. D.; Branda, N. R. *J. Am. Chem. Soc.* **2010**, *132*, 15766.
(445) Zhang, B. F.; Frigoli, M.; Angiuli, F.; Vetrone, F.; Capobianco, J. A. *Chem. Commun.* **2012**, *48*, 7244.
(446) Zhang, C.; Zhou, H. P.; Liao, L. Y.; Feng, W.; Sun, W.; Li, Z. X.; Xu, C. H.; Fang, C. J.; Sun, L. D.; Zhang, Y. W.; Yan, C. H. *Adv. Mater.* **2010**, *22*, 633.
(447) Boyer, J. C.; Carling, C. J.; Chua, S. Y.; Wilson, D.; Johnsen, B.; Baillie, D.; Branda, N. R. *Chem.—Eur. J.* **2012**, *18*, 3122.
(448) Jayakumar, M. K. G.; Idris, N. M.; Zhang, Y. *Proc. Natl. Acad. Sci. U.S.A.* **2012**, *109*, 8483.
(449) Yang, Y. M.; Shao, Q.; Deng, R. R.; Wang, C.; Teng, X.; Cheng, K.; Cheng, Z.; Huang, L.; Liu, Z.; Liu, X. G.; Xing, B. G. *Angew. Chem., Int. Ed.* **2012**, *51*, 3125.
(450) Yang, Y. M.; Liu, F.; Liu, X. G.; Xing, B. G. *Nanoscale* **2013**, *5*, 231.
(451) Yang, Y.; Velmurugan, B.; Liu, X.; Xing, B. *Small* **2013**, *9*, 2937.
(452) Liu, J. A.; Bu, W. B.; Pan, L. M.; Shi, J. L. *Angew. Chem., Int. Ed.* **2013**, *52*, 4375.
(453) Garcia, J. V.; Yang, J. P.; Shen, D. K.; Yao, C.; Li, X. M.; Wang, R.; Stucky, G. D.; Zhao, D. Y.; Ford, P. C.; Zhang, F. *Small* **2012**, *8*, 3800.
(454) Burks, P. T.; Garcia, J. V.; Gonzalezirias, R.; Tillman, J. T.; Niu, M.; Mikhailovsky, A. A.; Zhang, J.; Zhang, F.; Ford, P. C. *J. Am. Chem. Soc.* **2013**, *135*, 18145.
(455) Yan, B.; Boyer, J. C.; Branda, N. R.; Zhao, Y. *J. Am. Chem. Soc.* **2011**, *133*, 19714.
(456) Yan, B.; Boyer, J. C.; Habault, D.; Branda, N. R.; Zhao, Y. *J. Am. Chem. Soc.* **2012**, *134*, 16558.
(457) Viger, M. L.; Grossman, M.; Fomina, N.; Almutairi, A. *Adv. Mater.* **2013**, *25*, 3733.
(458) Xiao, Q.; Zheng, X.; Bu, W.; Ge, W.; Zhang, S.; Chen, F.; Xing, H.; Ren, Q.; Fan, W.; Zhao, K.; Hua, Y.; Shi, J. *J. Am. Chem. Soc.* **2013**, *135*, 13041.
(459) Zhang, P.; Steelant, W.; Kumar, M.; Scholfield, M. *J. Am. Chem. Soc.* **2007**, *129*, 4526.
(460) Guo, Y. Y.; Kumar, M.; Zhang, P. *Chem. Mater.* **2007**, *19*, 6071.
(461) Shan, J. N.; Budijono, S. J.; Hu, G. H.; Yao, N.; Kang, Y. B.; Ju, Y. G.; Prud'homme, R. K. *Adv. Funct. Mater.* **2011**, *21*, 2488.
(462) Tian, G.; Ren, W. L.; Yan, L.; Jian, S.; Gu, Z. J.; Zhou, L. J.; Jin, S.; Yin, W. Y.; Li, S. J.; Zhao, Y. L. *Small* **2013**, *9*, 1929.
(463) Wang, C.; Tao, H. Q.; Cheng, L.; Liu, Z. *Biomaterials* **2011**, *32*, 6145.
(464) Wang, C.; Cheng, L.; Liu, Y. M.; Wang, X. J.; Ma, X. X.; Deng, Z. Y.; Li, Y. G.; Liu, Z. *Adv. Funct. Mater.* **2013**, *23*, 3077.
(465) Cui, S. S.; Yin, D. Y.; Chen, Y. Q.; Di, Y. F.; Chen, H. Y.; Ma, Y. X.; Achilefu, S.; Gu, Y. Q. *ACS Nano* **2013**, *7*, 676.
(466) Lim, M. E.; Lee, Y. L.; Zhang, Y.; Chu, J. J. H. *Biomaterials* **2012**, *33*, 1912.
(467) Shen, J.; Chen, G.; Vu, A. M.; Fan, W.; Bilsel, O. S.; Chang, C. C.; Han, G. *Adv. Opt. Mater.* **2013**, *1*, 644.
(468) Xie, X.; Gao, N.; Deng, R.; Sun, Q.; Xu, Q. H.; Liu, X. *J. Am. Chem. Soc.* **2013**, *135*, 12608.
(469) Wang, Y. F.; Liu, G. Y.; Sun, L. D.; Xiao, J. W.; Zhou, J. C.; Yan, C. H. *ACS Nano* **2013**, *7*, 7200.

## NOTE ADDED AFTER ASAP PUBLICATION

This paper was published to the Web on March 10, 2014, with an error in the Web TOC graphic and the title-page-graphic. This was fixed in the version published to the Web on May 5, 2014.